Федеральное государственное автономное образовательное учреждение
высшего образования «Уральский федеральный университет имени первого
Президента России Б. Н. Ельцина»

Уральский энергетический институт
Кафедра «Атомные станции и возобновляемые источники энергии»

На правах рукописи

Касим Мухаммед Абдулхалик Касим

Разработка и оптимизация термоэлектрических генераторов и их интеграция с фотоэлектрической панелью для применения в отдаленных районах Республики Ирак

2.4.5. Энергетические системы и комплексы

ДИССЕРТАЦИЯ
на соискание ученой степени
кандидата технических наук

Научный руководитель:
Доктор технических наук, доцент,
Велькин Владимир Иванович

Екатеринбург – 2023

Federal State Autonomous Educational Institution Higher Education «Ural Federal University named after the first President of Russia B.N. Yeltsin»

Ural Power Engineering Institute
Department of «Nuclear Power Plants and Renewable Energy Sources»

As a manuscript

Qasim Mohammed Abdulkhaleq Qasim

Development and optimization of thermoelectric generators and their integration with a photovoltaic panel for applications in remote areas of the Republic of Iraq

2.4.5. Energy systems and complexes

DISSERTATION
Degree of Candidate of Technical Sciences

Scientific supervisor:
Doctor of Technical Sciences, Associate Professor,
Velkin Vladimir Ivanovich

Yekaterinburg – 2023

ACKNOWLEDGMENT

I would like to express my special thanks of gratitude to my supervisor, Prof. Vladimir Ivanovich Velkin, Department of Nuclear and Renewable Energy, Ural Power Engineering Institute of Ural Federal University, Ekaterinburg, Russia for the continuous support of my Ph.D. study. His encouragement and guidance helped me in doing a lot of research and gain knowledge of so many new things that contributed to preparation of my dissertation and presenting the work in this way. Besides my supervisor, I would like to express my sincere gratitude to Prof. Sergey Evgenvich Shcheklein (Head of Department) for his support and encouragement.

I would also like to give special thanks to my family, and all my friends and colleagues for supporting me throughout my Ph.D. study.

Last but not least, I am extremely grateful to Ural Federal University for giving me this golden opportunity to complete my study and research.

Table of Contents

List of Figures

List of Tables

INTRODUCTION

The relevance of the research topic and the degree of its development: The economic development and growth, a well as the countries urbanization involve a substantial increase in electricity demand worldwide. Currently, electricity generation from non-renewable energy sources is 71.9%, while it is 28.1% from renewable sources. Developed countries, such as the USA, China, Russia, and the EU countries, are increasing the pace of development of nonconventional and renewable energy sources. According to the International Renewable Energy Agency (IRENA), in 2022 the installed capacities of renewable energy sources reached 3,064 GW.

At present, only 2% of electricity in Iraq is generated from renewable energy sources (the installed capacity of hydroelectric power plants is 1,864 MW, and solar power plants is 50 MW). This is because the country has significant stores of fossil fuels, which are used to generate electricity.

Currently, the supply-demand gap has increased in Iraq. The peak electricity capacity was 28 GW, while the power generation was only 16 GW, and most of it is accounted for by fossil fuel power plants. Thus, despite the country's large stores of oil and gas, there is a shortage of electricity with increased environmental degradation in Iraq. Traditional and renewable energy sources can be used to increase power generation. Iraq is located in a hot climate zone, so the country has the opportunity to use thermal and solar energy more efficiently.

In the last 5-10 years, along with solar photovoltaic panels (PV), the use of thermoelectric generators (TEG) has been investigated. TEG modules can operate autonomously, which is well suited for remote areas. Moreover, TEGs should be used in conjunction with PV technology to increase efficiency and reduce environmental impact. TEGs work without intermediate energy conversion. As such, they are highly reliable, noise-free, and environmentally friendly. An important advantage of the TEGs is their absence of moving parts, and, consequently, vibrations. In Iraq, photovoltaic panels are used to generate power. The efficiency of PV depends on the correct location related to the sun, and the level of radiation. These factors do not affect TEGs. Thus, research on efficiency improvement of TEG is relevant.

The degree of elaboration of the research topic: Well-known Russian scientists have been engaged in research about renewable and hybrid energy supplies for rural and remote areas and the improvement of the power plants using renewable energy sources. These esteemed researchers include Alekseev V.A., Alferov Z. I., Alekseenko S.V., Strebkov D.S., Bezrukikh P. .P., Elistratov V.V. Kharchenko V.V.,

Shcheklein S.E., Sheryazov S.K. Foreign scientists involved in this research are the well-known Fini M. A. (K. N. Toosi University of Technology, Iran), Zhang J. (Nanjing University of Aeronautics and Astronautics, China), R. Monnier (Solid State Physics Laboratory, ETH Zurich) and Gao Min (Cardiff University, United Kingdom).

The purpose of the study: Development and optimization of a TEG system based on solar energy for operation in remote areas of the Republic of Iraq.

The following tasks were performed in order to accomplish the study goal:

1. To develop, create and investigate designs of thermoelectric generators based on solar energy using Fresnel lenses and heat exchangers to increase the amount of extracted energy.
2. To develop, create and investigate designs of a TEG panel from a serial and parallel TEG configuration in arrays of (2×10 TEG, 15×10 TEG) panels. This is done to study the efficiency of electricity generation with the use of tap water and a solar heater.
3. To develop, create, design and investigate an experimental hybrid system consisting from PV and TEG (HPVTEG) with a water heat exchanger to increase overall efficiency of the installation.
4. To carry out theoretical and numerical analyses of parameters (efficiency, power) in the developed TEG modules using (CFD) code based on program ANSYS.
5. To conduct theoretical analysis and research of a system consisting of a solar panel and a thermoelectric generator (PV-TEG) to improve the efficiency and stability of the system using the MPPT algorithm based on MATLAB SIMULINK.

The object of the study: A thermoelectric generator based on the Seebeck effect to generate power.

Subject of research: Efficiency of TEG modules that can be used with various types of RES and cooling methods.

Research methods: : During the experiment, the Seebeck effect and the photovoltaic effect were employed to study the electrical power output of TEG and PV systems. Methods of waste heat recovery and transfer were used to evaluate the performance and efficiency of TEG and PV systems, and experimental studies were conducted. Algorithms in MATLAB and ANSYS were used to carry out theoretical calculations. The theoretical model is based on algorithms and CFD code. For the proposed system, MPPT algorithms were tested, and parametric methods were studied, while experimental and theoretical results were compared.

The main provisions of the dissertation submitted for defense:

1. The experimental results of the panels with a use of solar energy and Fresnel lenses along with heat exchangers show an optimization of generated power.
2. The experimental results of 2x10 TEG, 15x10 TEG panels from serial and parallel configurations of TEG arrays for generating electrical energy using water as a cooler with two-layer heat exchangers
3. The experimental results of the hybrid PV-TEG system show an efficiency improvement of the installation with a water heat exchanger.
4. The results of theoretical and numerical analysis of heat exchange processes in the TEG using the ANSYS program were based on the CFD code.
5. The theoretical results of modeling a hybrid PV-TEG system show improvement of efficiency and reliability. This hybrid PV-TEG uses the methods of the MPPT algorithm.

Scientific novelty of the dissertation research:

1. For the first time, a new method has been proposed to increase the power and efficiency of TEG modules powered by solar energy. This system can work in the hot and dry areas of Iraq.
2. For the first time, a new method was proposed to increase the power and efficiency of a TEG using a double-layer heat exchanger and tap water. A stable electrical connection for TEG modules was proposed.
3. An experimental hybrid PV-TEG system is proposed to increase the overall efficiency of the installation using a water heat exchanger that can operate in the hot and dry areas of Iraq.
4. A theoretical analysis of the TEG was carried out: . the The effect of increasing the thickness of the plate facing the sun; and the water flow rate (on the cooled side of the TEG) at the output power and efficiency were considered. The TEG module was created with using the ANSYS program and the code (CFD).
5. A hybrid system PV-TEG using MPPT algorithms in the MATLAB SIMULINK program has been developed and proposed.
6. It is shown that the electrical power of the TEG modules decrease if a Fresnel lens is used for panels with a large area. This occurs since a panel collects heat only on a small portion of its area. The converse is also true, power increases if a Fresnel lens is used for panels with a small area.

7. A method was developed and implemented for cooling solar photovoltaic modules in combination with TEGs and a heat exchanger, which made a 10-16% development of the solar cells efficiency an achievable task.

The theoretical and practical significance of the work is: This work describes designs of various types of TEG panels made of serial and parallel connection of modules to obtain desired voltage and power levels. Experimentally, mechanisms for obtaining thermal energy directly from solar radiation or from pipelines that are used for household needs have been implemented. Then thermal energy is converted into useful electrical energy. CFD code is used for validation and parametric research. During the study, a hybrid PV-TEG system was investigated using several MPPT algorithms to improve its efficiency

Credibility and validity: The scientific results obtained during the work are based on experiments and mathematical modeling of TEG modules. These results and the previously generated experimental and theoretical data from previous researchers were compared.

Personal contribution: The author personally participated in:

1. Proposed combinations of new ways to increase generation of electricity from TEG modules using Fresnel lenses and a solar energy.
2. Experimental studies were done to develop TEG panels (TEG 2x10 and 15x10) for TEG efficiency enhancement using a two-layer heat exchanger.
3. Experimental studies of the effectiveness of the developed methods for increasing the efficiency of a solar cell with a TEG under conditions of high ambient temperatures were carried out.
4. A theoretical analysis of TEG models was performed using ANSYS programs.
5. A theoretical model of the PV-TEG hybrid system was developed using MATLAB programs.

Approbation of the work: The results are presented and discussed at the following conferences: First International Conference on Advances in Physical Sciences and Materials (ICAPSM 2020) held at SNS College of Technology, Coimbatore, Tamil Nadu, India during 13 – 14 August 2020 ; International Youth Danilov Energy Forum (All-Russian Student Olympiad with international participation "Energy and Resource Saving", "Non-traditional and Renewable Energy", "Nuclear Energy", UrFU, 2022); All-Russian Conference with International Participation Ural Project of Energy Conference, Ural Federal University, December 19, 2022; Exhibition of research works and engineering developments of young scientists, November 29, 2022; XIX international conference "Renewable and small-scale energy - 2022". Energy saving. Autonomous power supply systems for stationary and mobile objects, NRU Moscow

Power Engineering Institute (MPEI), Moscow, Russia, October 20-21, 2022; Third International Conference on Advances in the Physical Sciences and Materials, (ICAPSM 2022) 2022 Coimbatore, India, August 18-19, 2022; Second Global Conference on Recent Advances in Sustainable Materials (GC-RASM 2022), Mangaluru, India, 28-29 July 2022; International Conference on Emerging Technologies in Electricity, Electronics and Computing (ICE4CT2022), Malaysia, December 28-29, 2022.

Publications: The results of the dissertation were published in 25 articles. Seventeen of these articles were indexed in the Scopus Web of Science international citation databases. Two articles were published in peer-reviewed scientific publications recommended by the Higher Attestation Commission of the Russian Federation and the UrFU Attestation Council. Six articles were presented international and Russian scientific conferences.

Structure and scope of the dissertation: the dissertation contains an Introduction, 5 chapters, Conclusions, 208 references and appendices. As a result, the dissertation consists of 160 pages, 98 figures and 21 tables.

CHAPTER ONE: LITERATURE REVIEW

1.1 Preface

Electricity sector is an important sign of the progression and the economic development of a country. It also represent a vital player to support the growth and the strength of the economic and industrial divisions [1]. After the 1% fall in global electricity demand due to the Covid-19 pandemic, in 2020, it has shown growth rates of 5% and 4% in 2021 and 2022, respectively. This is because of the recovery of the economic worldwide, as reported by the resent semi-annual Electricity Market Report released by the International Energy Agency (IEA). The most portion of this demand comes from China, India, and Asia Pacific region. In 2021 and 2022, Fossil fuel signifies 45% and 40% of the total electricity generation [2]. Consequently, the carbon emissions associated with the electricity generation increased by 3.5% in 2021 and by 2.5% in 2022 compared to lower level during the pandemic period (2019-2020).

Worldwide electricity demand is developing at a higher rate than renewables, which leads to sharp increase in fossil fuels-base electricity generation. An IEA report stated a 5% increase in electricity need in 2021, half of the increase is met by fossil fuels, particularly coal, which pushes CO_2 2022 emissions in to record levels.

Renewables, on the other hand, are escalating quickly but not enough to fulfill the global demand. The present economic trends and policy settings indicates that the renewables-based electricity generation; including wind, hydropower, and solar PV is on the way to develop intensely worldwide. The increase rate in 2021 was 8%, and it is anticipated to be more than 6% in 2022. Though, renewables are only able to meet 50% of the increase in electricity demand [2].

1.2 Status of Energy Generation in Iraq

Iraq has an oil-dependent economy which lacks other developed divisions. According to the International Monetary Fund, crude oil exports, in 2017, represents about 89% of the whole government revenues. Petroleum industry grabbed the main concern of the Iraqi government which resulted in neglecting the industrial and electrical sectors. Also, electrical sector became extremely reliant on the money gained from exporting oil which is already known to be unstable.

After 2003, the war significantly hindered the electricity generation in Iraq, and citizens suffered from long hours of power outages. Even after the war, the electricity generation continued to struggle for many years which negatively affected the economy. In addition to that, the weak infrastructure, unstable situation, subsidies policies, unreliable grid, mismanagement, and gas flaring, were another factors that effectively contributed to electricity generation issue in Iraq.

The Iraqi grid electricity was not able to meet more than 55% of demand in 2011 [3]. This undependable energy supply led to the extensive use of private diesel generators. Natural gas is an economic option if efficiently used in electricity generation. The amount of gas flared was 9 billion cubic meters in 2010, while in 2018 the production touched 16.8 billion cubic meters [4]. In 2018, the grid maximum supply was projected at 16.4 GW whereas the demand peak was 27.3 GW [4].

In 2018, the total Iraqi energy consumption was 22,552 ktoe [5]. The sector-wise energy consumption was categorized as: transport (50%), the households (24%), industry (19%), and others (7%) (Figure 1-1). Figure 1-2 shows that the energy was mostly made up of fossil fuels. Out of this energy, oil detained a 78%, natural gas formed 21%, while a negligible share of 0.3% was given for renewable energies [5]. The wasteful gas flaring practice is another accountable reason for increasing the natural gas consumption [4].

Figure 1-1 The sector-wise whole energy consumption (in ktoe) in Iraqi between 1990 and 2018 [1]

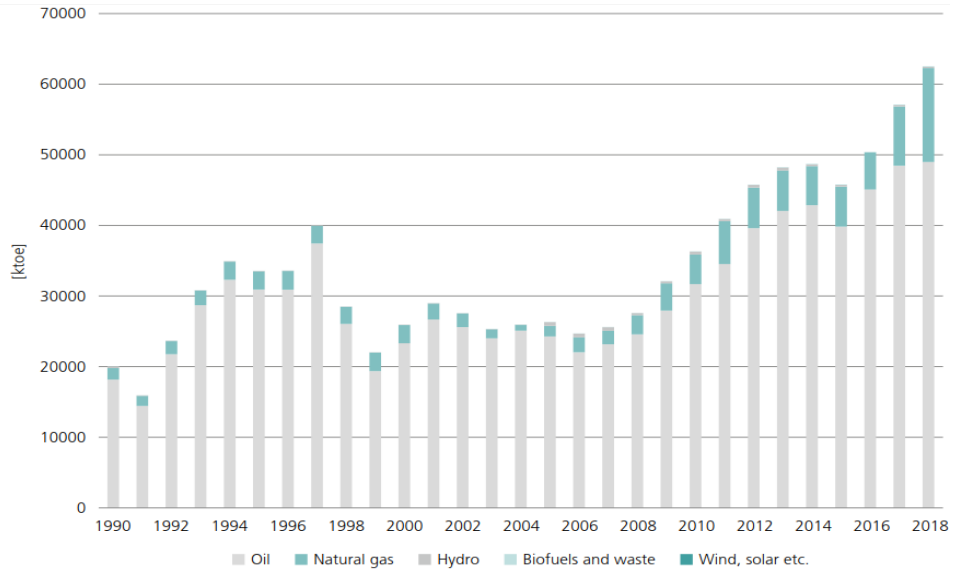

Figure 1-2 The source-wise whole energy supply (in ktoe) in Iraq between 1990 and 2018 [1]

Since 2012 a substantial development has been made in a number of areas. In the oil production sector, a 50% increase was achieved to reach around 5 million barrels per day (mb/d) by the end of 2018. This has propelled Iraq to the rank of the world's third-largest oil exporter. However, this progress has not been even across the whole energy sectors.

1.2.1 Electricity Generation and Demand

Electricity consumption in Iraq has more than doubled since 1990. Figure 1-3 shows that the energy consumption is almost 50 TWh in 2018. It is anticipated that the demand will approach 170 TWh by 2035 [6]. The increase in demand is motivated by economic and population increase reached by the surge in consumer investment and purchases. Moreover, the wide use of an older version of the equipment that consumes high energy in residential uses is another cause for the increased demands. The operational capacity in 2018 was in the range from 14 GW to 15 GW whereas the real existing capacity was 26.2 GW, with a peak demand of 25 GW in summer [7].

Figure 1-3 Electricity Consumption (TWh) in Iraq between 1990–2018 [7]

Due to many reasons including lack of fuel, age of the equipment, need for routine maintenance, and breakdown, the generation units' capacity factor is low in Iraq. Moreover, reduction in water levels in the hydropower stations and dams results in huge unused potential capacity. This is partially due to the Ilisu dam which has been recently built by Turkey, it reduces the available Iraqi share of the water resources [7]. Figure 1-4 shows that oil and natural gas largely control the Iraqi electricity generation sector, and there is sign of an growing trend in generation over the latest years.

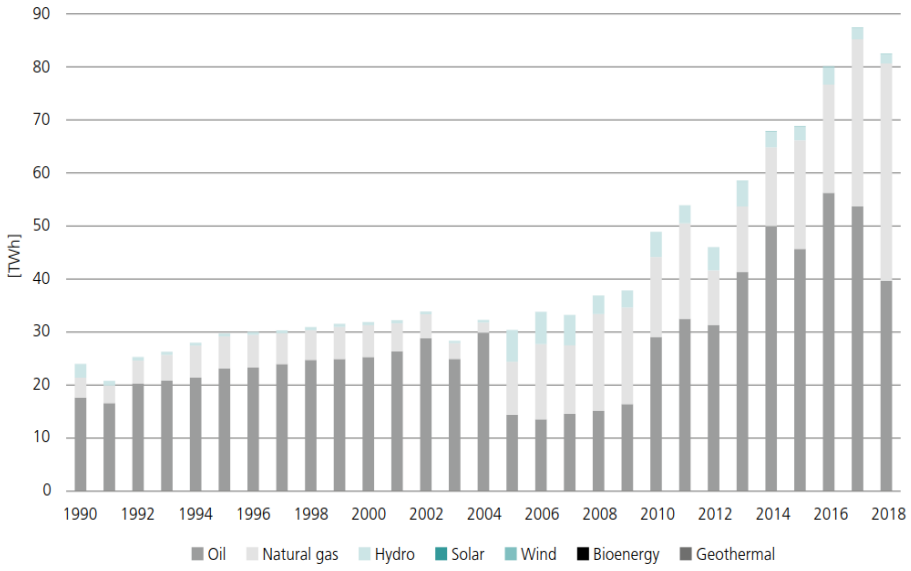

Figure 1-4 Electricity generation in Iraq (in TWh) during the period between 1990–2018 [5]

Despite electricity generation has been increased by approximately 90% between 2012 and 2018, the gap between demand and supply is wider now than in 2012. Chiefly in the summer, power supply is inadequate, and this is a main concern for the people across the country. Oil production in Iraq is expected to develop by 1.2 mb/d in the coming 10 years. This is slower than the 2.4 mb/d increase delivered since 2010, however, it still provide the global market with the third-largest increment of additional oil, after the United States and Brazil (Figure 1-5). When achieved, oil production in 2030 would represent around 6% of the global, up from 5% now.

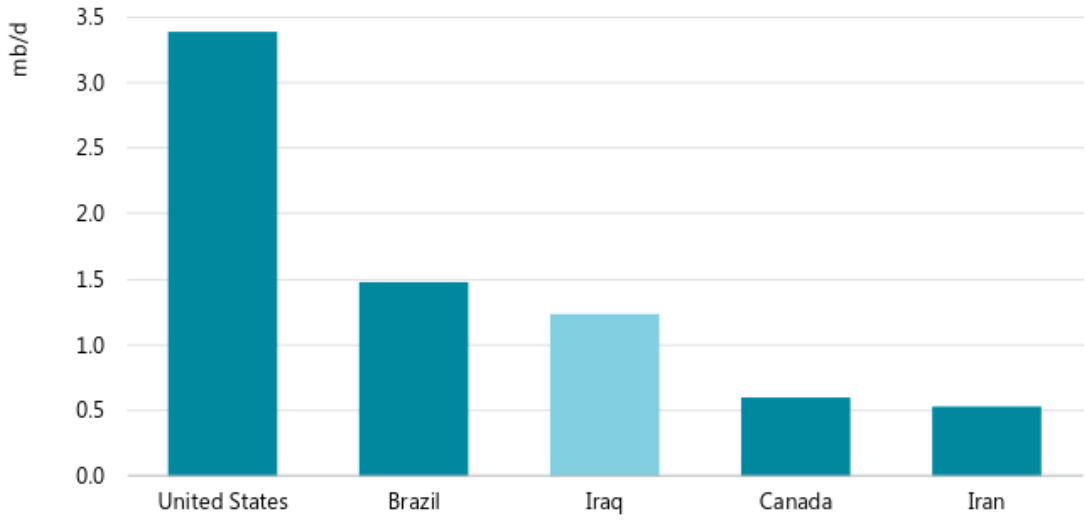

Figure 1-5 Top-five countries by increased oil production during the period between 2018 to 2030 [4]

1.2.2 Electricity Generation Problems

Fossil fuel is the main energy source for Iraq's energy generating systems. At the moment, Iraq is the third major global oil exporter and is anticipated, in the future, to continue as one of the three oil exporters. Between 2012 and 2018, the generation increased by 90%, though, the difference between supply and demand is bigger now than in 2012. Mainly, in the summer months, power supply to meet peak demand is inadequate and this is a major concern for Iraqis across the country.

Iraq suffered severe environmental degradation over the span of few decades. Water scarcity, intensified by increasing domestic demand, bad water management (particularly in agriculture), aged infrastructure, a climate change and the dams construction upstream have become a crucial restriction to economic growth and one of the foremost causes for public unrest recently. Approximately 70% of Iraq's water originates

from neighboring countries. The Ministry of Water Resources reported that Iraq's river levels have dropped by 40% in the last 20 years.

Power sector in Iraq has faced substantial challenges; outages still a daily occurrence for most households. The increased generating capacity was outrun by increasing the electricity demand, particularly by high demand for cooling during summer months. During the past few years, the gap between electricity demand and grid supply has widened, all though available supply was increased by one-third, as shown in Figure 1-6. Investment in developing the infrastructure, especially the distribution networks, has fallen behind what is designed due to the low oil prices. At the moment, tariff collection has not been enough to supplement the capital investment. Therefore, a negative cycle is created where lower revenues causes lower investment, which consequently limits the available supply and revenues.

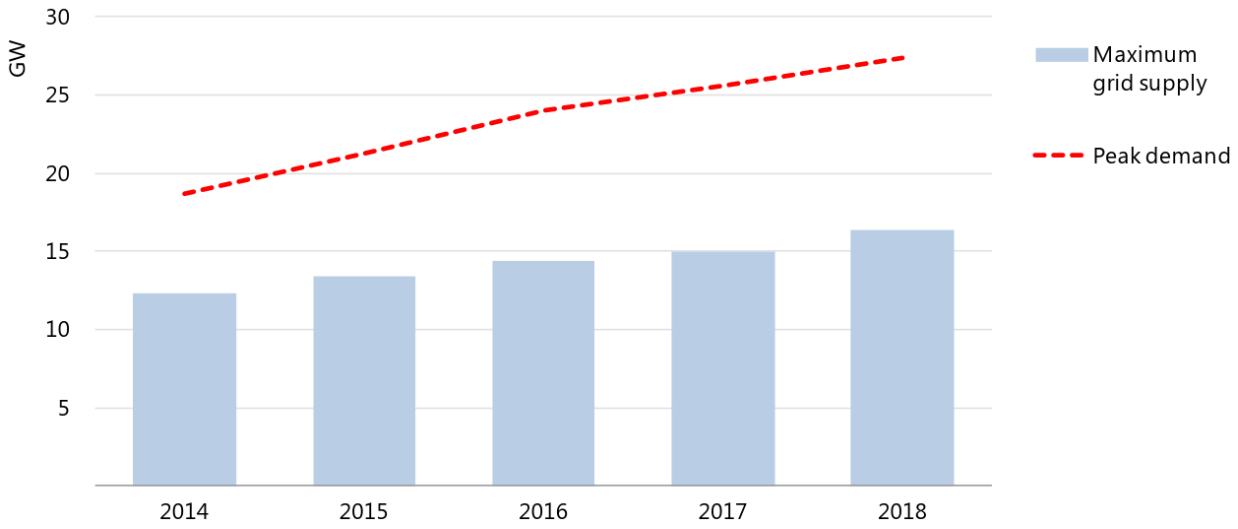

Figure 1-6 Maximum power supply and peak demand during the period between 2014-2018 [4]

Due to population increase the need for energy generation mix is an increased. Though, in the late 18th-century, energy was mainly generated using primary sources such as diesel, petrol, and coal [8]. This has led to increased Greenhouse Gases and diminution of the ozone layer. For this reason, most researchers around the world have considered Renewable Energy sources (REs) as an alternative energy source [9]. The REs are characterized to be reliable, clean, and productive. By using RE sources, the global warming effect can be reduced. Moreover, these REs that accepted around the world.

1.3 Status of Renewable Energy Generation in Iraq

Worldwide, electricity consumption is accompanied by development, urbanization of countries, and economic growth. At the present, around 71.9% of electric power is produced by non-renewable energy sources and 28.1% by renewable sources. Developed countries such as the Russia, China, and USA are taking real practical steps to develop a non-traditional and renewable energy sources every year. According to the IEA, the installed REs' capacity in the world is increased by 200 GW in 2020.

Renewables, including wind power and solar photovoltaic (PV), are progressively attractive options for most power schemes. This is principally accurate in Iraq due to the excellent solar resources. It provides significant RE source to enhance the affordability and reliability of electricity. The dropping costs of renewables provide an opportunity to reduce the electricity supply average cost, and to increase export revenue opportunities. Previous attempts to escalate the solar PV improvement were not very successful; however, they provided good preliminary insight and demonstrated the growing attention in Iraq. Solar PV is already on equal footing with oil-base generated electricity in terms of costs, it and would soon has a promising use if the solar market in Iraq were developed Figure 1-7. For USD 40/barrel oil price, the LCOE of oil-based electricity generation in Iraq ranges between USD 70 and 100/MWh, which indicates that solar PV is basically competitive already [4]. As for the gas-based electricity generation, power plants would be more challenging, even though gas is valued as USD 2 per million British thermal units (MBtu), solar photovoltaic would be capable to compete the gas-based electricity generation cost by 2030.

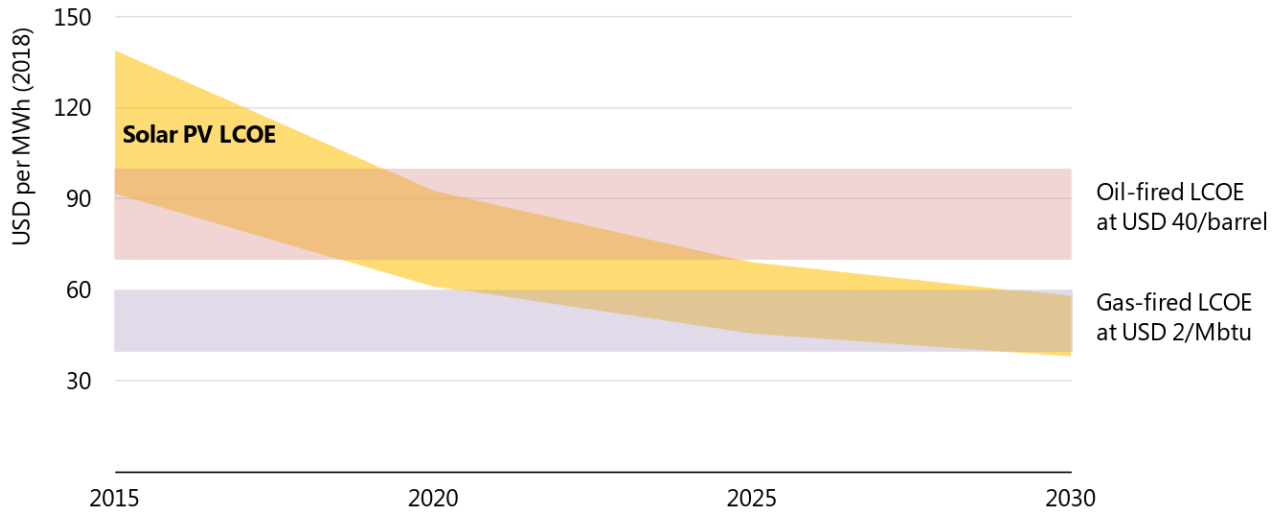

Figure 1-7 Solar photovoltaic levelised costs relative to oil- and gas-based electricity generation in Iraq during the period between 2015-2030 [4]

1.3.1 Wind Energy Potential in Iraq

According to Ersoy [5], the implementation of wind energy systems are limited in Iraq. Generally, Iraq is divided into dissimilar wind zones, as shown in Figure 1-8. The speed in these zones is ranging between 1.0 m/s and 3.5 m/s, with an energy density between 174 and 337 W/m^2. Only a small region of the country, approximately 8%, has a wind speed of approximately 5.0 m/s and energy density of 378 W/m^2 [10].

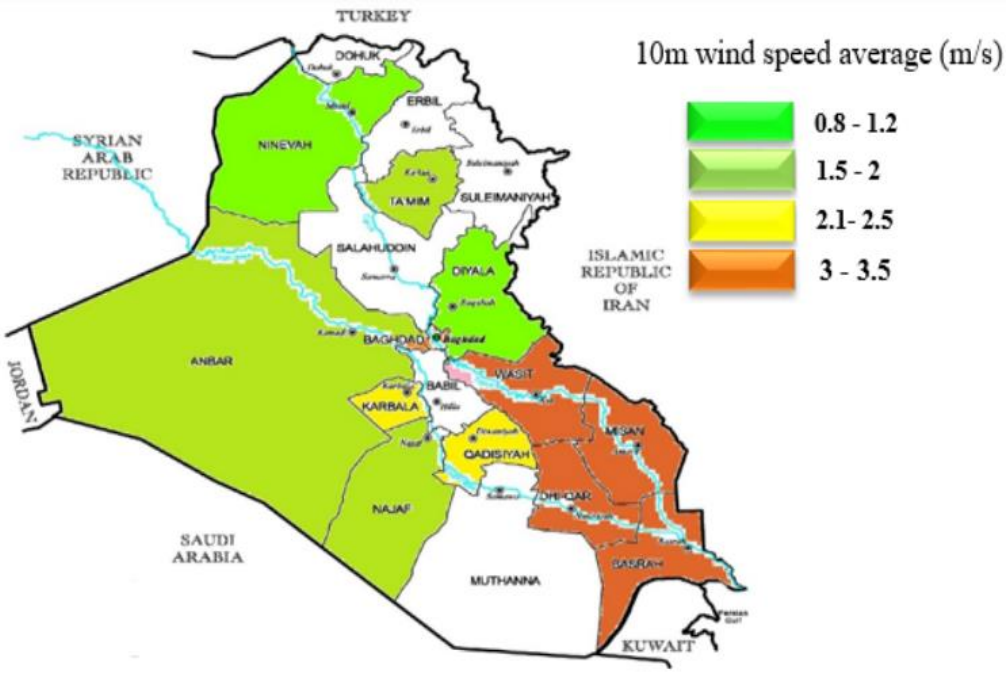

Figure 1-8 Map of wind speed distribution at different stations in Iraq [11]

First wind turbine built in Iraq was in Al-Jadiriyah / Baghdad in 2010, its capacity was 20 kW. Later on, many wind turbines were installed by the Ministry of Science and Technology in different places. Due to weak wind activity and difficulty to connect these turbines to the national network, these attempts did not effectively contributed to the improvement the wind energy sector in Iraq neither economically nor technically [5]. Technical location issues are other challenges that face the wind energy in Iraq. To overcome these challenges, it is essential to find an efficient solution to the low and intermittent wind speeds as well as poor grid infrastructures. Despite these represents critical challenges to overcome, they also offer chances for applying innovative solutions.

According to Darwish, Shaaban [12], the wind energy production in Iraq can be improved if it is used with the solar energy. Studies by [13, 14] assessed the opportunities of wind energy in Iraq, but unfortunately

they were without a comprehensive and strategic direction. To overcome this issue, Darwish, Shaaban [12] tried to develop a strategic implementation direction with a two-fold scientific contribution, practical and theoretical. An inclusive and novel methodology was developed to maximize the wind turbine production in low wind speed condition. The study considered Iraq as a case study where the low wind speed and other data were converted into a software package.

Darwish and Sayigh [15] studied the wind energy in Iraq, and evaluated wind data collected from nine Iraqi sites for a period of 11-years. The study reported availability of four dissimilar wind energy regions in Iraq. One-sixth of Iraq was reported to experience more than 5 m/s annual wind speed. Also, it was reported that wind farms had the possibility to deliver electricity to many locations of the country. Dihrab and Sopian [16] proposed a hybrid scheme, comprising photovoltaic and wind, as a steady and renewable power generation source. The study utilized meteorological data for the considered sites along with turbine sizes, as input parameters, to conduct a simulation and to propose 100 turbines of 10kW each with a photovoltaic area of 400m x 400m, according to the energy resources accessible at the sites. The study reported that at some rural villages, mainly in the southern Basrah province, Iraq can adopt integrated wind and solar energy systems to generate sufficient power. In another attempt to fill the gaps in existing wind speed data, Ali, Mahdi [17] investigated different techniques to determine the best wind speed estimation method for Iraq. A comparison was performed between the data obtained by five methods between 1971 and 2010.

Cost-wise, wind energy is an excellent choice for Iraq [4]. Despite that wind sources are modest in Iraq, modern technologies, such as low wind speed turbines and digitalized farm design are increasing the potential areas for development. To date, the wind energy and solar photovoltaic technologies have not been industrialized In Iraq. To develop these sectors, a cost is incurred. Though, with a Levelized Cost of Energy (LCOE) from USD 60-90/MWh, wind energy may compete the oil-fired generation. It also provides an excellent approach to diversify the power mix by enabling a generation scheme with a higher share of renewables. This would be of great importance for the generation mix, as the solar-dependent power generation is limited to the daylight hours only. Enhancing the wind and solar power generation would also enlarge the available capital for power generation investment which in turn expands the private players in Iraq. To boost and develop the wind energy industry in Iraq, a comprehensive feasibility studies and effective resource assessments are required.

Bashaer, Abdullah [11] built a novel program which was then developed using MATLAB to deeply analyze the wind energy in different locations in Iraq. MATLAB Graphical User Interface (GUI) was

employed to show the facilities of the developed “WIND ENERGY ANALYSIS” program. This program is capable of analyzing wind speed, processing missing data, estimating correlation coefficients, and plotting the analysis results. The program was built base on the Standard Deviation Method and the Energy Pattern Factor. It was used to present comprehensive details about the Weibull distribution parameters to propose an optimal wind turbine for a particular site based on minimum cost per kWh, or maximum generated capacity factor of the system.

1.3.2 Solar Energy Potential in Iraq

According to [5], Iraq gets a solar radiance for more than 3,000 hours per year with an hourly-base intensity fluctuation, between January and June, of 416 W/m^2 and 833 W/m^2 respectively [14]. However, Iraq uses minimal of renewable energy. The country occupies an excellent geographic location that permits it to get a daily global solar irradiance rate on a horizontal surface of about 5-5.6 kWh/m²/day as illustrated in Figure 1-9 [18].

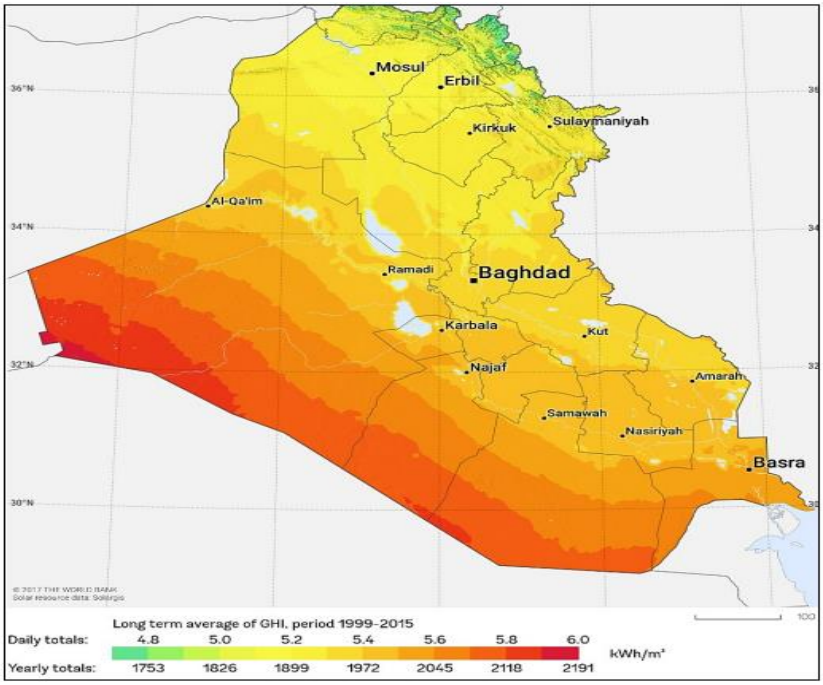

Figure 1-9 Solar GIS map illustrates the horizontal solar radiation in Iraq in kW/m² [18]

Although the government regulatory framework is lacking in Iraqi, the Ministry of Industry in this country has developed a instruction to surge the use of solar energy. According to this regulation, applications, like domestic water heater, drip irrigation, and street lighting systems, will be effectively improved [10]. However, the solar power potential, advantages, and importance are not adequately recognized by the

Iraqi government, which is a restraining factor for the development of this factor [19]. According to literature, no private company in Iraq has invested in renewable energy; moreover all planned projects remain under the government's instruction.

The Iraqi Electricity Law (No. 53 of 2017) expresses its objective of "supporting and encouraging the adoption of renewable energy, its activities and nationalization", however, the law is still in its draft form. On the other hand, the Ministry of Electricity, which is the executive and regulatory authority, has put its target to implement 1,000 MWp of solar energy. As a pilot project, an 8 MWp will be produced from roof fitted solar projects installed on government buildings [20]. Moreover, in 2019 the Iraqi government published a tender for a 755 MWp solar projects as shown in Table 1-1. The projects were planned to be executed under an IPP scheme and it was anticipated to be operational by the end of 2021.

Table 1-1 Iraqi planned large-scale solar power projects [5]

Planned solar power plants							
Project	Sawa-1	Sawa-2	Khidhir	Iskandariya	Jissan	Karbala	Diwania
Province	Muthana	Muthana	Muthana	Babil	Wassit	Karbala	Diwania
Installed Capacity (MWp)	30	50	50	225	50	300	50

The recent decrease in renewable energy technology cost has stimulated private sector to invest in Iraq [21]. Despite that the cost of the preliminary investment in Iraq is approximately 5 to 7 times the other Middle East/North Africa (MENA) countries; ACWA Power has offered to establish a large-scale photovoltaic power plant near to the Saudi border at the south of Iraq [21]. In addition to that, a contract has been signed with Siemens to perform projects under a 14 bn USD roadmap; this includes developing a wind atlas for Iraq [20].

According to Al-Kayiem and Mohammad [10], the hot water flat solar collectors installation by foreign suppliers is in the planning. Further to that, recently smaller companies have begun manufacturing solar cells, and solar photovoltaic is used for streets lighting in numerous cities.

Iraq has many challenges in the power sector; however, no schemes to foster projects for rooftop PV systems have been established yet. Iraqi government has adopted a mechanism to provide loans for citizens, through public and private banks, to procure and install rooftop solar systems. These loans are adequate to fit 3 to 10 kW capacity solar systems for residential applications. For bigger capacity projects above 10 MWp, the government declared bidding rounds after abandoning the feed-in tariff.

In addition to the step taken by the Iraqi government, the technologies of solar energy potential have been considers in a lot of studies conducted by Iraqi researchers. Abbood, Salih [22] proposed management techniques using solar photovoltaic systems for Baghdad city residential sector. Software was developed base on MATLAB, and used to estimate the photovoltaic system design and the solar radiation data. To control peak loads the study proposed a system comprises of 2kWp photovoltaic rooftop solar panels with an area of 10m² and 20% efficiency. Another study by Muslim, Alkhazraji [23] provided an optimization for the energy storage of a photovoltaic system designed to exploit the not beneficiary solar energy and to minimize the electricity peak loads at night. The study proposed six energy storing techniques and implemented them in MATLAB to minimize the losses and optimize the energy usage.

An economic and financial analysis was presented by Muslim, Alkhazraji [24] to assess the possibility of using a 2kWp photovoltaic system with a 500Ah battery system for each residential consumer in Baghdad compared to a 2.5kVA gasoline generator. The study objective was to determine the expected revenue from the considered solar system against the traditional gasoline generator. In another study, Abbood, Salih [25] investigated a 1MW photovoltaic system connected to the grid in Karbala city. The study considered the solar insolation estimations, losses of photovoltaic system, performance and economic calculations for this system, system technical design, and the environmental impact. An algorithm to optimize the solar tilt angle, based on MATLAB software, was proposed by Muslim [26]. The purpose is to maximize the electricity generation, and to calculate the optimum monthly and annually tilt angles for different case studies, including Najaf, California and New Delhi cities.

1.3.3 Biomass Energy Potential in Iraq

Biomass is known to be plant-based material which can be used as a fuel for heating or electricity generation. Biomass may be in the form of agricultural residues, wood residues, wood, and wastes from households, industry, and farms. Fortunately, Iraq is very affluent in biomass; according to Alhassany, Abbas [27] crop leftovers are available in amounts of around 10 million tons per year. These leftovers comprise mainly barley straw, wheat straw, rice straw, and pruning. According to studies, this amount of residues is able to produce 115.13 PJ of potential energy yearly. Moreover, the study estimates 10 million cattle in Iraq, this could produce a 72 million cubic meters of biogas per day, which represents an annual energy potential of 946 TJ. However, the abundant of the gas and oil in this country has negatively affected the potential to make use of the biomass. Biomass has been considered by several Iraqi scholars who tried to utilize bio-methanol and ethanol in mixed internal combustion fuels, like gasoline and diesel. Though, no actual and effective efforts have been presented yet to convert biomass-to-electric power [10].

In this context, Saleh and Chaichan [28] used PRODIT GR306/0001 type internal combustion engine with a single cylinder and variable compression ratio. The investigation was done on gasoline fuel (80 octane), with an equivalence ratio of Ø=1, wide range of air-fuel ratio, and different engine speeds (1500, 1700 and 1900 rpm). Ethanol was added in blends of 10% and 20% to the gasoline, and the engine performance and emissions were evaluated. The study reported that, for gasoline, the Highest Useful Compression Ratio (HUCR) was 8:1. By adding 10% ethanol, the HUCR increases to 9.5:1, which in turn increases the brake power. The brake specific fuel consumption also increases, whereas the CO and the CO_2 emissions reduce.

1.3.4 Hydro Power Plant Potential in Iraq

Iraq has two important rivers, the Tigris and the Euphrates, they represent 98% of Iraq's water, and both are originate in Turkey [29]. They are significant supply for energy generation in Iraq and they play a major role in agriculture irrigation [10].

Presently, hydropower is the a sustainable energy source that has maximum share in ppower generation in Iraq. Figure 1-10 shows that the hydropower source represents 90% of Iraq's renewable power. Though, this sector has met several complications due to conflicts, which damaged the infrastructure and transfer lines.

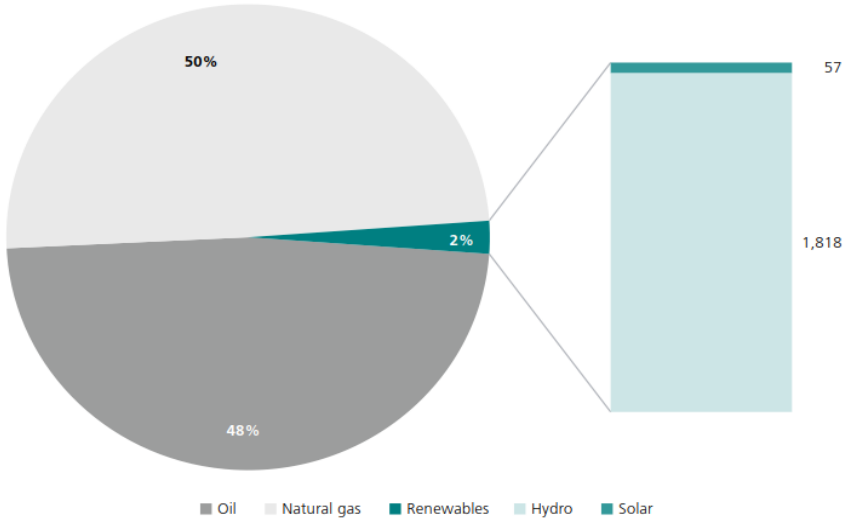

Figure 1-10 The Iraqi electricity generation mix in 2018 (in %, GWh) [5]

Climate change has been confirmed to be vital challenge for the hydropower generation. The capacity of installed hydropower stations in 2012 was 1,864 MW, however, this power potential could not be fully

utilized [10]. Even with the inadequate water resources, the strategy is to upsurge the hydropower to 14 TWh by 2035 [10]. Iraq has the most potential to utilize hydropower energy compared to the Arab countries. The current operational and planned hydropower dams in Iraq are given in Table 1-2.

Table 1-2 Iraqi operational and planned hydropower dams in Iraq [5]

Operational hydropower dams								
Dams	Dokan	Derbedkhan	Mousil	Himreen	Haditha	Samara	A-hidya	Kuffa
Power (MW)	400	240	750	50	660	75	15	5
Planned hydropower dams								
Dams	Bakhma	Taktak	Al-Khazer Comel	Badosh	Al-Baghdadi	Mendawa	Al-Udym	Al-Fatha
Power (MW)	1,500	300	24	171	300	620	27	2,500

After the solid biofuel, hydropower is the most vital renewable energy source in the Arab region with approximately 13% of the overall renewable energy consumption. Four countries, including Egypt, Iraq, Morocco and the Sudan account for almost 90% of the county's hydropower consumption. This indicates a high contribution of the hydropower resources in these countries. Due to the political instability in Iraq the maintenance processes of the hydropower facilities have been significantly hindered, which resulted in increased reliance on natural gas-fired power plants compared to hydropower.

1.4 The Current Iraqi Energy Policy

As a developing country Iraq is required to develop a firm strategy and to establish a long term policy, like other developing countries, for the RE mix. This would contribute efficiently in developing the electricity generating sector, reduce the averment impact, and ensure sustainability with reliable sources at an affordable coast. The government in Iraq has set in the low of electricity in Iraq, No. 53 for 2017. The fifth item of the first chapter of the low state that the Iraqi ministry of electricity "Support and encourage the use of renewable energies in various fields, and localize their industries" [30]. This represents a good step forward to enhance and encourage this technology in Iraq, and it opens the horizon for more successful implementation in the near future.

Recently, thermo electric generation (TEG) technology has emerged and has been employed in many fields depending on the availability of heat sources. Several countries have employed this technology for variety of applications, however, no studies have been found in the literature regarding the implementation of this technology in Iraq.

The TEG application spectrum includes the international space stations, USA, with an output power of 470 W, the Upravlyaemy Sputnik Aktivnyy station, Russia, with an output power of 390 W, the American Gentherm manufactures offshore platforms along pipelines, at altitudes or near gas wells with output power up to 550 watts, and the German car company (BMW) with a output power more 600 W. Also, it was used at homes with low power consumption applications in an independent manner or by integrating it with solar panels.

The ability to recover the wasted heat from the power generation processes and transform it to usable electrical power would massively enhance the power generation efficiency. Moreover, the reduced greenhouse emission that might be achieved by reducing this wastage would be beneficial for the environment due to the less fuel burning required for the same amount of electricity produced. Recently, TEG systems have attracted a considerable consideration in waste energy recovery due to their outstanding advantages [31, 32]. They have many benefits in generating electricity from heat energy; they do not moving parts, which makes its operation less costly [33]. Also, they have no economyscale-of effect, therefore they can be used for micro generation, in a limited space, as well as to generate kilowatts. Additionally, TEGs are environment friendly, and they run with no sound pollution [34]. Contrariwise, TEGs do have limited energy conversion efficiency and need a relatively constant heat source with high temperature difference across it two sides. This has limited their mass implementation in large scale power generating plants which is considered as a drawback in the literature [35]. The aforementioned advantages and drawbacks have attracted the researchers to consider the TEGs from different perspectives. Some of the research efforts were dedicated to implement the TEG in a variety of applications. For example, in waste heat recovery by Luo, Wang [36], in solar energy operation by Jouhara, Żabnieńska-Góra [33], and in thermoelectric generators with a peak efficiency of 9.6% and a system efficiency of 7.4% by Kraemer, Jie [37]. The other research efforts were directed towards overcoming the TEGs' drawbacks and enhancing their performance [38-40]: and to maximize their electrical energy generation [41, 42]. This was deliberated by scholars using either experimental or numerical methods. Experimentally, the researches built variety of TEG system designs, and assessed their productivity and performance in different operating conditions. On the other hand, the numerical approach adopted different modeling techniques to simulate the TEG performance using different software [43-46].

1.5 Conclusion for Chapter One

Despite the aforementioned attempts and inferences done by the researchers, the main TEG systems' challenges represented by their low energy conversion efficiency and the need for constant heat source

still exist. No study to date has provided empirical proof for the TEGs' hypothesized effects to implement them in a large-scale power generation utilities. Issues related to TEG design and applications in practical, powerful, and cost effective power conversion plants have not yet been elucidated. Further, the key questions related to the overcoming the drawbacks of the TEG are not fully addressed yet. Therefore, this study is conducted to provide an attempt to fill the identified gap and expand the knowledge through a series of critical experiments and numerical modeling. As a first step the study explores the direct effects of the TEG designs and operating conditions on their performance and energy conversion efficiency. Then, accordingly, a set of novel TEG designs was proposed and evaluated. The proposed designs involve different systems configurations, improved heating, and improved cooling techniques. Moreover, the electrical connection and the potential TEG hybridization with other energy harvesting systems were examined to explore their influence on the performance. To cut off the experimental investigation cost and to provide efficient parameters examination technique, the study develops a numerical model applicable for wide range of the geometrical configurations and operating conditions.

CHAPTER TWO: EXPERIMENTAL EVALUATION OF DIFFERENT MECHANISM METHODS TO MAXIMIZE THE OUTPUT POWER OF THERMOELECTRIC GENERATORS

2.1 Overview

Different TEG systems modification techniques were designed, built, and examined during the study. They are proposed to improve the performance and to enhance the energy conversion efficiency. The investigation of the designed systems was performed in Baghdad, Iraq (33.3152° N, 44.3661° E), during July 2020. Different TEG panel configurations with various connection methods were evaluated. Diverse heating and cooling techniques were assessed. Further, a solar operated TEG panel system was examined with the presence of a Fresnel lens.

2.2 Experimental Approach

2.2.1 TEG Performance Improvement Designs

Even though the high desirable advantages offered by the TEGs, their performance is nowhere close to other renewable energy harvesting technologies, such as the solar photovoltaic systems. The following review provides a summary survey for the state of the art to improve the productivity of the TEGs and to enhance their performance. This task was deliberated by researches using different strategies; some researchers considered improving the cooling of the TEG, the others adopted different materials to improve the performance such as the phase change materials and nano materials. Other research groups adopted modifying the TEG configuration design or their electrical connection, while others groups integrated the TEG in a hybrid systems with a variety of electricity generating devices.

2.2.1.1 Cooling Improvement Strategies

Alahmer, Khalid [40] proposed several strategies to develop efficient TEG device. The study provided an experimental method to employ the liquid evaporation heat transfer to improve the performance. The thermoelectric performance was investigated under various heat flux values and diverse forms of heat transfer, including free convection, forced convection, free convection with fins, and forced convection with fins. The results revealed that the forced liquid evaporation convection improves TEG voltage variation by 435.9% compared to free convection.

In another study, Mohammadnia, Ziapour [47] provided a self-cooling TEG system using cooling fans that consume a fraction of power generated by the TEGs. The system's design parameters were critically investigated to achieve maximum net power by using the optimum operating conditions of the fans. The study also investigated the effect of electrical input power of the cooling fans on the performance of the self-powered TEG system. The results demonstrated that the potential of using the cooling fans is strongly dependent on the thermal boundary conditions and the electrical load resistance applied on the coupled electric circuit of the TEG. Furthermore, the study reported that a minimum inlet airflow temperature and a minimum external load resistance are required in the proposed system to generate electrical power higher than that without the cooling fans.

Hilmin, Remeli [48] introduced titanium oxide (TiO_2) fluid as a cooling medium to increase the efficiency of a TEG set-up connected to a vehicle exhaust system. This fluid has been proven to have improved heat transfer properties; therefore it is anticipated to improve the cooling of the TEG surface. During the test, the engine was in idling conditions and the speed was varied between 700 and 1500 RPMs. The study reported remarkable enhancement in the TEG's thermal conversion and electrical power output, for various engine speeds, compared to water cooling.

In the same context, Lekbir, Hassani [49] proposed a new design of nanofluid-based photovoltaic (PV)/TEG hybrid system with cooling channel to improve the overall efficiency of hybrid system. The nano fluid performs as a coolant, it absorbs the heat from the TEG module resulting in raising its gradient of temperature, and eventually the overall performance of the system. The performance of the proposed novel design was investigated and compared with the conventional systems. The study revealed that at 35 °C operating temperature, the produced electrical energy by the proposed design is 10%, 47.7% and 49.5% higher than that of the nanofluid-based concentrated photovoltaic/thermal, CPV and CPV/TEG-heat sink systems, respectively.

Selimefendigil and Öztop [50] provided an assessment for a TEG module fitted to two channels where carbon-nanotube/water Nano fluid streams flow. The study provided an investigation for the effect of different combinations of nanoparticle inclusion and flow pulsations. Nanoparticle volume fraction between 0 and 0.04, pulsating flow frequency (Strouhal number between 0.01 and 0.1) and amplitude (between 0.25 and 0.95) on the power generation are examined. Higher power output is achieved when pulsation amplitude and nanoparticle solid volume fraction increase, though higher pulsation frequencies has been found to has inverse effect. At lowest pulsation frequency and highest amplitude a 14.2%

improvement in power is achieved for water compared to steady flow case. Though, the improvement rises to 31% for carbon nanotube nano fluid at the highest solid volume fraction.

2.2.1.2 Using Phase Change Materials

Phase change materials (PCMs) are able to absorb, store and release large amounts of latent heat over a defined temperature range when the material changes phase or state. Recently, they have been considered in solar energy storage applications due to their ability to absorb energy when the phase-changes from solid to liquid, and release energy when the phase changes from liquid to solid. This interesting feature has attracted many researchers to integrate the PCM materials with the TEG system to sustain the energy productivity.

Karthick, Suresh [51] developed a TEG design with a heat sink coupled with a thermal energy storage (TES) unit, as shown in Figure 2-1, for TEG modular solar reversible generation of power. The thermoelectric generation modules are alternatively cooled and heated through open and closed-circuit conditions. The developed design proposed a phase change material (PCM) packed heat sink. It keeps the thermal energy, providing energy generation continuity at night. The results demonstrate that the reversible process of TEG modules is useful for power generation during the day and the night. Also, the study highlighted that, during heating, the average power generated was 0.23, 0.31 and 0.39 W for heat flux of 4.5, 5 and 5.5 kW/m^2 respectively. Whereas in cooling, the average power generated was around 0.31 W.

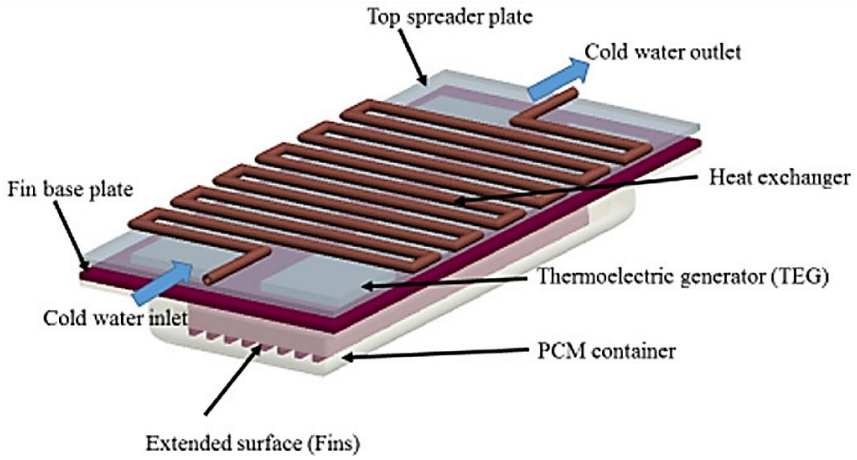

Figure 2-1 A 3-D schematic view of experimental setup for TEG system with cooling arrangement [51]

Borhani, Hosseini [52] examined the performance enhancement of a 5-TEGs by using PCM and porous medium. TEG's both sides were packed with paraffin, RT35 on the cold side and RT69 on the hot-side, as shown in Figure 2-2. Copper porous medium with different porosities and different pores per inches was

added to the PCM to improve its thermal conductivity. In the cold side, the PCM acts as a heat-sink, whereas in hot-side the PCM acts to reduce the output voltage fluctuations. The PCM in the hot-side generates a continuous heat when the heat source cuts-off. The study reported more electrical energy and output voltage when porous media is used on the cold side compared to use it on hot-side, and to PCM without porous medium on both sides. The results also pointed that the performance of the TEG can be improved 5.36% by reducing the porosity.

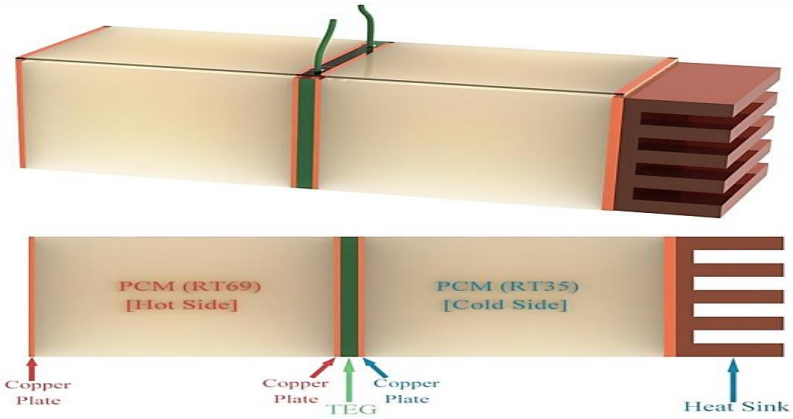

Figure 2-2 schematic of the TEG system with PCM [52]

To maintain electricity generation at night, Naderi, Ziapour [53] improved the photocell efficiency and power generation by integrating it with TEG and PCM. Practically, the proposed method acts to convert the heat energy into electricity energy using a thermoelectric generator, instead of dissipating it. The performance of the proposed system was compared to a solo photovoltaic system in terms of solar cell efficiency, temperature, and output power. The study findings demonstrated that, in the proposed system, the temperature of the cell was reduced from 74.43 ℃ - 53.72 ℃. Further, the electricity output and the solar cell efficiency were increased by 100% and 1.38%, respectively. Though, during night, the system's output power is low. The study also considered the wind velocity, packing factor, and the number of thermoelectric generators to optimize the system efficiency. The results showed that at packing factor of β_{sc}=0.4 and β_{sc}=0.93, the thermoelectric generator efficiency was 4.32% to 0.61% less, respectively. and the efficiencies of solar cell were 15.88%, 16.2% and 16.42% at average wind velocities of 1(m/s), 2(m/s) and 3(m/s), respectively.

Huang, Yan [54] integrated the PCM with TEG to improve the transient performance and total efficiency in an automotive related application. This was done by reducing the exhaust gas temperature fluctuations, and thereby improving the efficiency under various driving conditions. The Pentaerythritol (PE) PCM was selected based on the thermal properties of the exhaust gases. It has low rate of volume change during the

phase transition, and its phase transition is more compatible with the automotive exhaust temperature range. The results revealed that the improvement of open circuit voltage and power output are 0.7% and 1.16%, respectively.

Wang, Peng [55] tried to improve the TTEG system performance by adopting the PCM and heat transfer enhancement to establish improved thermal conditions. The study provided an experimental investigation for the effects of the PCM and the heat transfer enhancement on the open-circuit voltage and the electrical energy. Results indicated that the temperature, thickness and thermal conductivity of the PCM are of great impact on the electrical energy generated. The results also indicate that suitable PCM and heat transfer enhancement measures should be considered according to the TEG's working conditions.

2.2.1.3 Modifying the TEG Configuration

Wang, Liu [56] designed a power generator (Figure 2-3) made of four TEGs arranged in a half-ring form. The design utilized a polymer-based composite materials and used on hot water pipes to recover the waste heat. The experimental work succeeded in producing a 3.4 mV output voltage and 126 nW output power using a temperature difference of 10.5 K. Another study by Susanto, Salim [57] proposed parallel and series connected TEG modules to exploit a rocket stove heat. The heat is collected by water flow in a copper pipe wrapped around the stove, where water temperature reaches 90ºC. A resistor of 1kΩ - 10kΩ was used to test the power produced by the proposed TEG. Highest efficiency of 5.38% was obtained at the 5kΩ.

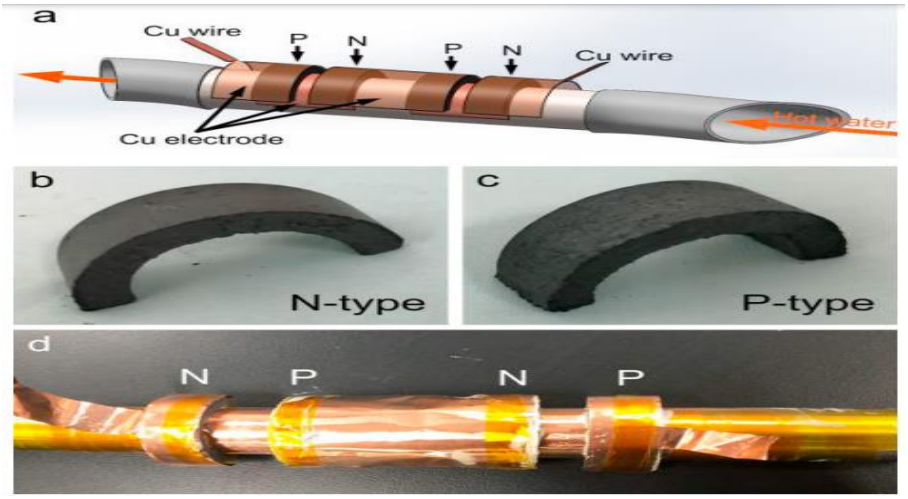

Figure 2-3 (a) Schematic of the TEG on a hot water pipe. (b) and (c) are the photographs of n and p-type half rings synthesized by compression molding, respectively. (d) Photograph of the TEG on a stainless steel pipe [56].

Qasim, Velkin [41] developed and evaluated the performance of a new TEG panel for converting the solar radiation into electricity. The TEG panel was made of many TEG modules, and was exposed to solar radiation using a Fresnel lens. The other side of the TEG modules is cooled with water at ambient temperature. To achieve an active cooling, the water passes through an aluminum heat exchanger. The study reported maximum open-circuit output voltages of 9.35 V and 11.75 V for the TEG panel with and without the Fresnel lens, respectively. These voltages where obtained in Iraq during July at 14:00 h local time.

Hoang, Nguyen [58] investigated the generation characteristics including voltage and power output, and conversion efficiency of a TEG with added fishbone-fins to enhance heat exchange. Also, the effect of cooling water mass flow rate (MFR) on the power generation characteristics was analyzed for hot inlet air temperatures between 200–500°C. The results showed that the fishbone-shaped fins improve the output voltage and power by 31.37 V and 16.49 W, respectively. In the same way, the conversion efficiency was increased 2.93% due to the use of the fishbone-shaped fins compared to conventional one. Moreover, the cooling water outlet temperature was measured to evaluate the fishbone-shaped fins effect on the flux transferred from hot side to cold side of the TEG.

Garmejani and Hossainpour [59] considered a TEG system equipped with hot and cold heat-exchangers and optimized the performance using automobile exhaust. The study analyzed the system to calculate the objective functions including power output, second law efficiency, investment and a compound function which is a sum of power, second law efficiency and the investment. The heat exchangers' hydraulic diameter and the mass flow rate of the hot fluids are considered as input variables. A MATLAB code was used to conduct a multi-objective optimization for co-flow and counter-flow system. The results revealed that the efficiency of 6.56% with the power of 118.72 W can be achieved using the optimization method. The study concluded that, by reducing the power output by 9.58% a 44.81% enhancement in the second law efficiency, and a 37.31% reduction in the investment are achieved.

Karana and Sahoo [60] provided an attempt to design and develop a modified annular TEG (MATEG) design which has a heat transfer along its longitudinal direction. This design has a good potential application in fluid-carrying bend pipes. It is also applicable for round-shaped heat sinks and source, where the performance suffers due to the mismatch of geometries. A steady-state theoretical approach was developed to predict the proposed system performance using parallel flow and counterflow cooling configurations. The study provided an investigation for a number of the effective parameters. This includes the TEG geometric dimensions, number of the modules, length of the module, angle ratio, total

angle, and of the height of junction. The study reported that the maximum power is obtained with five numbers of the module. Further, by increasing the length of TEG module, the power density decreases with slight fluctuation in the conversion efficiency.

Zarifi and Moghaddam [61] proposed a novel laboratory TEG design, shown in Figure 2-4, based on combined heat and power (CHP) model to maximize the energy output level by a compensating method. The study employed an economizer section where the temperature gradient for the TEGs can rise. By introducing the economizer, the wasted heat from the TEGs can be significantly compensated in the economizer part. To assess the functionality of the proposed design, the research group investigated the performance of developed design in two different modes, with and without the economizer. The results confirmed that the efficiency of the suggested TEG system was enhanced by up to 90% when the economizer is used.

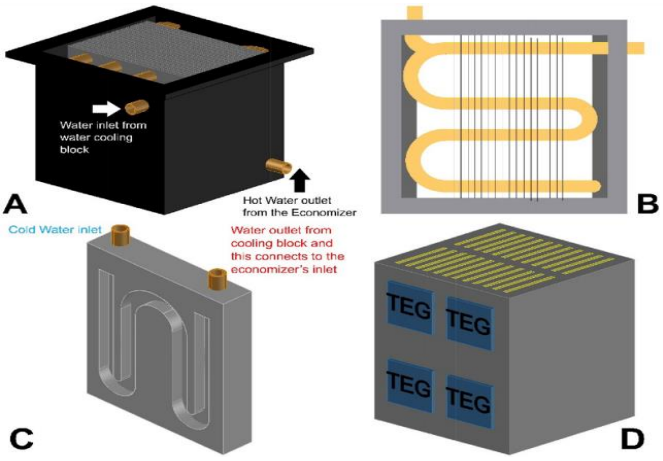

Figure 2-4 Finned tube economizer (A and B)-water cooling block (C) and hot sink (heat sink) comprised of four TEGs (D) [61]

2.2.2 Hybrid TEG System Designs

One the most motivating study field in renewable energy is the progress in energy harvesting techniques which are used to produce electricity from solar irradiance. One of these technologies is the PV-TEG hybrid scheme which is gaining growing interest [62]. Since TEG generators electricity, it acts to raise the electrical performance when integrated with PV in the hybrid PV-TEG system. This can result in approximately 10% more produced energy than a single PV solar cell, however, this depends on TEG's material, geometry, and connections [63].

Hybrid PV-TEG systems are designed by two methods, the first is called spectral splitting method where energy below 2,500 nm cut-off wavelength is transmitted to the PV while the higher wavelength is transmitted to the TEG. The second is known as direct method, where the TEG is directly connected to the back of the PV. The TEG uses the extra heat produced by the PV to generate extra energy. To determine the hybrid PV-TEG system optimum operating condition, several studies have considered the effects of various operating parameters. The investigated parameters included the cooling system [64], system structure [65], and the contact thermal resistance [66]. However, most of the researchers focused on the solar irradiance effect on the PV-TEG system's performance.

Yin, Li [67] experimentally optimized the concentrating photovoltaic thermoelectric hybrid CPV-TE system's (Figure 2-5) operating conditions taking into consideration the connection modes, system structure, coupling characteristics of the devices, and total input energy. The study evaluated the hybrid PV-TEG at different concentration ratios to determine the influence of the optical concentration ratio on the efficiency of the system. Also, to evaluate the performance features and the output voltage effect of the photovoltaic system, the TEG load resistance influence on the power output was examined. The influences of structural design and thermal resistance on the PV-TEG system's efficiency were also analyzed. The study also provided an investigation for the series and parallel connections of the TEG modules. The results revealed a 28.9°C temperature difference through the TEG when the optical concentration was changed from 74 W/m^2 to 217 W/m^2, specifying a considerable improvement in the TEG efficiency.

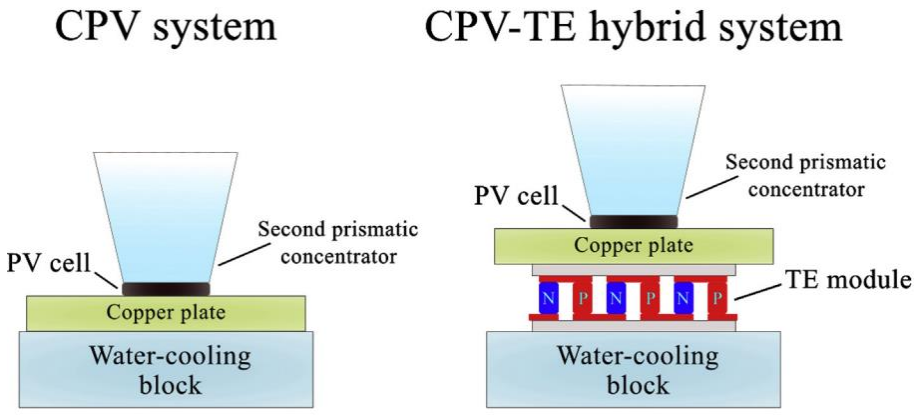

Figure 2-5 Schematic diagrams of the CPV system and the CPV-TE hybrid system

Riahi, Ali [68] investigated a concentrated photovoltaic thermal (CPVT) and concentrated photovoltaic thermal thermoelectric (CPVT-TE) hybrid solar systems. The results showed that the output electric power of the CPVT-TE is greater than that of the CPVT. Also, an improvement in the electrical efficiency

can be achieved through the integration of the thermoelectric generators. The study reported a 7.46% improvement in the daily electrical efficiency of the CPVT-TE system, in a sunny day with 935 W/m^2 radiation level and 33 °C ambient temperature, compared to the CPVT system.

Wu, Zhang [69] studied the load and the main geometric parameters of an alkali metal thermal electric converter AMTEC/TEG hybrid system. The study provided an evaluation for the evaporation temperature and condensation temperatures of the AMYEC and the operating temperature of the TEG. A considerably effect for the electrode current density on the AMYEC and TEG systems was reported in the study. Also, the results show that the AMTEC and AMTEC/TEG systems' maximum conversion efficiency was 27.42% and 31.33%, respectively. Interestingly, the optimal thermoelectric module area to electrode area was reported as 0.2 regardless the ratio of evaporator heat transfer area to electrode area. Additionally, the study concluded that the thermoelectric arms' length and the ratio of thermoelectric couple area to the total area of the thermoelectric module should be $\leq$ 11 mm and $\geq$ 0.55, respectively, to obtain a compact and low-cost system.

Wu, Zhang [70] incorporated a thermionic converter (TIC) and an AMTEC to the TEG to develop a novel thermoelectric TIC/AMTEC/TEG hybrid system driven by a concentrated solar radiation (Figure 2-6). The study considered the effect of a set of load and geometrical parameters on the conversion efficiency of the developed hybrid system (η_{ALL}). These parameters include the TIC output voltage (V_1), the AMTEC electrode current density (J_2), the TEG dimensionless current (i), and dimensionless geometric parameters (the ratio of total electrode area of AMTEC subsystem to emitter area of TIC subsystem (r), the ratio of TEG subsystem area to total electrode area of AMTEC subsystem (c)). Furthermore, comparisons with two-stage hybrid systems were presented to evaluate the contribution of the developed hybrid system. The study highlighted that booth of V_1 and i have a positive effect on η_{ALL}. Also, the η_{ALL} increases first and then decreases under the influence of J_2 and r, and low c can achieve better η_{ALL}.

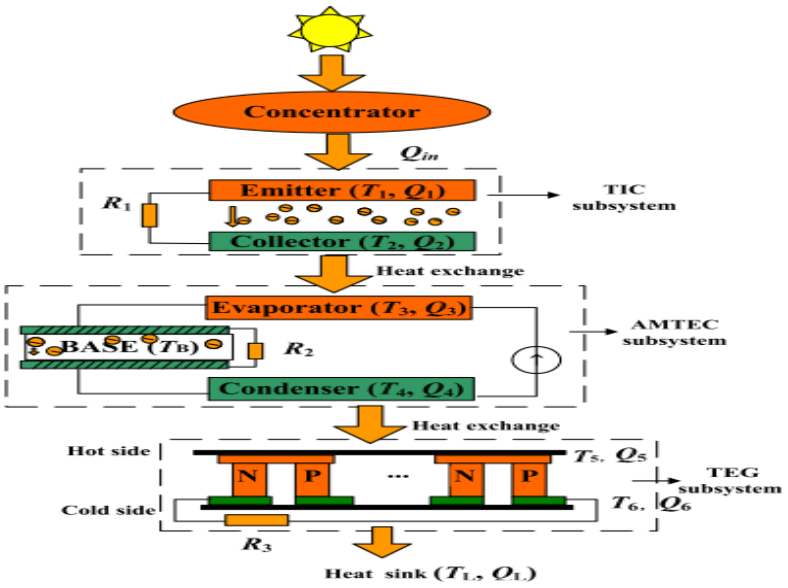

Figure 2-6 The schematic diagram of the concentrated solar-driven TIC/AMTEC/TEG hybrid system [70]

Al-Widyan and Al-Oweiti [71] examined a hybrid TEG/thermal radiator unit to generate electricity while heating a cold space. The TEGs were fitted on the two sides of the aluminum sheet of the radiator to exploit the temperature difference between the hot water inside the radiator and the surrounding air. An assessment for the system's performance was performed, under free and forced convection conditions, based on the TEG's parameters, temperature, and velocity of the hot water and air. The results revealed that the ambient air velocity is the most effective parameter on the generated power with an optimum value of 0.5 m/s. Furthermore, the generated power decreases 15.39 % for 5 K increase in ambient temperature. Though, it increases 24.6 % when the hot water temperature increases by 5 K.

2.3 Experimental Setup

2.3.1 Principle and Mechanism of the TEG Module

Typically, a thermoelectric power generation module contains up to 100 TEG elements. These TEGs comprise *p*-type and *n*-type semiconductors [72]. They consist of components involve big concentrations of positive and negative charges in p-type and n-type junctions respectively. A large amount of the positive charges or holes are doped into the p-type material, which results in a positive Seebeck coefficient [35]. The negative Seebeck coefficient, on the other hand, is achieved when an n-type material is doped with a large concentration of negative charges or electrons. Figure 2-7 demonstrates a schematic of a TEG module.

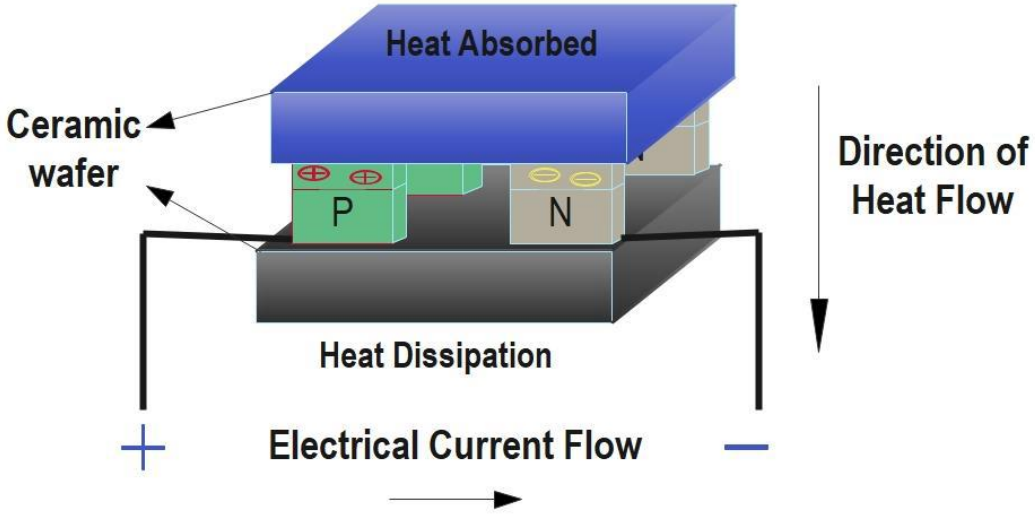

Figure 2-7 Schematic depiction of a TEG module

Seebeck effect is the basic working principle of the thermoelectric generator module. When the TEG module is exposed to heat, charge carriers off the semiconductor material. Normally, they are holes in p-type and electrons in n-type semiconductors. They diffuse from high temperature area (T_h) to a lower temperature (T_c) area. Hence, it is essential to have a temperature gradient between the two sides of the TEG module in order to get the electrical charge. When the diffusion process take place, an electrical current is induced, this accordingly leads to voltage potential build up at the TEG module's terminals. Because of these characteristics, different TEG module applications and configurations are exist [73]. A suitable ΔT enables heat transfer and subsequent electron flow from the n-type to the p-type semiconductors and the generated voltage is as follows:

$$V_{oc} = \alpha \times \Delta T \qquad 2.1$$

$$\Delta T = T_h - T_c \qquad 2.2$$

$$\alpha = (\alpha_p - \alpha_n) \qquad 2.3$$

here V_{oc} represents the open circuit voltage, α denotes the coefficient of Seebeck effect (V/K), α_n and α_p are the Seebeck coefficients of the *n*-type and the *p*-type TE legs, respectively.

$$\alpha = \Delta v / \Delta T \qquad 2.4$$

where, Δv , ΔT are the voltage and temperature change, respectively.

The TEG electrical power across the externally connected load produced a current flow in the circuit, which can be designed using the power balancing formulas given below [74].

$$W = Q_h - Q_c = V.I \quad 2.5$$

here, Q_h , Q_c denote the absorbed and dissipated heat rate at the hot and cold junctions of a TEG module respectively. they are determined by

$$Q_h = \left(K_p - K_n\right)(T_h - T_c) + \left(\alpha_p - \alpha_n\right)IT_h - \frac{I^2R}{2} \quad 2.6$$

$$Q_c = \left(K_p - K_n\right)(T_h - T_c) + \left(\alpha_p - \alpha_n\right)IT_c + \frac{I^2R}{2} \quad 2.7$$

where K_p represents the thermal conductivity of the *p*-type, and k_n is the thermal conductivity of the *n*-type TEG legs. Also, T_h and T_c denote the temperatures of the hot and the cold junctions, while *R* and *I* are the electrical resistance and current, respectively.

When Equations 2.6 and 2.7 are rearranged and simplified we get:

$$V = \left(\alpha_p - \alpha_n\right)(T_h - T_c) - IR \quad 2.8$$

2.3.2 Solar TEG System Panel

To develop a solar operated TEG panel with a maximum output voltage, the study proposed a TEG panel that collects the heat from the solar energy while the low temperature sink is cooled with a normal tap water. Table 2-1 below lists the technical specifications of a used TEG module, and Figure 2-8 shows it configuration. This module is manufactured specifically for power generation; it can also be used for cooling and/or heating applications. However, it is far superior compared to the standard peltiers for power generation applications.

Table 2-1 Technical properties of a single TEG module (SP1848-27145)

Properties	Value
Material	Ceramic/bismuth telluride
Model	SP1848-27145
Temperature	150^{o}C
Open-circuit voltage at temperature difference 20, 40, 60, and 80^{o}C	0.97, 1.8, 2.4, 3.6, and 4.8 V
Current at temperature difference 20, 40, 60, and 80^{o}C	225, 368, 469, 558, and 669 MA

Color	White
Weight	25 g
Size (Length × Width × Height)	(4 × 4 × 0.4) cm

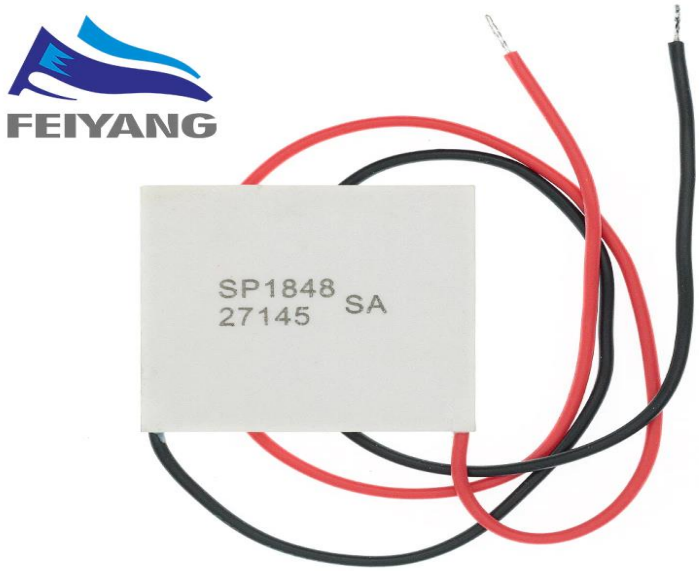

Figure 2-8 The TEG module (SP1848-27145)

The panel consists of 150 TEG modules arranged in a 15 × 10 array; it has a group of 10-TEG modules connected in series, and 15 lines connected in parallel, as shown in Figure 2-9.

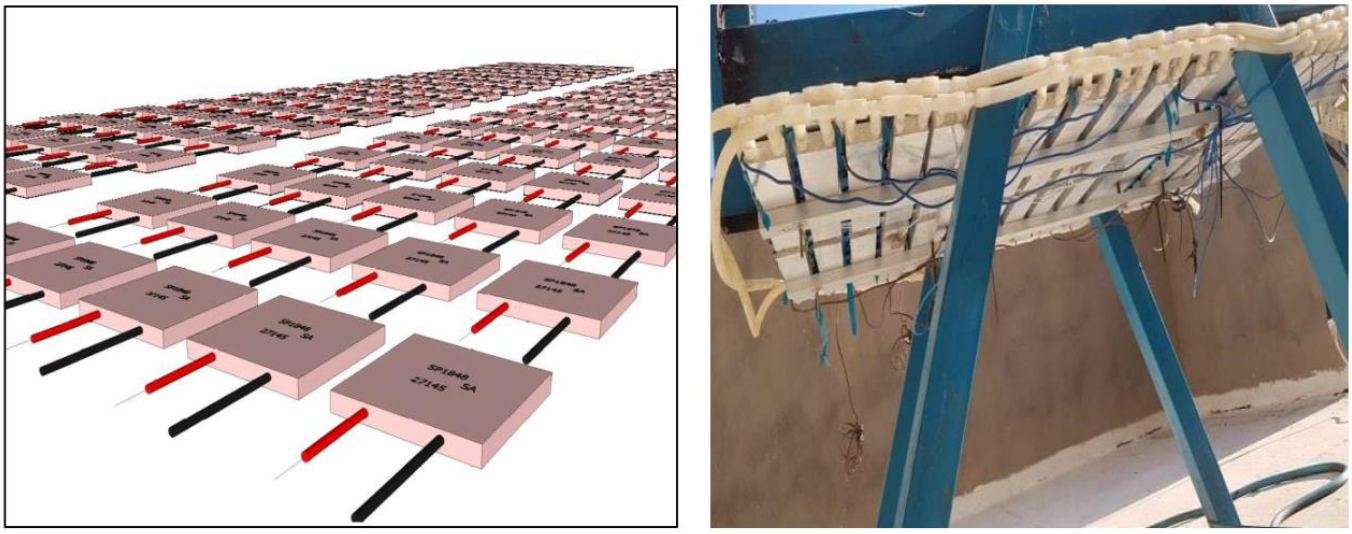

(a) (b)

Figure 2-9 TEG modules (a) the series and parallel connection (b) The integration of the TEG modules into the system.

The panel is positioned on a flat table; and a 4 mm thick glass sheet was placed at a distance of 5 mm above the TEG hot surface. The glass cover helps to upsurge the heat transfer on the hot surface

particularly when it is exposed to the solar radiation. Also, to guarantee a uniform temperature distribution among the TEG modules and to increase the solar radiation heat storage, a 16 mm thick black aluminum plate was fitted to the hot side of the TEG panel. To ensure sufficient cooling for the other side of the TEG modules 30 heat exchangers were fitted to the modules and were supplied with tap water at a flow velocity of 0.8 m/s. The properties of the each heat exchanger were ClYXGS Aluminum blocks, cooled with water, and has dimensions of 40 × 240 × 10 mm [75]. Figure 2-10 shows the configuration, internal design, and the connection ports of the used aluminum block.

Figure 2-10 The configuration, internal design, and the connections of the water cooled ClYXGS aluminum block

Water cools each heat exchanger to guarantee an excellent temperature distribution on the TEG panel low temperature side. Several temperature sensors were fitted on each sides of the TEG panel. Figure 2-11 shows a schematic cross-section of the designed TEG panel.

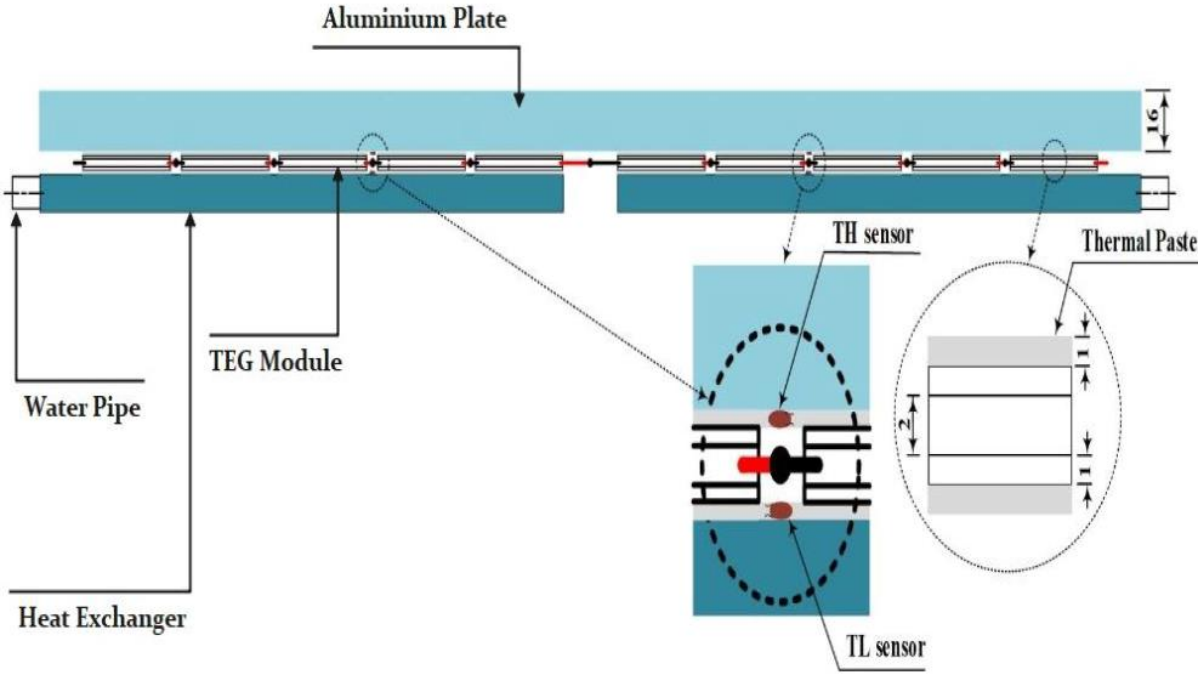

Figure 2-11 A schematic shows the cross section of the TEG panel.

The coolant that was employed in this study retained its low temperature, and it did not leak from the system. A thermal paste was used to do the installation to guarantee excellent contact between the cooling block and the TEG modules. The thermal paste is a high thermal conductivity soft silica gel 200*400*0.3/1.2/1.5/2.5/5/6mm Gray and white heat sink 1.5w/m.k GPU CPU silicone pad. STARS-922 5g heat sink plaster strong viscous thermal silica gel. The application of sufficient thermal paste was very important, and it must be used carefully to maximize the contact surface area between the ends of the Peltiers on the back of the panel. Thermocouples (heat sensors) were fitted at different locations on the panel to monitor the temperature distribution on the panel. Signals from these sensors were sent to a custom designed Arduino Mega.

To achieve maximum voltage out of the TEG panel, two distinct methods were adopted. The first involves using a Fresnel lens to focus the solar radiation on the TEG panel. In the second method, the solar radiation is directly applied to the TEG modules with no lens. Similar conditions and at same solar irradiance intensity were applied when operating the two TEG panels during the experiment. The experiment was performed and a comparison was done between the proposed designs of a TEG panel system. The first system was integrated with a Fresnel lens (L-TEG panel), while the second is without Fresnel lens (NL-TEG panel).

In most previous studies, the researchers adopted a single TEG module or set of modules at various high temperatures. In this current study, a TEG module at lower temperatures was used. The voltage and current were both manually and automatically measured using instruments and a microcontroller, respectively.

2.3.2.1 TEG Panel Subjected to Solar Radiation through a Fresnel Lens (L-TEG Panel)

In this system, the suggested approach is novel and simple. A Fresnel lens is used in the L-TEG panel system, while in the NL-TEG no lens is employed. A major problem was to provide adequate heat transfer by improving contact with heat and cold sources. This was done using thermal paste in the form of strips placed on both ends of the Peltiers, which minimize the replacement and maintenance costs. Generally, two types of Fresnel lenses are used in solar-related applications. First is a spot Fresnel lens, it focuses light into a single point on a required area. The second is a linear lens, it focuses solar light into a line on a particular plane [76, 77]. In this study the spot Fresnel lens was used as shown in Figure 2-12.

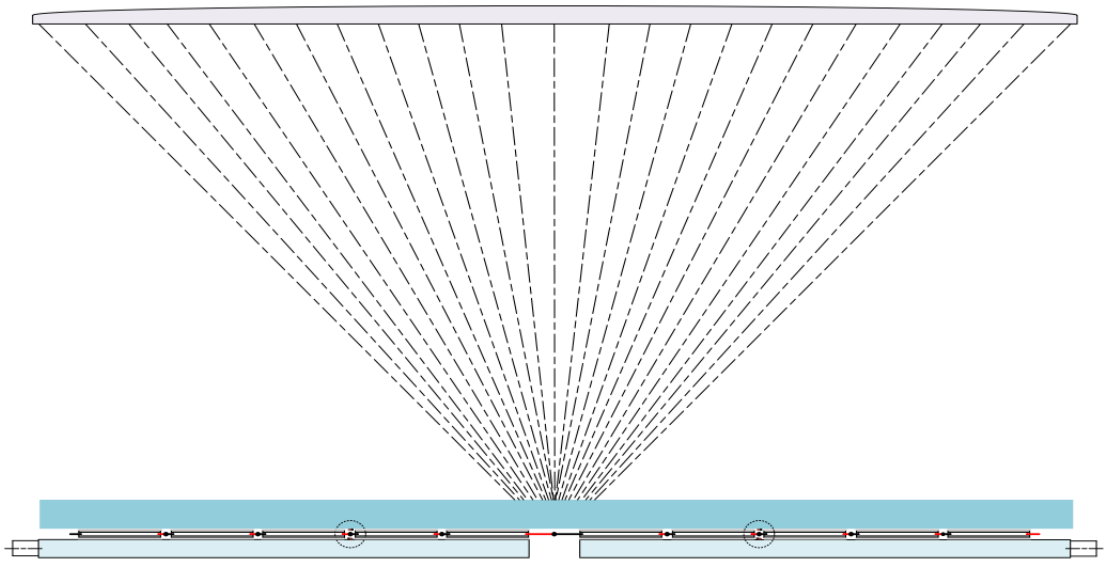

Figure 2-12 A side view of the adopted arrangement of Fresnel lens and the TEG panel system

The TEG panel was placed beneath the lens at a distance equal to the focal length of the lens which is protected by a metal frame. The lens has dimensions of 1100 × 1100 mm. During the experiment the lens focused solar light into a single spot. The glass cover and the aluminum plate ensure an approximately equal and uniform heat energy distribution on the TEG panel hot side. The entire system design and arrangement during the experimental test is shown in Figure 2-13.

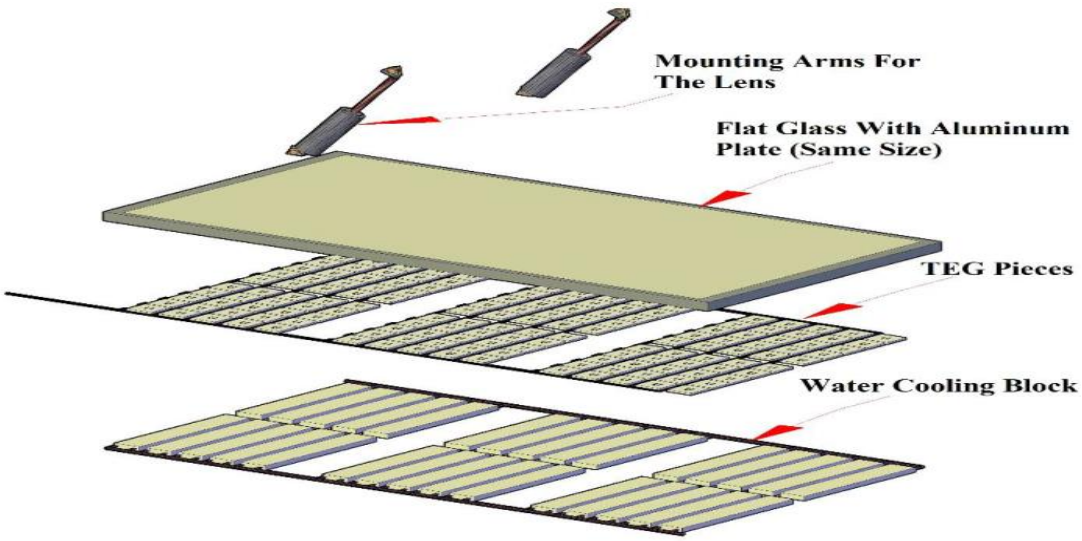

(a)

(**b**)

Figure 2-13 (a) the TEG system schematic diagram, (b) the exposure of the TEG panel to solar radiation via Frensel lens

The focal length of the TEG panel-lens system was adjusted using a linear DC motor. An Arduino Mega microcontroller was employed to control the system tilt angle via a driver circuit, as shown in Figure 2-14 below. The Arduino Mega data logger system collects the data from a set of thermocouples, logged measurements were presented on a serial monitor, and they were saved in a text file. The controller, also, collects data from a photo sensor fixed on the lens's steel frame, and accordingly adjusts the focal length of the lens and the tilt angle of the TEG panel.

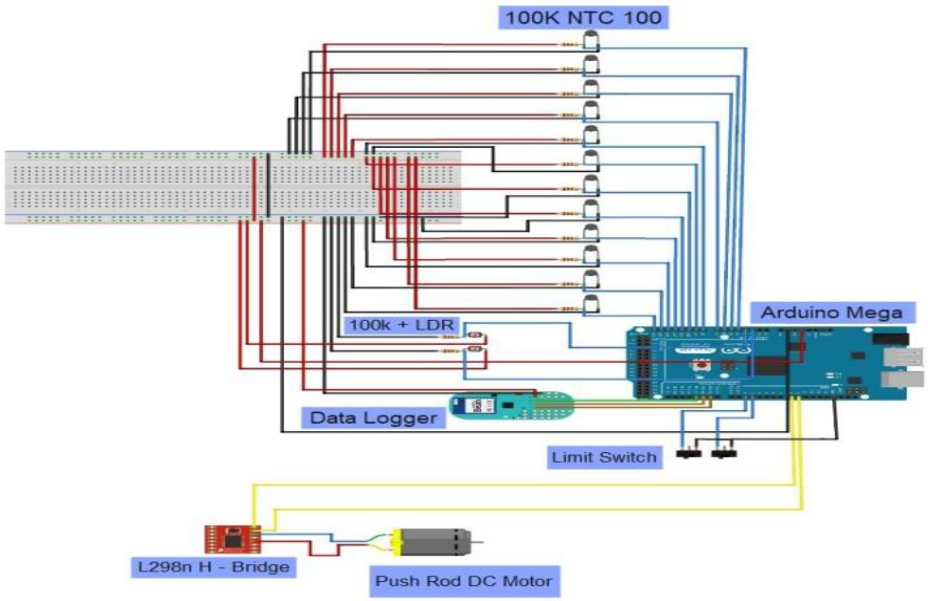

Figure 2-14 A schematic diagram illustrate the temperature measuring system including the data logger and Arduino Mega.

2.3.2.2 TEG Panel Subjected to Direct Solar Radiation without Lens (NL-TEG Panel)

The NL-TEG Panel was direct exposed to solar radiation, as illustrated in Figure 2-15. Temperature reading data was logged using temperature sensors connected to an Arduino Mega. The TEG panel was oriented for collection of maximal solar radiation during the day. Its panel was aligned using a magnetic compass, compensating for magnetic variation [78]. In the northern hemisphere at latitudes greater than 23.5◦, the solar collecting system should be oriented to face south. The current study was done at approximately 33◦ north latitude. To gain maximum solar radiation, the no lens TEG panel must directed toward the geographic South Pole [79].

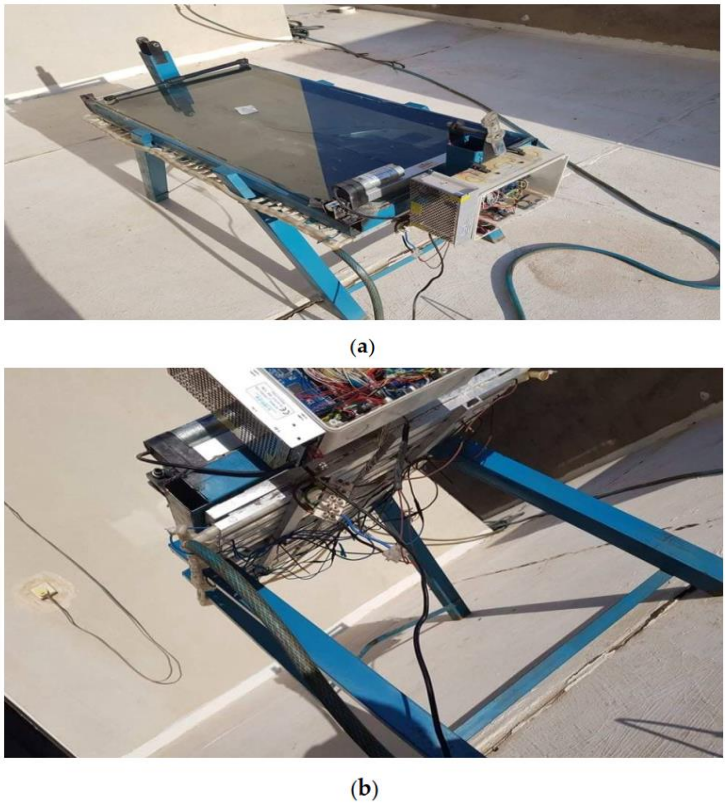

(a)

(b)

Figure 2-15 (a) top view, and (b) side view of the no Fresnel lens TEG panel exposed to solar radiation

2.3.2.3 Analysis of Measurement Errors

In this part a brief discussion for the effects of measurement errors, during the experiments, is provided. This comprises the measurement devices error rate in addition to the errors of the microcontroller (Arduino) and sensors. A range of parameters were measured to determine the uncertainty related to the used instruments in the experiments. Table 2-2 depicts the various used instruments accuracies, this includes the ambient temperature measuring recorder, the digital clamp meter, the humidity meter, the TES 132 solar power meter, the Handheld Pro HVAC CFM anemometer, and the NTC single-end glass

seal thermistor temperature sensor. To evaluate the standard uncertainty (u_n), Equation 2.9 is used [80, 81].

$$u_n = \frac{a_n}{\sqrt{3}} \qquad 2.9$$

here the instrument accuracy, as given by the manufacturer, is indicated as a_n. Equation 2.10 is used to determine the uncertainty of *z*, where *z* is a several inputs dependent [81].

$$u(z) = \sqrt{\left(\frac{\delta z}{\delta y_1}\right)^2 u^2(w_1) + \left(\frac{\delta z}{\delta y_2}\right)^2 u^2(w_2) + \cdots + \left(\frac{\delta z}{\delta y_n}\right)^2 u^2(w_n)} \qquad 2.10$$

where potential errors are given as $\Delta y_1, \Delta y_2, \ldots \ldots \Delta y_n$. The total uncertainty percentage of the TEG system was 2.61%. This is satisfactory in systems similar to the one used in our study.

Table 2-2 Technical properties, uncertainties, and accuracies of the measuring instruments

Instrument	Range	Accuracy	Uncertainty, %
Digital Temperature Humidity	−20 °C ~ 70 °C	±1.0 °C%	0.58
Meter, °C, RH%	0 ~ 100%RH	±3.0%RH	1.73
AC/DC Digital Clamp Meter, V	−20 °C ~ 70 °C	±0.01%	0.01
TES 132 Solar Power Meter, W/m2	−0 ~ 2000 W/m2	±0.7%	0.40
Pro HVAC Anemometer Handheld CFM Meter Wind Speed Meter, m/s	0.001 ~ 45 m/s	±3%	1.73
NTC single-end glass seal thermistor temperature sensor	−200 ~ 260	±1%	0.58

2.3.2.4 Maximum efficiency

The TEG module maximum efficiency is influenced by the temperatures of the TEG's hot and cold sides, in addition to the ambient temperature. This is due to the module's voltage and current are considerably affected by its temperature. The maximal TEG module efficiency is determined according to Equation 2.11 [82-84].

$$\eta_{max} = \frac{T_h - T_c}{T_h} \frac{\sqrt{1+Z\bar{T}} - 1}{\sqrt{1+Z\bar{T}} + \frac{T_c}{T_h}} \qquad 2.11$$

where $\bar{T} = \frac{T_h + T_c}{2}$, T_h and T_c are source and sink temperatures, respectively. $Z\bar{T}$ is called a figure of merit, the thermoelectric figure of merit *Z*, which is given by Equation 2.12 below, predicts the performance of any thermoelectric generator [85]:

$$Z_{p,n} = \frac{\alpha^2}{\rho k} \quad 2.12$$

where ρ represents the electrical resistance, and k denotes the thermal conductivity. If linked to the thermoelectric module average temperature ($\bar{T}$), this figure of merit becomes dimensionless value for the *n*-type and *p*-type TE legs. It can be given by the following equations:

$$Z\bar{T}_{p,n} = \frac{\alpha^2 \bar{T}}{\rho k} \quad 2.13$$

$$Z_{p,n} = \frac{\alpha^2 \sigma}{\lambda} \quad 2.14$$

In the above equation α, σ, and λ are the Seebeck coefficient, electrical conductivity, and thermal conductivity, respectively. All of these quantities are dependent on the TEG material, which is Bi_2Te_3 in this study. The ($Z\bar{T}$) appears as constant; however, $Z\bar{T}$ is a temperature dependent through Equation 2.11. For this reason and due to the dependence of $Z\bar{T}$ on the properties of the manufactured materials, we set the value of $Z\bar{T}$ base on the temperature at which the experiment was performed where $Z\bar{T}$ has a range of (0~1). The $Z\bar{T}$ value was taken (0.85) as specified by [86].

2.3.2.5 Results and Discussion

In both solar panels investigated in this chapter, the total time of the conducted experiments was 240 min. The experiments started at 11:30 h., and it ended at 15.30 h. local time, lasting four hours. The weather, effect of the Fresnel lens, power production, and maximum efficiencies of the two panels are presented and discussed in this section.

2.3.2.5.1 Weather during the Experiments

The weather during the experiments was recorded (see Figure 2-16). The highest solar radiation, 950 W/m2, was recorded at 11:30 h Conversely, the lowest solar radiation, 200 W/m^2, was observed at 17:00 h although the data collection period ended at 15:30 h. Over the course of the day, the average solar radiation was 694.59 W/m^2. The highest ambient temperature, 46.8 ◦C, was recorded at 17:00 h. while the lowest temperature was at around mid-day, 11:30 h., at the start of the experiments. The average temperature during the experiments was 44.91 ◦C.

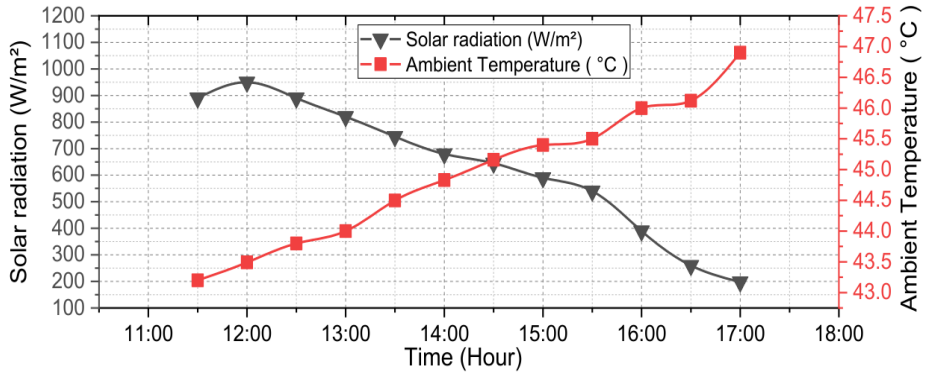

Figure 2-16 Solar radiation and ambient temperature for the L-TEG and NL-TEG during the day of the experiment

2.3.2.5.2 Effect of Fresnel lens at Different ΔT Values on the TEG System

This section discusses the impact of the Fresnel lens on the electrical performance of the two TEG systems. The influence of the devices presented in this research on the thermoelectric system has been investigated, as well as the extent to which they can be employed to save time and effort in the future. As can be seen from Figure 2-17, the NL-TEG presented the highest ΔT across the TEG modules throughout the experiments. The highest ΔT recorded between the cold and the hot side of NL-TEG panel was at 13:05 h. local time. The ΔT of the NL-TEG showed uniform changes and higher values compared to the L-TEG. The reason for this is that a Fresnel lens focuses solar radiation on a single spot which yields an irregular temperature distribution on the hot side that affects even the lower or the cold side temperature of the TEG panel. In comparison, the NL-TEG panel showed its highest ΔT, 35.62 °C, against 29.18 °C for the L-TEG panel during the same period. The system with no Fresnel lens worked very well, even at quite high temperatures. The mean ΔT for an NL-TEG panel during the experiments was 31.69 °C and 25.80 °C for the L-TEG. This is a 5.89 °C reduction for the NL-TEG, as shown in Figure 2-18. In both systems, there was an enhanced temperature difference, even though the systems operated under relatively low temperatures. This was attributed to the use of M-shaped cooling blocks, so that the temperature rise on the cold side was reduced compared to previous research [87].

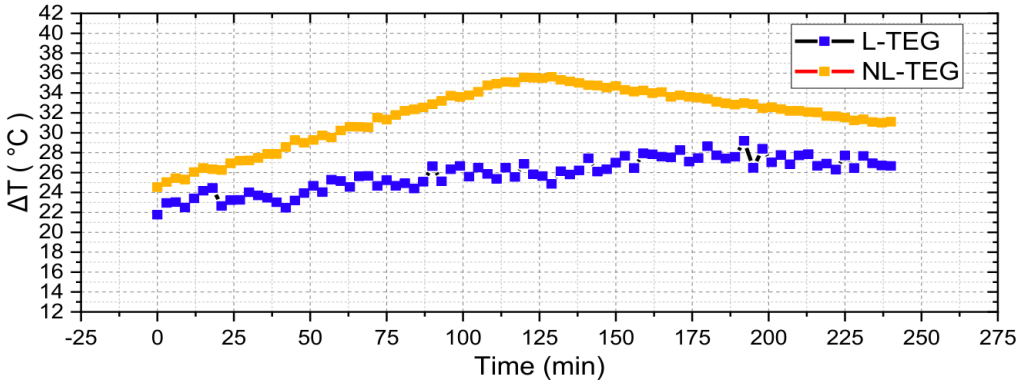

Figure 2-17 ΔT for each of NL-TEG and L-TEG system

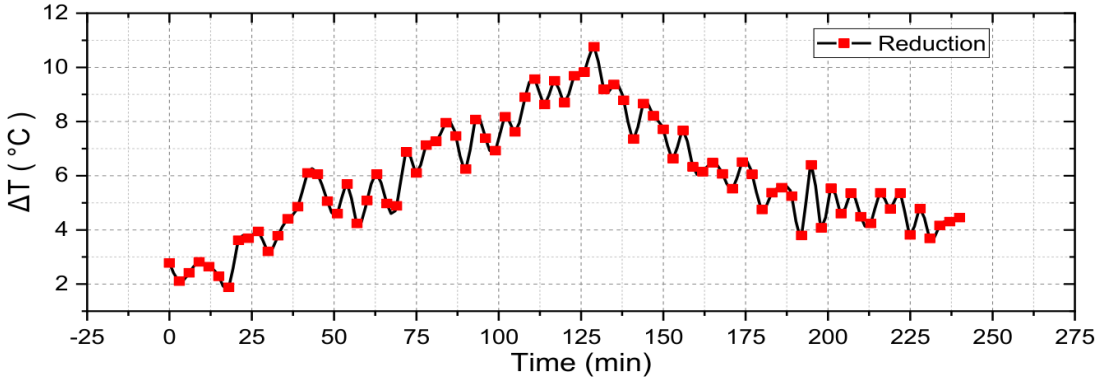

Figure 2-18 ΔT reduction for each of NL-TEG and L-TEG systems

2.3.2.5.3 Electrical Performance of the Module

The experimental electric voltages and currents are illustrated in Figure 2-19. The voltage dropped considerably with decreasing ΔT. During the experiments, the average voltage for the NL-TEG system was 10.33 V, while the L-TEG panel produced 8.74 V. This was a 1.59 V difference and a significant reduction of the L-TEG panel in the voltage. The proposed NL-TEG mechanism showed its effectiveness during the experiments. The voltage using no Fresnel lens was consistently higher than the L-TEG panel. Similarly, the NL-TEG current was slightly higher than the L-TEG. This was expected since the ΔT value was affected when there was no lens. The NL-TEG panel presented an average current of 1.68 A, while the L-TEG panel produced only 1.36 A. The change was insignificant as both panels produced nearly the same current until after mid-day when the ambient temperature increased sharply, affecting the system temperature.

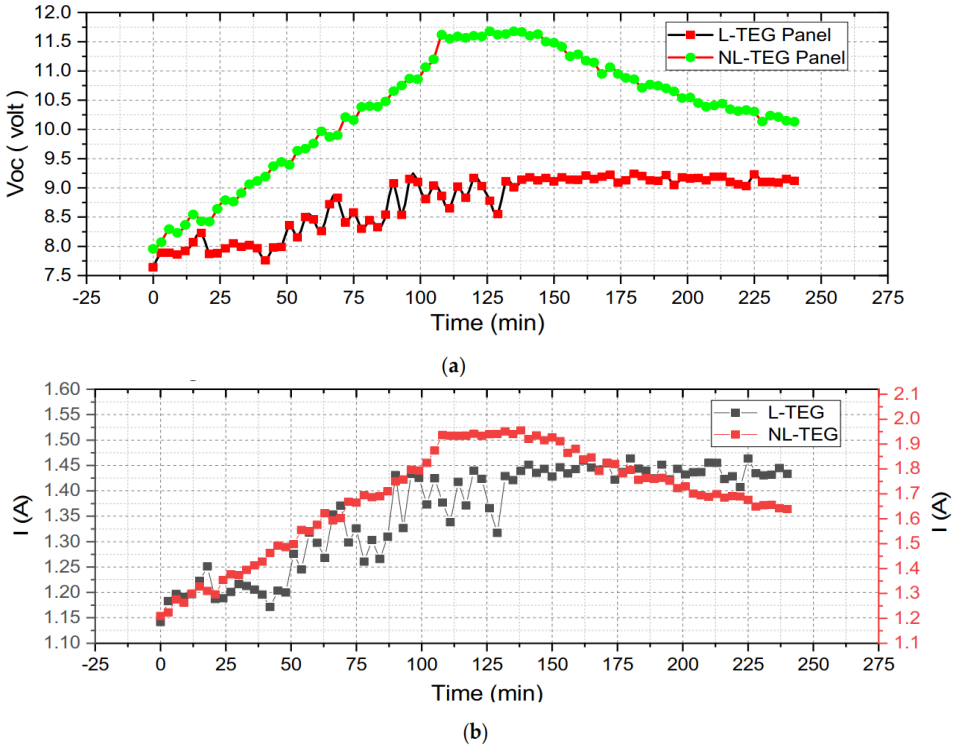

Figure 2-19 (**a**) Voltage for L-TEG and NL-TEG systems, (**b**) Current for L-TEG and NL-TEG systems

The power output of both panels is shown in Figure 2-20. The NL-TEG panel had the highest output power during the experiments. Both panels presented increased power with greater levels of solar radiation, and hence had different temperatures during the experiments. The modules reached their highest temperature differences (ΔT) at exactly 13:00 h However, output power subsequently began to decrease as decreased due to reduced solar radiation. The NL-TEG presented an average power of 14.37 W versus 9.26 W for the L-TEG panel. Thus, there was a difference of 5.10 W between the panels. This means that a 35.52% improvement in the output power was due to the different temperature profile of the NL-TEG panel.

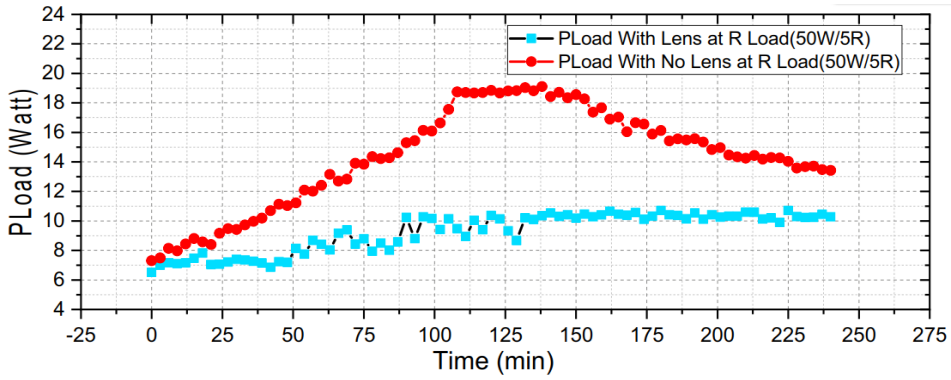

Figure 2-20 Power for both L-TEG and NL-TEG systems at load of (5 Ω/50 W)

2.3.2.5.4 Maximum Electrical Efficiency for TEG Related to Thermoelectric Materials

The maximum conversion efficiency of a TEG module was dependent on the of the material used in the fabrication, which was bismuth telluride BI2 TE3 here. The differences in the on the module surface were due to variations in the tap water temperature and solar heat from the sun. The maximum efficiencies of the NL-TEG and L-TEG modules were determined from Equation 2.11, and Figure 2-21presents the results. The calculated average maximum efficiencies realized for the NL-TEG and L-TEG panels were 1.49% and 1.25%, respectively. This represents an improved efficiency of 16.09% in the TEG module, a significant increase since the proposed mechanism does not depend on an active mechanism such as forced convection cooling or heating from outside of the system.

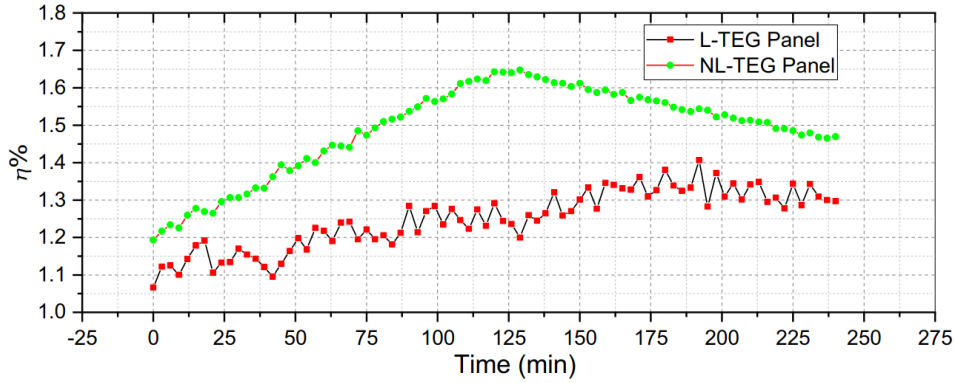

Figure 2-21 Efficiency for L-TEG and NL-TEG systems

2.3.2.5.5 Economic Analysis and Cost Estimation of System Implementation

This section presents a cost estimation of such a TEG panel. The estimation is based on the cost of system components. Due to a low generated voltage, the Fresnel lens is excluded from the cost estimation. Table 2-3 represents the cost of the components of the TEG panel.

Table 2-3 Component costs of the TEG panel

Components	Cost US $
TEG module	1.70
Aluminum alloy 6063	15.00
Water cooling Block (Heat Exchanger)	1.10
Glass	2.00
Metal stand	10.00
Flexible plastic water pipes	5.00

The total cost of the entire panel could be reduced if special modules were used to serve as a central heat exchanger with larger TEGs. In comparison with PV cells, TEGs need less maintenance since the former is affected by dust and high temperature, especially during the summer in hot areas like Iraq.

Heat exchangers generally represent much of the thermoelectric generator system costs, which vary from $1/(W/K) to $10/(W/K) and higher. Further considerations in economic analysis have been published [88, 89] for such systems. The cost of a heat exchanger is expressed in one US dollar per Watt and temperature units ($/W/K). The lowest thermoelectric cost is found at the maximum power point, but not at the highest power density of the thermoelectric module or the efficiency of the system.

According to the literature [87], the cost of a water-cooling block exchanger is approximately $13.81/(W/K). Other heat exchangers, such as air-cooled exchangers, have costs of approximately $15.12/(W/K).

Due to its simplicity and its low initial investment, air-cooled exchangers are most commonly used to improve the efficiency of the hot side of a thermoelectric module, although the actual thermoelectric gain of income is rather modest [88]. Water cooled block exchangers are less costly, more efficient, and help to optimize thermoelectric systems.

2.3.3 TEG System Panel with Two-Pass Flow

In this section, two TEG panels were designed and investigated using a multi-pass flow for the required electrical power generation actions. First panel consists of 20-TEG modules arranged as a 2×10 array while the second comprises 150-module arranged as 15×10 array.

2.3.3.1 The Design of the 2×10 TEG Panel

Series and parallel connections of TEGs are used to fabricate a TEG panel. The aim of this research is to convert waste heat from hot water pipelines that are fed from solar water heaters into electricity, as depicted in Figure 2-22. The TEG panel will convert the ΔT on both sides of it into an electric voltage that can charge a battery. The DC voltage of the battery can be converted into AC through an inverter to supply loads such as LED lights. During the night, the TEG can supply electric current since the hot water is fed in pipelines using an electric heater. Certainly, this will reduce electricity bills of homes.

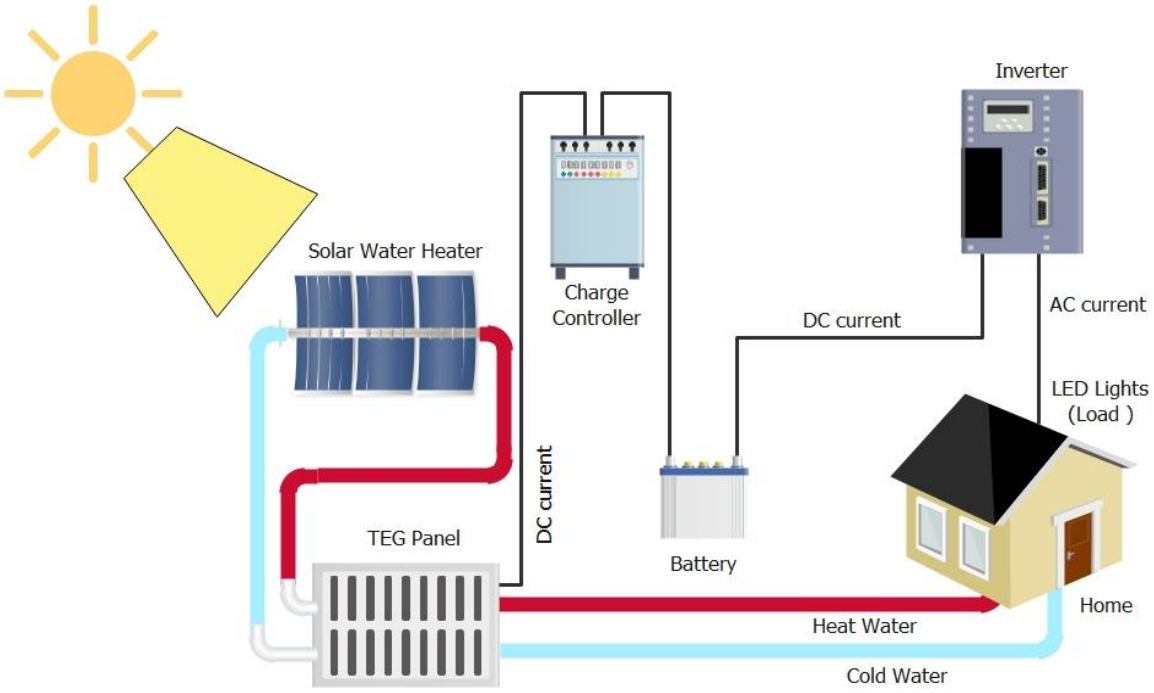

Figure 2-22 Role of TEG panel with solar water heater as renewable energy system

2.3.3.1.1 Proposed 2×10 TEG Panel

The series connections of 10 TEG modules are connected in parallel to form two lines of TEG modules, as shown in Figure 2-23.

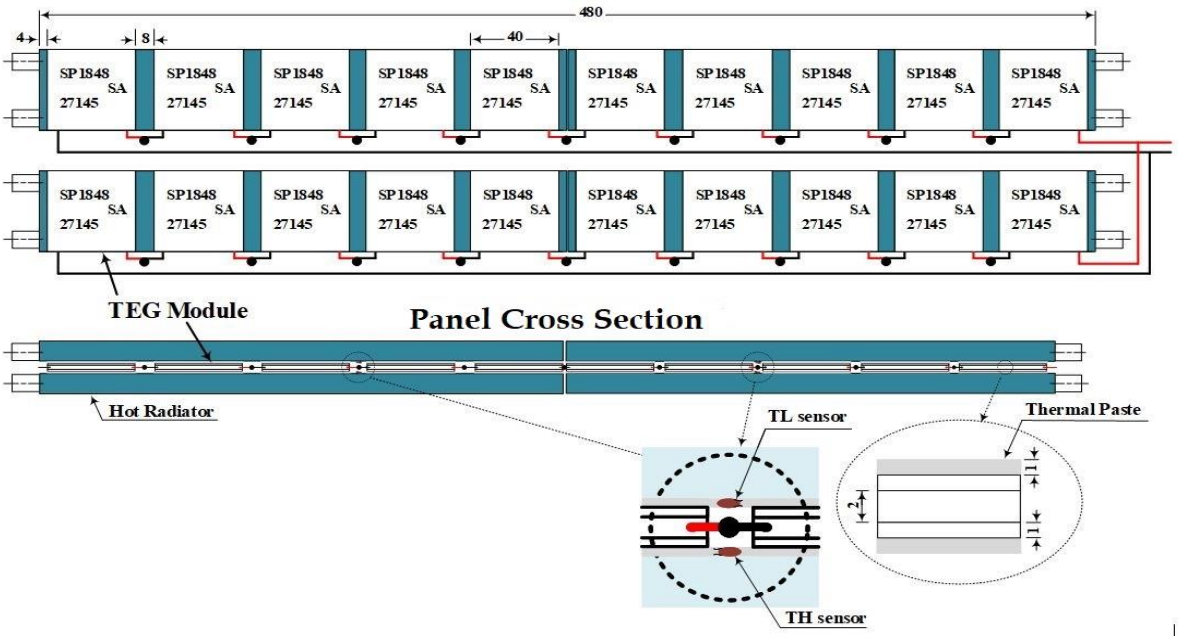

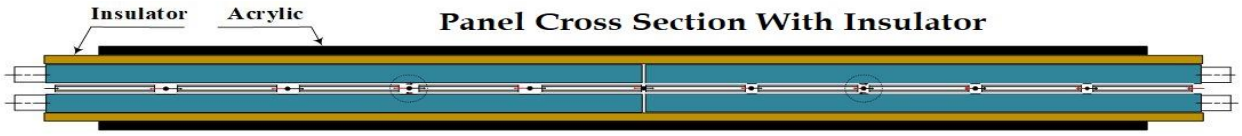

(a)

(b)

Figure 2-23 (a) Schematic diagram of a 2×10 TEG panel, (b) TEG module connections of the panel used in the current study.

The source of heat is hot water supplied from a solar water heater. The active cooling effect is from tap water. Both hot and cold water are passed through pipes connected at the appropriate sides of the TEG panel. The significant difference between this system and solar panels is that the former can be used continuously during the day and night hours. This is unlike solar systems that operate during daylight hours because they depend only on solar radiation. Thermal paste is used to allow for a uniform temperature distribution at each side of the TEG panel. Additionally, thermal insulators are used at both sides of the TEG panel to mitigate heat losses from the system. Acrylic glass covers both sides of the TEG panel, as shown in Figure 2-24. A ClYXGS aluminum water-cooling block is used on the other side of the TEG. The size this heat exchanger is (40 x 160 x 10) mm^3 and it is constructed from an aluminum alloy [41]. Water enters each heat exchanger in parallel flow to ensure good low temperature distribution on the cool side of the TEG panel. On each side of the panel, multiple temperature sensors are used to measure the temperature at various points. These readings are fed to an Arduino Mega microcontroller as shown in

Figure 2-25. The role of the Arduino Mega board is to record temperature readings and save them to a text file. So, it serves as a data logger.

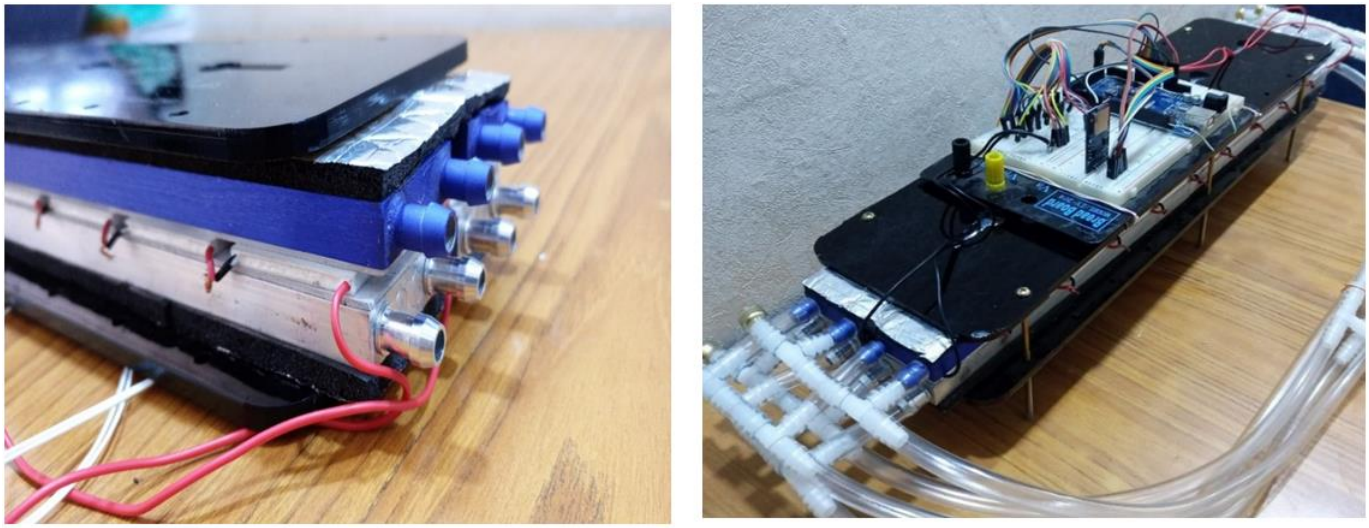

(a) (b)

Figure 2-24 Implementation of the designed TEG panel experimentally, (a) side view showing the various layers of the panel, (b) connection with an Arduino Mega microcontroller and measuring devices

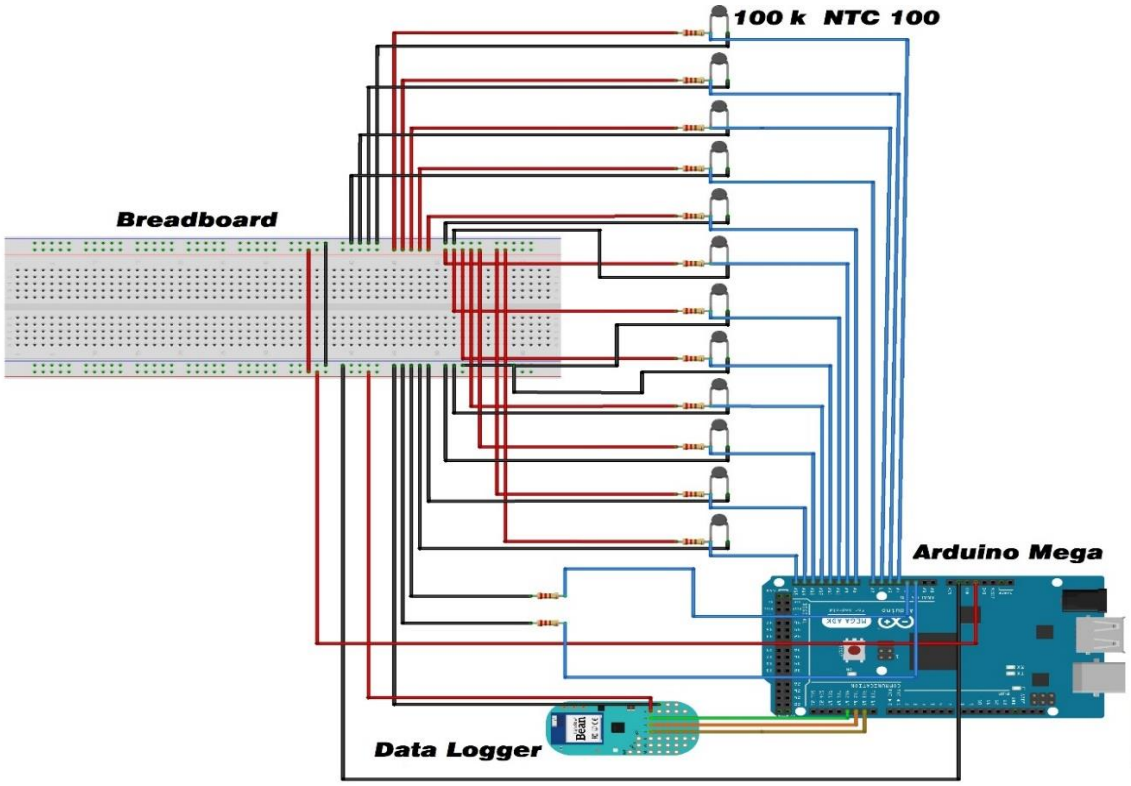

Figure 2-25 Temperature data logging via an Arduino Mega microcontroller

2.3.3.1.2 Efficiency of the TEG System

The highest possible efficiency of any energy conversion is the Carnot efficiency. The Seebeck effect uses a temperature differential to generate electricity in a thermoelectric device built from the junction of two materials. Temperature differentials can be converted to other kinds of energy by several technologies [90, 91]. Thermoelectric and pyroelectric systems, for example, convert temperature differentials to electricity, whereas Stirling engines and steam turbines transform them to mechanical work. Any device that transforms a temperature differential into another source of energy has its Carnot efficiency as a fundamental limit. The Carnot efficiency can be calculated using Equation 2.15 below [82, 92]. T_h and T_c, respectively, represent the hot and cold temperatures that comprise a temperature differential,

$$\eta_c \frac{T_h - T_c}{T_h} \qquad 2.15$$

2.3.3.1.3 Results and Discussion

2.3.3.1.3.1 Effect of Active Cooling and Heating Methods on the Temperature Difference of a 2×10 TEG Panel

Cooling and heating of the appropriate sides of a thermoelectric material leads to increased efficiency. These methods are either active or passive cooling methods [31]. Passive cooling appears to be the better option at first glance because it requires no electrical inputs. However, the yield of a thermoelectric material is sensitive to the magnitude of the temperature differential across it. Here, passive cooling has a comparatively large thermal resistance that detrimentally impacts the power yield. The temperature differential can be considerably increased using an active approach. However, a pressure differential must be established for active cooling and in most situations, this requires electrical power, which might negatively impact the net electrical output power. On further consideration, the net output power can be increased because, in many circumstances, the temperature differential has a bigger positive impact on the net output power than the active cooling's negative effect. The proposed TEG panel is tested experimentally. The experimental work was started at 12:00 PM and lasted for two hours. The hot (Th) and cold side temperatures (Tc) are depicted in Figure 2-26. In this figure, it can be seen that at the beginning of the experimental work, (Tc) is low. Then, it increased since (Th) affects (Tc) over time until a stable or equilibrium condition is reached. This effect decreases the ΔT between the hot and cold sides of the 2 x 10 TEG panel. The TEG panel recorded a low temperature of 67.3 ℃ and a high temperature of 67.59 ℃ on the hot side. Nevertheless, its average temperature was 67.44 ℃. The cold side saw a low

temperature of 25.2 ℃and a maximum temperature of 33.12 ℃, with an average temperature of 29.86 ℃. Thermocouples of the microcontroller recorded an average temperature difference of 37.58 ℃ on the surface of the panel. The highest and lowest temperature differences were 42.38 ℃ and 34.19 ℃, respectively, over the same time period. These results were obtained using thermocouples that were in direct contact with panel surfaces, providing more precise results.

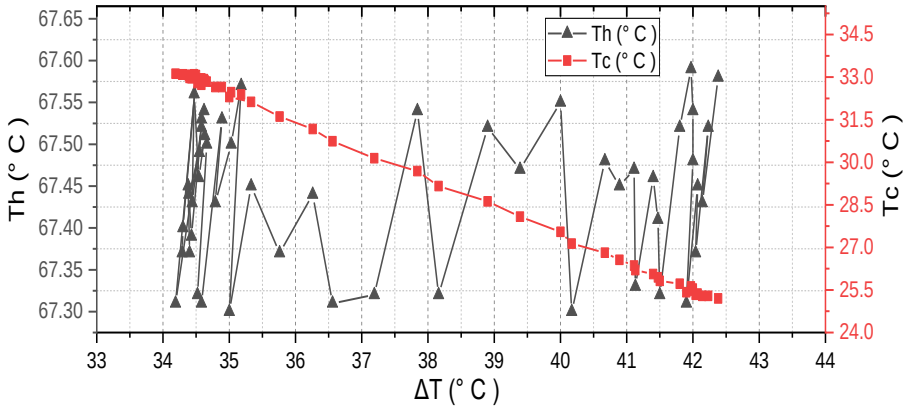

Figure 2-26 ΔT, Th and Tc of a 2×10 TEG panel

2.3.3.1.3.2 Performance in Terms of Electricity for the 2×10 TEG Panel

With a ΔT across the TEG module, an output voltage at the TEG terminals is generated, as shown in Figure 2-27. In this figure, it can be seen that the output voltage is proportional to ΔT. At the beginning of the experimental work, the open circuit voltage (Voc) is 15.05 V and then its value settled to 12.7 V.

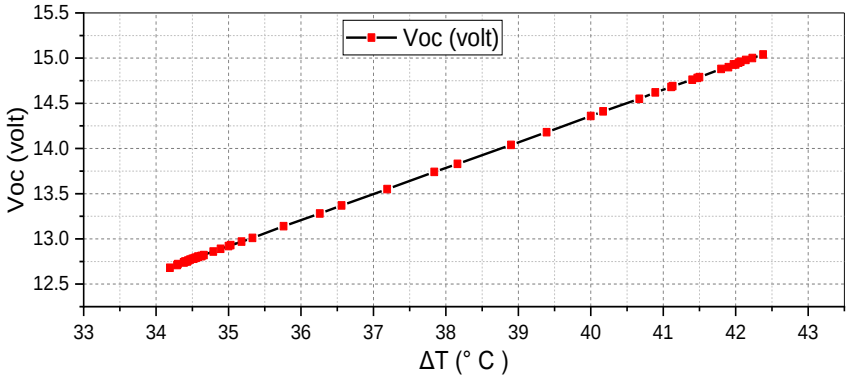

Figure 2-27 Open circuit voltage of the proposed 2×10 TEG panel

If a 5 Ω resistance is connected at the TEG panel terminals, current will flow. Figure 2-28 represents the output power versus ΔT. Since the initial generated voltage is higher than the steady state condition, the output power behaves the same since it is proportional to the squared value of the voltage. The minimum

and maximum power values are 3.04 W and 4.28 W, respectively, with an average of 3.55 W. However, it is notable that good output power is obtained due to the use of active cooling and heating systems compared to less efficient (passive) TEG systems [31]. The output voltage and power of the panel can be increased if the ΔT is made greater or by increasing the number of TEG modules.

Carnot Efficiency of the Proposed System

The Carnot efficiency (ηc) of a TEG depends on the temperatures of the hot and cold sides of the module. The TEG showed Carnot efficiencies at various ΔT values determined using Equation (9) and the results are presented in Figure 2-29. The calculated average efficiency of the module is 11.04%. Its maximum and minimum efficiencies are 12.44% and 10.43%, respectively, which are acceptable in small systems such as this.

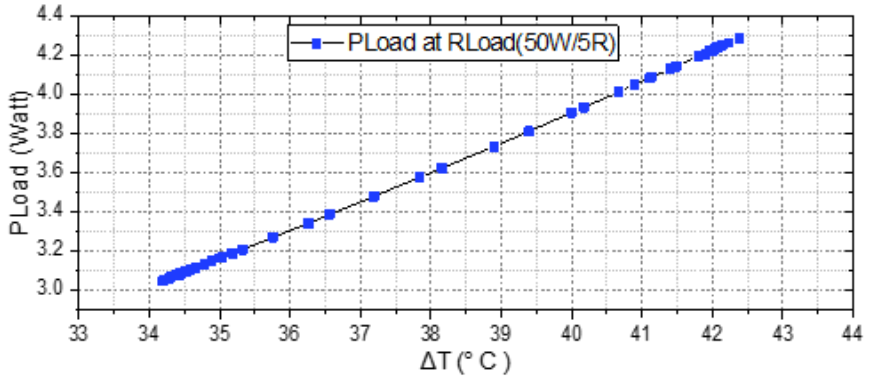

Figure 2-28 Load power of the proposed 2×10 TEG panel versus ΔT

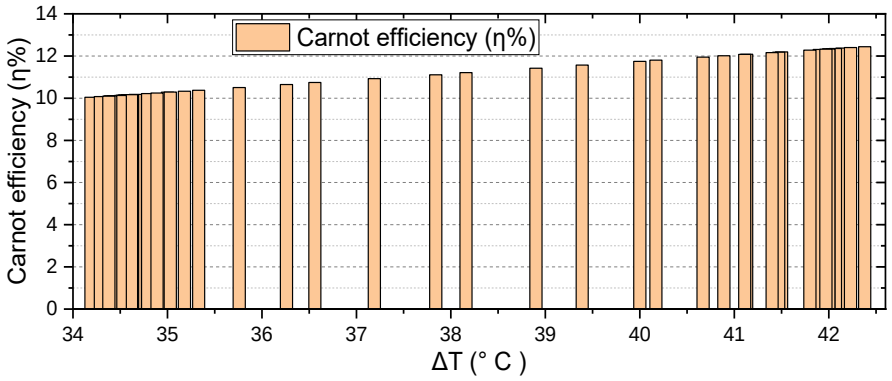

Figure 2-29 Carnot efficiency of a 2×10 TEG panel

2.3.3.1.3.3 System Implementation Cost Estimation and Economic Analysis

Economic analysis and cost assessment for system installation are two important considerations of the project [32]. This section estimates the cost of a 2 x 10 TEG panel from its key components, as shown in Table 2-4.

Table 2-4 Component costs of the TEG panel

Components	Cost US $
TEG module	0.95
Water cooling block (Heat exchanger)	1.10
Flexible plastic water pipes	3.00

A thermoelectric system was improved using water cooling block heat exchangers, which are less expensive, more efficient, and less energy intensive [88]. Other consideration for the system's economic analysis has been presented [88, 89, 93]. In reality, the heat exchanger accounts for the majority of the cost of a thermoelectric generator system, which can range from $1/(W/K) to $10/(W/K) and higher. The heat exchanger costs are measured in dollars per the ratio of Watts and degrees of absolute temperature $/(W/K). At maximum power, the lowest thermoelectric cost is determined, but not at the highest power density, largest thermoelectric module, or system efficiency. The cost of a water-cooled block exchanger, according to literature [94], is nearly $13.81/(W/K), which is reasonable when compared to other heat exchangers.

2.3.3.2 Design of the 15×10 TEG Panel

The construction of this panel is similar to the 2×10 panel; the only difference between the two panels is that the earlier is built from 20 TEG modules whereas the latter is built from 150 TEG modules. The

required temperature difference across the two sides of the TEG panel to generate electric power is achieved by using tap water. Two water passes were designed for this task. In the first, a normal tap water, between 25 and 33^{o}C, is used at a flow rate of 0.8-0.9 m/s to dissipate heat from the cold surface of the TEG panel. The same water is then heated about 1-2 ^{o}C and directed back to the TEG panel, as a second pass, to supply heat to the hot surface. Practically, this design is of great importance in domestic application, particularly for houses fitted with hot water solar panels. In this application, fresh tap water cools the cold surface, gets heat from the solar panel, heats the hot surface, and then the excess hot water is used for domestic purposes, as illustrated in Figure 2-30.

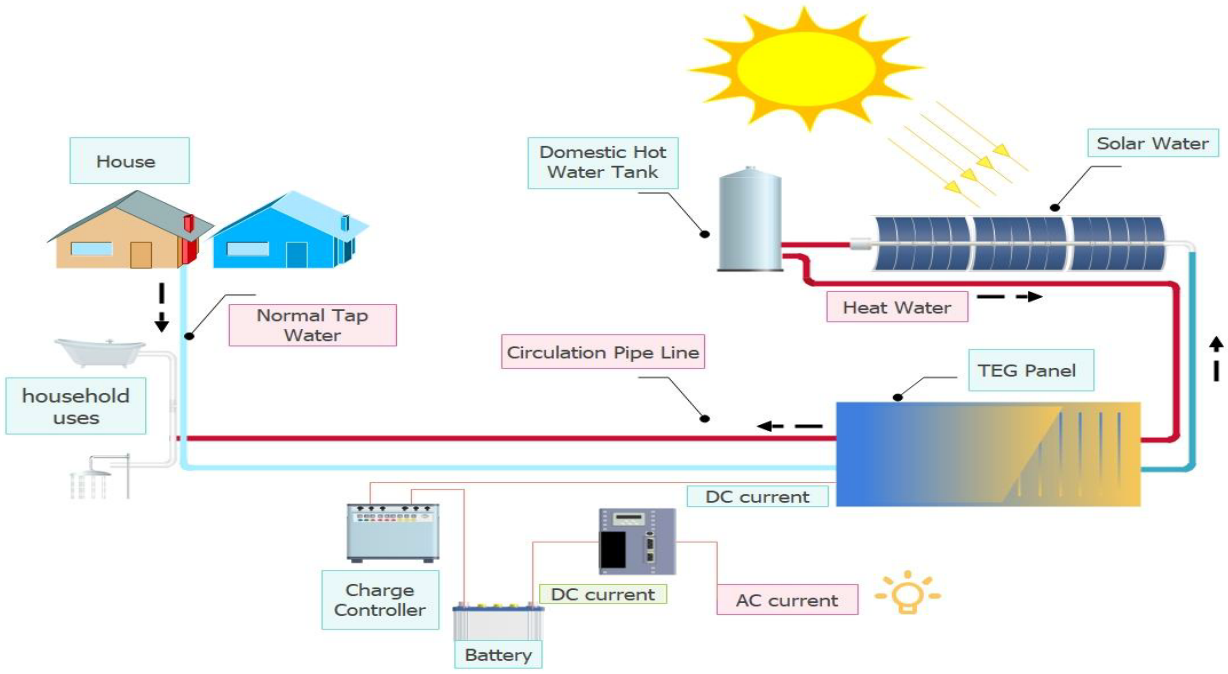

Figure 2-30 Domestic application of a TEG panel operated by two pass flow water system with a hot water solar panel.

2.3.3.2.1 Experimental Setup of the 15×10 TEG Panel

As illustrated in Figure 2-31, the series connections of 10 TEG modules are linked in parallel to produce 15 lines of TEG modules. Experimental work was done during a July day in Iraq. The aim of the proposed system is to generate and maximize output power from the thermoelectric modules (TEGs).

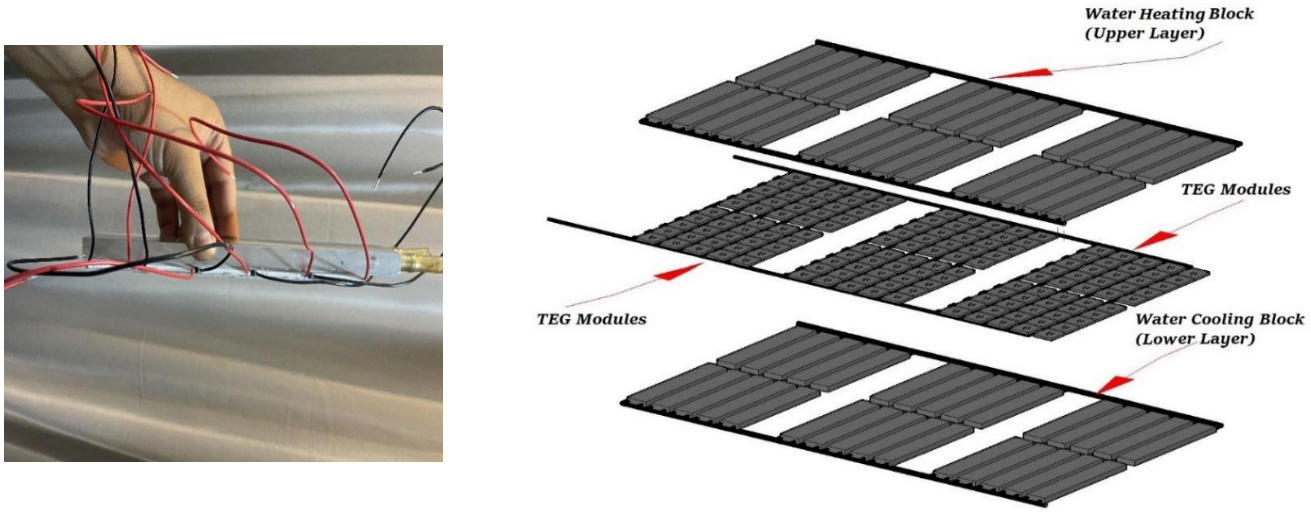

(a) (b)

Figure 2-31 (a) Single line of the TEG panel, (b) a schematic diagram of the 15×10 TEG panel.

The process system consists of three parts. The first part represents the hot surface of the system, where 30 pieces of an aluminum heating block are used. The dimensions of each piece are (40 x 240 x 10 mm), with an identical cooling block on the opposite side of the panel. This was built as in the Figure 2-32. Then the hot water coming from a solar water heater passes these pieces in parallel flow, with a constant velocity (0.8 m/s), to ensure a constant flow rate of water evenly enters the heating block, as shown in Figure 2-33. Then, this water goes into the house for domestic purposes after it heats the upper surface of the panel. The second part represents the cold surface of the TEG panel, which is at the bottom of the panel. Here, the technology is the same as for the upper surface, which is an aluminum water-cooling block. However, here, normal tap water enters the cooling block, at temperature that ranges from 25 to 34^{o}C. The flow of this water will dissipate heat coming from the hot surface of the plate to outside of the system. Then, this water is returned to the solar water heater. Here, an important new idea of this work emerges. This is to heat the water in two stages. The first stage is when it passes through a (TEG panel). The second time is in a solar water heater.

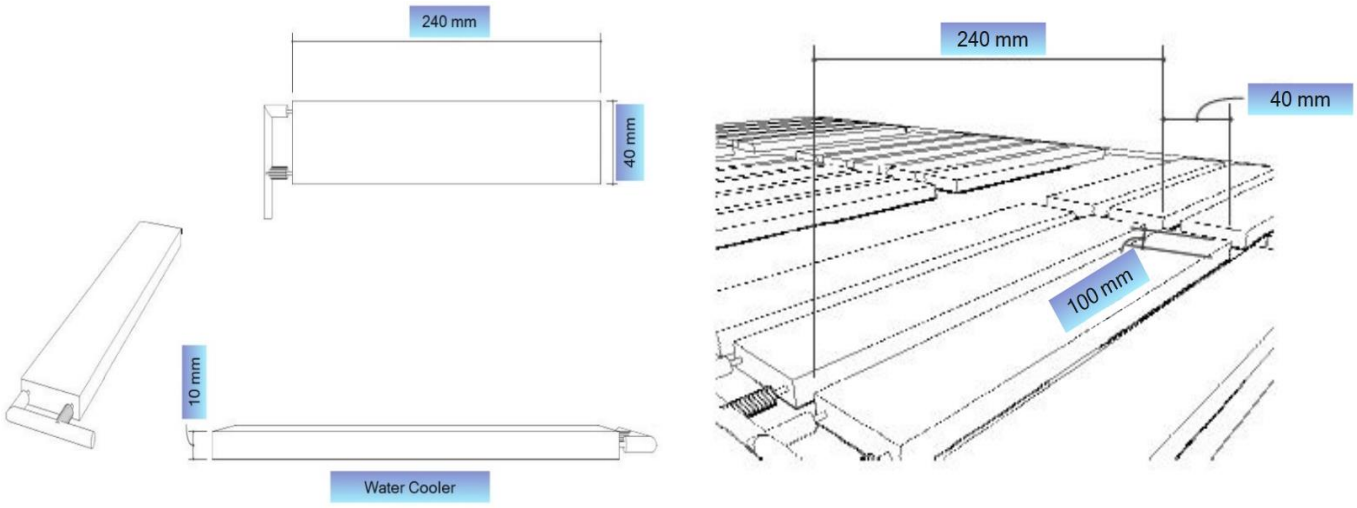

(a) (b)

Figure 2-32 (a) Schematic diagram of CLYXGS aluminum water block, and (b) individual pieces comprising aluminum water block in the as-built system.

Figure 2-33 Hot and cold water pipe systems

The third part represents the many TEG modules, as shown in Figure 2-34. They are connected electrically in series and parallel to obtain the required voltage. Thermal paste is used to improve thermal contact between the module components and allow for a uniform temperature distribution at each side of the TEG module, as shown in Figure 2-35. Also, insulators are here between the wires and the electrical connections passing between the TEG pieces to ensure that no electrical short-circuit occurs. Then, acrylic plates are installed on the two surfaces of the panel in a sandwich configuration so that all the connecting parts are installed correctly and evenly.

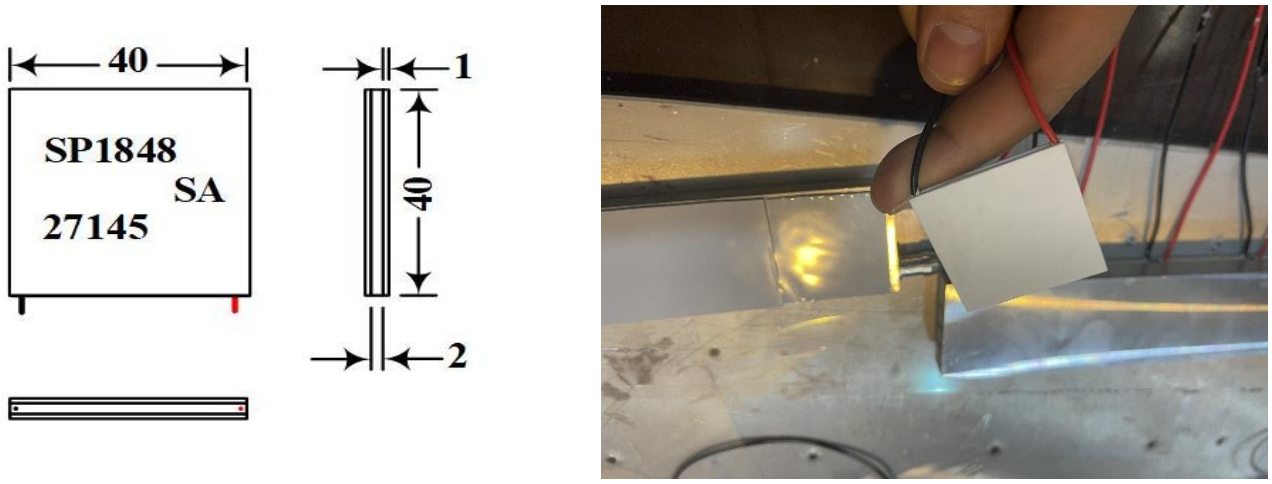

(a) (b)

Figure 2-34 (a) Schematic diagram, and (b) image of single TEG module implementation

Figure 2-35 Thermal paste, arrays and insulators used in the panel

The significant difference between this system and solar panels is that the former can be used continuously during the day and night hours. This is unlike solar systems that operate during daylight hours because they depend only on solar radiation.

2.3.3.2.2 Electrical Connections and Data Measurements

In practice, many measuring devices were used during the experiment (digital clamp meter, a single-end glass seal (NTC) thermistor temperature sensor, digital temperature humidity meter) integrated with a microcontroller to obtain more accurate results. Heat sensors (thermocouples) are attached at various

places on the panel to determine the temperature distribution on the test panel. All of the mentioned sensors here are sending their measurements signals to an Arduino Mega which is shown in Figure 2-36.

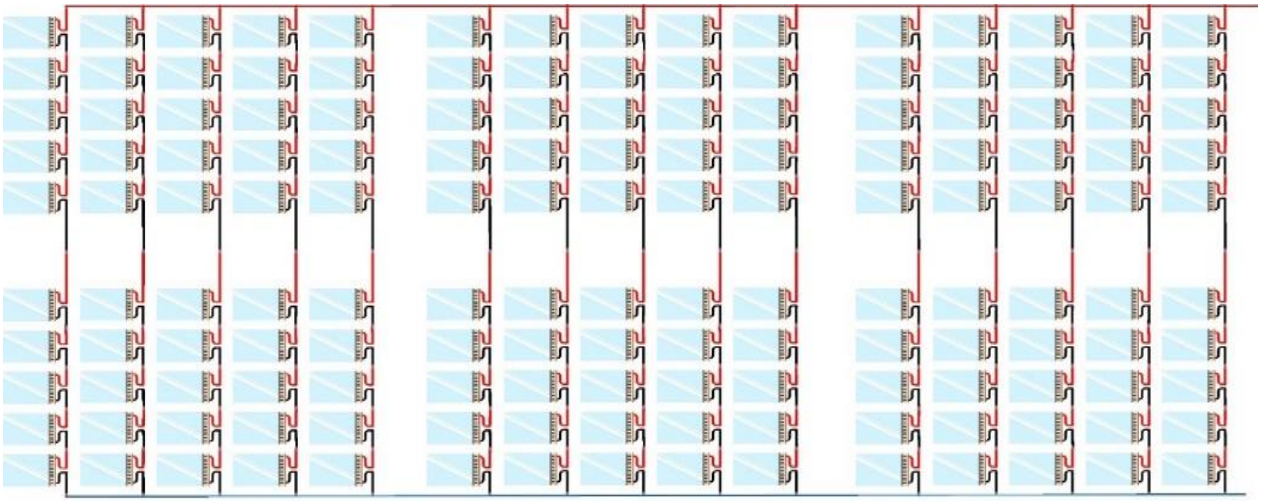

(a)

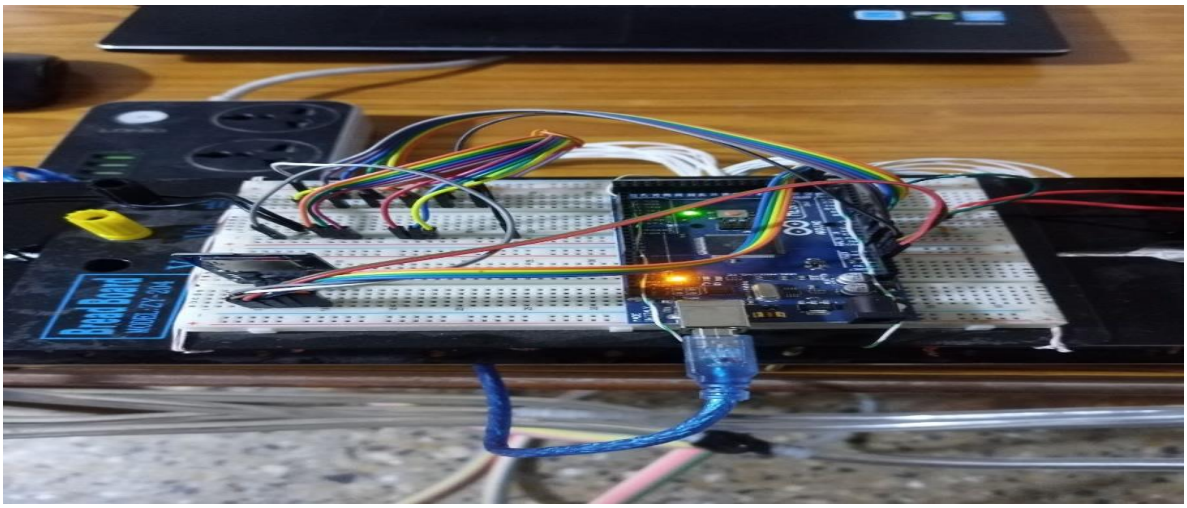

(b)

Figure 2-36 (a) Electrical connections of the TEG modules, and (b) Electrical connections of a microcontroller (Mega)

The recorded data is shown by Arduino IDE serial monitor and saved into text file. To optimize the TEG panel output voltage, two approaches are used in this study. A microcontroller (Mega) was used to measure the current and voltage in real time in conjunction with some manual measurements.

2.3.3.2.3 Results and Discussion

2.3.3.2.3.1 Effect Solar Water and Normal Tap Water on the Temperature Difference across a 15×10 TEG Panel

A TEG module relies on the temperature difference between its surfaces to generate electric power using the Seebeck effect. In the proposed system, two methods are used to provide this temperature difference, depending on the renewable energy source. The first method, directs the passage of normal tap water through the TEG panel, as this water performs the task of dissipating heat on the surface of the cold panel. This is usually at a temperature ranging from 25 to 34 ◦C. The other way is by flowing this same water after it leaves the panel to the solar water heater, and then the water is used to heat the hot surface of the TEG. After that, the water is used for domestic purposes. In this way, a temperature differential is formed, and thus electrical energy can be generated by the panel. The proposed TEG panel was tested experimentally on a July day in Iraq. The hot (Th) and cold side temperatures (Tc) are given in Figure 2-37.

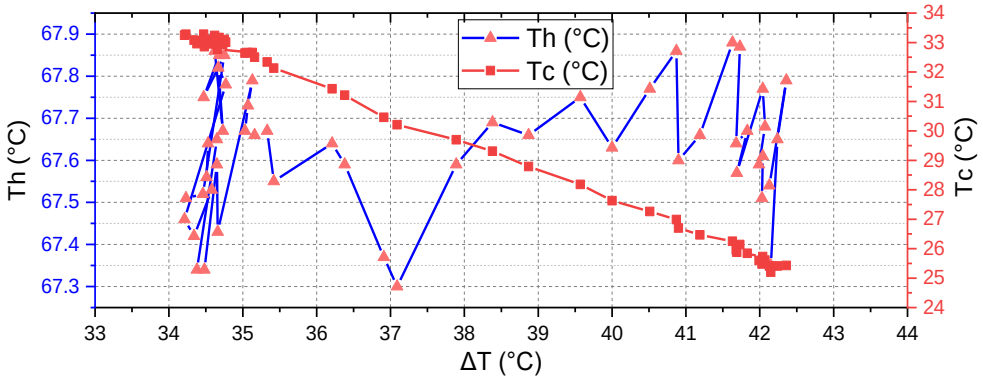

Figure 2-37 ΔT, Th, and Tc of a 15 × 10 TEG Panel

In this figure, it can be observed that (Tc) is low at the start of the experiment. Then, it increased because (Th) has an effect on (Tc) over time until an equilibrium condition is established. The ΔT between both the hot and cold sides of the 10×15 TEG Panel is reduced as a result of this impact. On the hot side, the TEG panel measured low and high temperatures of 67.22 ◦C and 67.88 ◦C, respectively. Despite this, the temperature averaged 67.62 ◦C. Low and high temperatures of 25.40 ◦C and 33.28 ◦C were, respectively, recorded on the cold side, with an average temperature of 29.95 ◦C. On the surface of the panel, microcontroller thermocouples detected a temperature differential of 37.67 ◦C. During the same time period, the largest and lowest temperature variations were 42.35 ◦C and 34.22 ◦C, respectively. These

results were acquired employing thermocouples in direct contact with panel surfaces, which allowed for more exact results.

2.3.3.2.3.2 Electrical Performance of the Proposed Panel

Figure 2-38 depicts the experimentally measured electric voltages. With a decrease in ΔT, the voltage fell dramatically. The average voltage for the 15 × 10 $TEG\ panel$ was 13.73 V, with the greatest and lowest voltages of 15.3 V and 12.51V, respectively.

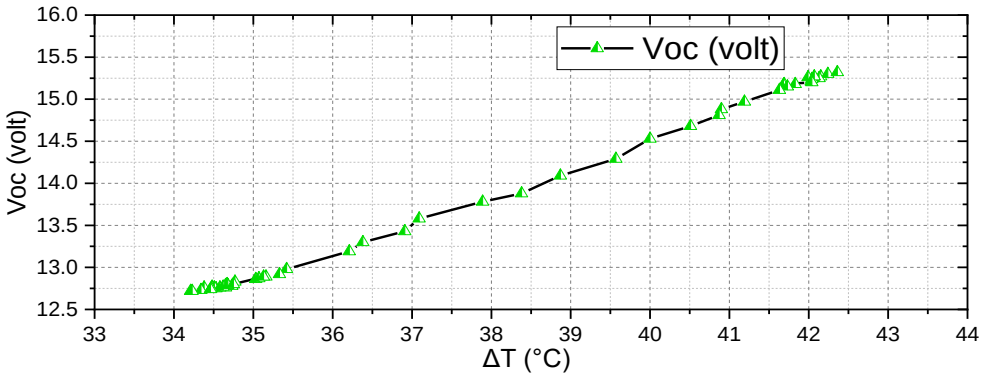

Figure 2-38 Voltage for 15×10 TEG panel systems

The illustration in Figure 2-39 shows that the power output of the 15×10 TEG panel ranged from 19.72 W to 29.49 W during the experiments, with an average power output of 23.92 W where the resistance of the used load is 5 Ω. The panel experienced varying temperatures during the studies and as a result, it demonstrated enhanced power with higher temperature differentials. The greatest temperature difference (ΔT) across the panel was 42.35 $°C$. However, when ΔT decreased, the output power of the panel also decreased.

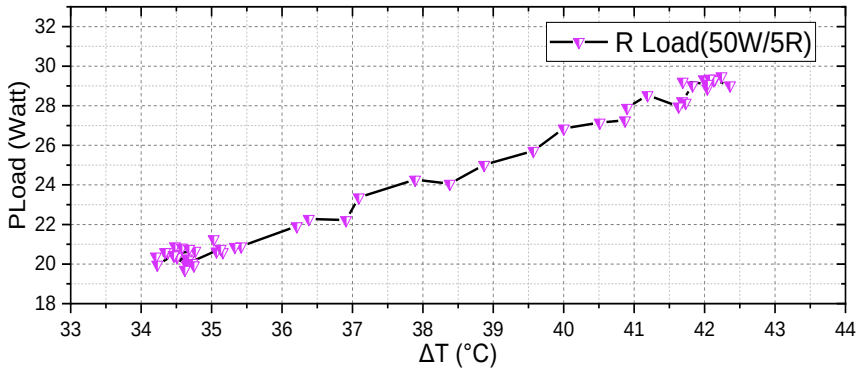

Figure 2-39 Power for 15 × 10 TEG panel at load of (50W/5Ω)

2.3.3.2.3.3 TEG's Maximum Electrical Efficiency in Relation to Thermoelectric Materials

The value of the figure of merit ($Z\bar{T}$) of the semiconductor behavior of a TEG module depends on the type of materials used. Bismuth telluride BI2TE3 was used in the current study. Figure 2-40 depicts that the average maximum efficiency achieved by the TEG panels was 1.77% . The lowest and highest values obtained during the experiments were 1.601% and 2.1%, respectively. The increase in this proposed mechanism is significant. This efficiency is considered important because the system operates under a low temperature difference compared to other systems, such as car exhaust and chimneys, among others. These conditions have twice the temperature difference used in the current work.

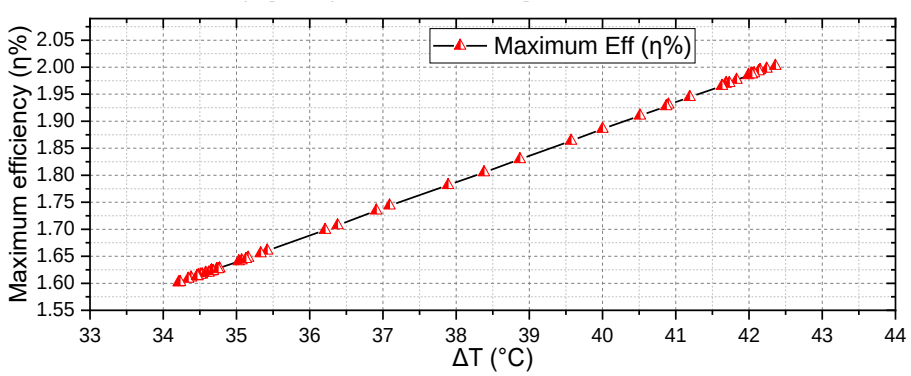

Figure 2-40 Efficiency of a 15 × 10 TEG panel system

In the Figure the relation between ΔT and ηmax seems linear. The estimated regression equation for the data of this figure is: $\eta_{max} = -0.089 + 0.049\ \Delta T$, where the value of the correlation between ΔT and η_{max} is 0.9998 i.e., positively high correlated.

A significant improvement in efficiency and output power is observed. This occurs since this proposed system uses heat sources that depend on available water rather than relying on other variable and unstable heat sources. As such, this system is independent, cost-effective, and does not use complex mechanisms. Table 2-5 represents a comparison of the research discussed above in this paper as well as others with the results of the current work. The results are either better than or competitive with systems presented in earlier studies. Most often, the proposed system gives better results, especially if utilization time is extended for many hours. The duration of each experimental run was only a few minutes, but if it lasted for many hours then the energy production would have been 1.435 kWh.

Table 2-5 Comparative analysis with earlier research

References	No. of TEG modules	Maximum output power	Maximum of ΔT	Maximum efficiency	Source of Heat
[95]	1	1.03 *W*	38.6 ℃	1.81 %	Solar radiation focused by a Fresnel lens
[96]	48	1.033 *W*	39 ℃	2.218 %	Waste heat of a biomass engine
[97]	18	5.6 *W*	110 ℃	Not specified	Hydrothermal power generation
[98]	4	0.03 *W*	32 ℃	Not specified	Walls of a building
[99]	1	3.13 *W*	133 ^{o}C	1.2 %	Not specified
[100]	10	0.85 *W*	58 ℃	2 %	Hot water
[101]	Not specified	21.17 *W*	40 ℃	0.68%	Heat Storage
[102]	Not specified	24.4 *W*	100 ℃	0.87%	Humidified flue gas
[103]	18	6.5 *W*	61.5 ℃	0.55%	Hot water
Proposed	150	29.49 *W*	42.35 ℃	2.1%	Hot water pipelines

2.3.4 Conclusion for Chapter Two

With the aim of developing TEG systems with maximum output voltage, three TEG panel systems have been developed in this chapter. In all systems the TEG modules were connected in series and parallel to achieve the best output voltage. In the first system, the TEG panel collects heat from the solar energy throughout the hot side of the TEG modules while a low temperature sink was used to dissipate the heat from the cold side of the TEG modules. To ensure uniform temperature distribution and to increase the energy storage, a 16 mm thick black aluminum plate was mounted directly on the hot side of the TEG panel. On the other a 30 ClYXGS Aluminum blocks of 40×240×10 mm were used. These blocks are water cooled, and they function as heat exchangers to dissipate the heat from the cold side of the panel. In this system, two panel designs were proposed; the first comprises using a Frensel lens with adjustable focal distance while the second is directly exposed to the solar rays. However, both designs involve a set of embedded temperature sensors and a photo sensor to monitor the temperature across the panel and the solar incident on the hot side of the panel. All sensors were linked to an Arduino Mega controller which processes the received signals and, accordingly, activate electrical motors which adjust the tilt angle of the panel and the focal distance of the Frencel lens.

The second developed system consists of 20-moodules arranged in a panel of 2×10, and uses hot water as a source of energy. Tap water at a flow rate of 0.8-0.9 m/s and temperature between 25 and 33^{o}C was used to cool the cold side of the panel before it get heated in a solar hot water system and then used again to heat the hot side of the panel. The heating and cooling processes were done using ClYXGS aluminum blocks attached to either sides of the panel. This novel design enables the storage of the solar energy as a hot water in an insulated water tank which can be used later on to sustain the electricity generation even after the sunset. This is unlike the solar operated system in which the power generation is limited to the presence of the solar radiation during the day time. The water operated system has a great potential in domestic applications, particularly for houses that already equipped with a hot water solar system. Another advantage of this system is that the excess energy of the hot water after leaving the TEG panel can be reused again in different house applications.

The third system is similar to the second one in terms of the principle of operation, however, the panel configuration and the number of the modules in the panel is different. The panel consists of 150-modules arranged in 15×10 array configuration. Both of the second and third systems were provided with a set of temperature sensors and equipped with an Arduino Mega controller.

In each of the systems, the TEG panel converts the ΔT across its sides into a DC electric voltage that can be used to charge a battery. The DC voltage is then converted into AC through an appropriate inverter to supply the energy to loads, such as LED lights which certainly contributes to reducing the houses electricity bills.

Different measuring devices, such as the digital clamp meter, single-end glass seal (NTC), thermistor temperature sensor, and digital temperature humidity meter were used to measure the systems' parts operation parameters and the generated electricity. According to obtained data the performance and efficiency of each system was determined, assessed, and evaluated.

CHAPTER THREE: EXPERIMENTAL STUDY ON HYBRIDIZATION OF A PV-TEG SYSTEM FOR OVERALL EFFICIENCY ENHANCEMENT USING HEAT EXCHANGERS, ENERGY, EXERGY AND ECONOMIC LEVELIZED COST OF ENERGY (LCOE) ANALYSIS

3.1 Introduction

The need for energy is growing. Since natural resources are becoming scarcer, it is crucial to provide clean, reusable, and ecologically friendly energy. The largest source of renewable energy, which can be directly transformed from light and heat to electricity, is solar energy [104-106]. When compared to a stand-alone PV system, combined photovoltaic (PV) and thermoelectric generator (TEG) systems have received considerable attention over the past ten years and have been shown to be an excellent way to utilize waste solar heat [106-109]. Using a temperature differential between the back of the PV and the TEG cold junction, the Seebeck effect allows TEG modules to directly convert waste thermal energy into electricity. TEGs have several advantages since the heat supply is constant, they make no noise, are clean and they are compatible with PV systems. Furthermore, they can function for many years [110, 111]. However, it is probable that the PV TEG efficiency is lower than PV systems alone [112]. Increased temperature differences will raise TEG efficiency but reduce PV efficiency. Therefore, the connection between the PV and TEG technology is complicated, which affects the performance of such systems [113].

Zhang et al. increased the open-circuit voltage and doubled energy harvesting. They developed a combination of polymer solar cells with TE modules [114]. Kil, Kim [115] concentrated on developing a photovoltaic/thermoelectric hybrid generator with a single-junction. Their system employed a GaAs-based solar cell and a conventional thermoelectric module. They found the conversion efficiency of this hybrid system is 23.2 % compared with 22.5 % for a single PV. This improvement was about 3% at a solar intensity of 50 suns [115].

Rajaee, Rad [116] conducted studies on a system that included photovoltaic cells, thermoelectric generators, nanofluids, and phase-change materials. They found that the system's total electrical efficiency can reach 15.8%. Moreover, they were able to increase the system's overall output by 42% [116]. Fini, Gharapetian [117] conducted a 24 hour analysis that involved experimental build testing, mathematical

modelling and finite element simulation of a hybrid PV/TEG system using water-cooled heat exchangers that had been proposed to extract more power from the system. They found that the average maximum photovoltaic panel temperature in both the experimental measurements and simulations of the hybrid system was 44.2 ◦C at maximum irradiation, while it was 57.1 ◦C for a reference PV panel. Also, they found the efficiency of a pure PV panel is 13.82% while its hybrid systems was 15.6% [117].

Mahmoudinezhad, Cotfas [118] tested the performance of PV, TEG, and PV-TEG hybrid systems using a spectrum beam splitter (BS). According to the results of their analysis, the system using only TEGs generated more power than the TEG in the hybrid system because it made better use of the whole spectrum of energy available to it. While the efficiency of the TEG component did decrease, the total efficiency of the hybrid system improved because of increased PV efficiency. More power was produced by the hybrid system than by either the PV or TEG systems [118].

Lorenzi, Mariani [108] designed a BI2TE3 TEG device for hybridization with three distinct panels. These were amorphous silicon (a-Si), gallium indium phosphide (GaInP) and perovskite photovoltaic panels. At an intensity of 5 suns and a panel temperature of 340 K, the Perovskite panel had the greatest efficiency improvement among three hybrid PV-TEG systems. Then, they experimentally constructed a Perovskite PV-TEG model. Their tests revealed a change in efficiency, from 16.8% to 19.5%, a 16.07 % improvement [108].

Babu and Ponnambalam [65] also used the MATLAB/Simulink environment to do a theoretical study of a non-concentrated hybrid PV/TEG system. This hybrid system was 6% more efficient overall and could produce 5% more energy [65]. Shatar et al. considered the load requirements of an indoor farm to design an unconcentrated photovoltaic-thermoelectric generator (PV-TEG) hybrid system. The performance of the hybrid system was evaluated during three months of testing in Malaysia. The planned system has proven that it can accommodate an extra load while also supplying enough power to service its intended load [119].

Direct coupling was done by Van Sark [120] to combine thermoelectric modules with solar cells to create a hybrid PV/TEG system that achieved improved electrical performance [120]. This technology was offered as an efficient thermal management strategy for photovoltaic cells. Two case studies were provided from Utrecht, Netherlands, and Malaga, Spain. The outcomes also indicated that the energy of Malaga and Utrecht might be increased by approximately 14.7% and 11%, respectively, using the annual

irradiance and temperature profiles of these cities. Nevertheless, this study overlooked radiation losses and the idealized model overstated the outcomes for real PV/TEG systems by roughly 10% [120].

Ko and Jeong [121] used MATLAB software to quantitatively examine the transient behavior of a PVTEG system incorporated into a building in combination with phase change materials (PCMs). They investigated the impact of PCM layer thickness and its melting point on PV TEG efficiency. According to their findings, the hybrid system was 1.09% more efficient than a PV system alone, with 0.18% coming from TEGs and 0.91% from the PV. Additionally, the proposed system produced 0.91% more energy in spring, 1.32% more in summer, 2.25% more in autumn, and 3.16% more in winter. It was suggested that the hybrid system might possibly produce 4.47% more power than a single PV when TEGs having a higher figure of merit were employed [121].

Beeri, Rotem [122] presented experimental and theoretical data for a combined PV-TEG system to convert concentrated sunlight, with a factor of X up to 300, into electricity. These results demonstrate that when the X value and system temperature were increased, the efficiency of the PV cell decreased and that of the TEG increased. As a result, the direct electrical contribution of the TEG began to predominate in the overall system, reaching a 20% power contribution at an X value of 290. Efficiency changed from 28.95% to 30.53% with an improvement of 5.45% at a concentration factor of 205. By utilizing more sophisticated PV cells and TE materials, it is demonstrated that the hybrid system may exceed 50% overall efficiency [122].

Khan, Khan [123] demonstrated an experimental hybrid photovoltaic-thermoelectric generation (PV-TEG) system. A 10 W polycrystalline silicon panel with ten bismuth-telluride TEG modules was mounted to the panel back to recover and convert waste heat into usable electrical energy, while simultaneously cooling the PV cells. The results showed that this hybrid system achieved increased output power and conversion efficiency values for PV modules. In the hybrid system, the PV module operating temperature decreased by 5.5%, from 55 °C to 52 °C. When compared to a straightforward PV system, the total output power of the hybrid system increased from 8.78 to 10.84 W, a 19% increase. Additionally, the hybrid PVTEG system efficiency rose from 11.6 to 14%, a total improvement of 17% [123].

Li, Zhou [124] showed inconsistency of thermoelectric load resistance for photovoltaic–thermoelectric modules from a theoretical perspective. Two types of PV cells were employed to build and test a model PV-TE. Under various working conditions for a TE module, a TE in the PV-TE, and a PV-TE, the maximum load resistance of each TE was examined. The efficiency of crystalline silicon alone is 9.5%

and increase to 11.07% in a hybrid system with a TE load resistance of 0.75 and a figure of merit of 0.0085/K. The efficiency of GaAs alone is 21.91% and increases to 22.94% in hybrid mode when the TE load resistance is 1.60 and the figure of merit is 0.0022/K [124].

Zhang, Xuan [125] used three-dimensional numerical modeling to calculate the potential and characteristics of an integrated system consisting of new perovskite solar cells and thermoelectric modules. They found that the temperature coefficient of the perovskite solar cell is lower than 2%. Due to such a reduced temperature coefficient, the efficiency of the perovskite solar cell-TEG hybrid system was 18.6%, whereas that of a pure perovskite solar cell is 17.8%, making it a good alternative in a PV-TEG hybrid system. Concentration of heat can be changed, and thus the required bulk TEG material may be decreased, leading to significant cost savings for a hybrid system [125].

Cui, Xuan [126] experimentally utilized a phase change material (PCM) to develop a unique PV-PCM-TE hybrid system to maintain system function at an optimal temperature. The temperature, efficiency, and output power of the hybrid system are compared with those of a stand-alone PV system under identical conditions. The effects of the optical concentration ratio and cooling approach on the conversion efficiency of the hybrid system are experimentally explored. According to the results, a hybrid PV-PCM-TE system has an efficiency of 13.45%, compared to that of a stand-alone system, 13.43%. The study indicates that such a hybrid system has good potential for full-spectrum conversion of solar energy [126].

Generally, previous studies do not consider some issues. Most PV-TEG systems link many thermoelectric modules in a series and parallel array to achieve the necessary power level. The uniform temperature distribution of thermoelectric modules, the influence of pressure distribution on the assembly, thermal contact between the modules and the heat exchangers, and the thermal bridge between the heat exchangers and PV panel were given little attention. Additionally, the issues of concentrated and non-concentrated solar irradiation techniques were given little consideration in PV-TEG systems. For non-concentrated PV-TEG systems, the electrical performance of PVs and gradient temperature for TEGs is low, and most of the electricity is produced by the PVs. While for concentrated PV-TEG systems, the operating temperature of the PV increases, sometimes to levels higher than 100 ^{o}C, significantly reducing its performance. This led to high temperature gradients for TEGs and more electricity production.

Therefore, creation of a hybrid system that balances the performance of solar panels and TEGs, with appropriate electrical connections and assembly of TEG modules to obtain the appropriate voltage is extremely important, where the modules are attached to the back of generic PV panels. In this chapter, a

TEG configuration test method was used to measure and analyze data obtained from TEGs, one of which was highly efficient in the proposed system. Also, a hybrid PV-TEG system was fabricated using an experimental design for the Iraq climate using an energy, exergy, and analysis of economic levelized cost of energy (LCOE) approach. The overall objective of the current chapter is to quantify the performance of this system and its associated parameters with the goal of enhancing conversion efficiency and heat recovery from a PV panel in a hybridized system (HPVTEG) for comparison with a standalone PV panel. The experimental investigations are examined under actual weather conditions in on the roof of a building in Baghdad, Iraq.

3.2 Thermodynamic Calculations

As we know, energy, and exergy calculations evolved with the thermodynamics analysis. Therefore, in the present, a detailed thermodynamic analysis was presented.

3.2.1 Computation of Energy

3.2.1.1 Solar Photovoltaic Subsystem

The reduction in operating temperature (caused by the thermoelectric device) is the prime source of the performance improvement for solar cells integrated into a PV-TEG hybrid configuration. It is, therefore, necessary to describe the performance parameters of the cell with respect to temperature to determine the source of improvement [127]. Using Equation 3.1, it is possible to determine the PV cell efficiency η_{mpp} (G,T_{pv}) for an operating temperature, T_{pv} [128]. Also, Energy efficiency is also well known as the first law of thermodynamics, and it is quantitative measurement.

$$\eta_{mpp}(G, T_{pv}) = \eta_{mpp}(G, T_{ref}) \cdot [1 - \beta(T_{pv} - T_{ref})] \qquad (3.1)$$

where, T_{ref} represents the reference air temperature and G is the incident solar irradiance. The temperature efficiency coefficient, often given by the cell manufacturer, is denoted by β, while η_{mpp} (G,T_{ref}) represents the photovoltaic cell efficiency at STC (standard test conditions).

After defining the photovoltaic conversion efficiency η_{mpp} (G,T_{pv}), Equation 3.2 may be used to calculate the PV cell power output at a previously determined temperature, T_{pv} [129].

$$P_{pv} = \eta_{mpp}(G, T_{pv}) \cdot G \cdot A \qquad (3.2)$$

where A is the PV cell's solar-facing frontal area.

3.2.1.2 Thermoelectric Subsystem

Each TEG thermocouple has p- and n-junctions (legs). Thermal transmission losses, as well as the electrical and thermal contact resistances are neglected. At steady state, the power absorbed at the hot side of the TEG module and the power discharged at the cold junction are [130]:

$$P_h = n\left[IT_h\alpha - \frac{1}{2}\,I^2R\ + K(T_h - T_c)\right] \tag{3.3}$$

$$P_c = n\left[IT_c\alpha + \frac{1}{2}\,I^2R\ + K(T_h - T_c)\right] \tag{3.4}$$

In Equations 3.3 and 3.4, the first terms on the left hand side indicate Peltier heat in power transmission, whereas the second and third terms imply Joule and Fourier heat in power transmission. Internal resistance (*R*) and thermal conductance (*K*) are expressed as [131]:

$$\alpha = (\alpha_p - \alpha_n) \tag{3.5}$$

$$R = \frac{\rho_p\, l_{TEG_l}}{A_p} + \frac{\rho_n\, l_{TEG_l}}{A_n} \tag{3.6}$$

$$K = \frac{K_{TEG}}{l_{TEG_l}} + (A_p + A_n) \tag{3.7}$$

where α is the Seebeck coefficient, ρ_p, ρ_n are the density of legs , l_{TEG_l} is the TEG leg length, and A_p, A_n are the cross-sectional area of the TEG legs, which are equal.

Using the difference $P_h - P_c$, the system's output power may alternatively be represented as current and load resistance, RL.

$$P_h - P_c = I^2R_L \tag{3.8}$$

Additionally, the current and Seebeck emf can be calculated as:

$$V_{oc} = \left(\alpha_p - \alpha_n\right)(T_h - T_c) \tag{3.9}$$

$$W = I = \frac{V_{oc}}{R+R_L} \tag{3.10}$$

Combining Equations (3.3), (3.4), (3.8) and (3.10), TEG module efficiency can be expressed as Equation (3.11) [132] :

$$\eta = \frac{P_h - P_c}{P_h} = \eta_c \frac{\beta}{(1+\beta)+(1+\beta)^2\,.(ZT_h)^{-1}-\eta_c/2} \tag{3.11}$$

where $\beta = \frac{R_l}{R}$L, $Z_{p,n} = \frac{\alpha^2}{\rho\, k}$ and $\eta_c = \frac{T_h - T_c}{T_h}$. The maximum efficiency occurs at $\beta = \frac{R_l}{R} = (1+ZT)^{0.5}$, where T_h and T_c are averaged to yield T.

$$\eta_{max} = \frac{T_h - T_C}{T_h} \frac{(1+ZT)^{0.5} - 1}{(1+ZT)^{0.5} + \frac{T_C}{T_h}} \quad (3.12)$$

3.2.1.3 HPVTEG system

A hybrid system was developed that combines PV and TEG modules with four wires in parallel for an isolated load, where the energy harvesting process is separately executed. This system is illustrated in Figure 3-1 as its electrical equivalent circuit.

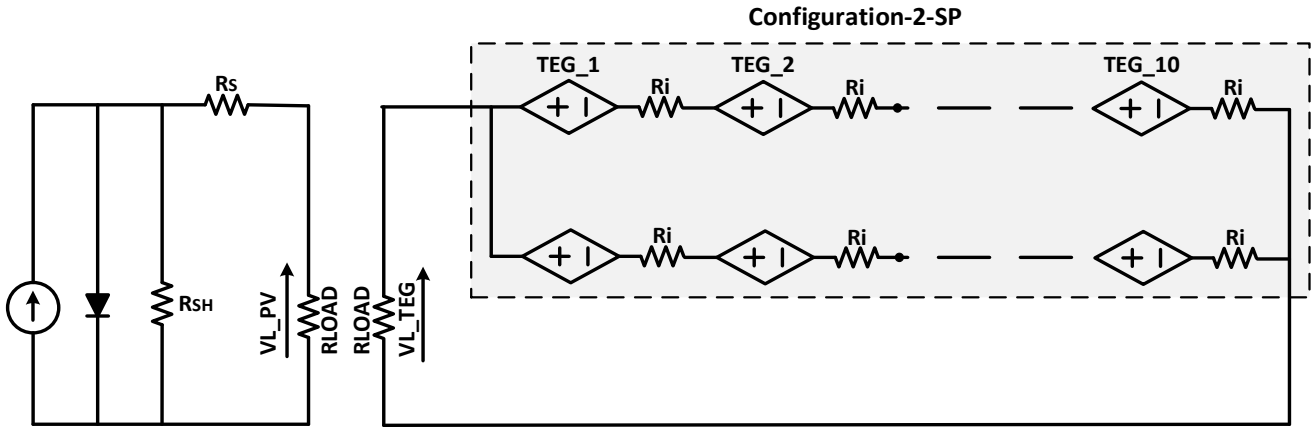

Figure 3-1 Circuit diagram for the HPVTEG system

Solar energy, *Q*, illuminates the PV cell, which produces electricity, p_{pv}. Heat is produced that is not converted to electricity by the PV cell, which is then transferred to the hot side of the TEGs, transforming it into extra electrical power p_{teg}, that is removed from the system at the cold side of the TEGs. Equations 3.13 and 3.14 provide the total system electrical power output p_{tot} and efficiency η_{tot} [133] .

$$p_{tot} = P_{pv} + P_{teg} \quad (3.13)$$

$$\eta_{tot} = \frac{P_{tot}}{\mathrm{Q}} \quad (3.14)$$

$\boldsymbol{Q}$ is the incident solar irradiance input energy, which is equal to $G \cdot A$, where G, A are sun intensity and solar module area.

The improvement of efficiency of a hybrid system and stand-alone PV can be estimated by Eq.

$$\eta_{improvement} = \left(\frac{\eta_{HPVTEG}}{\eta_{ref,PV}} - 1\right) \times 100\% \quad (3.15)$$

3.2.1.4 Exergy Modeling

This section presents a thorough exergy analysis of the HPVTEG system under investigation. Exergy analysis is a helpful technique for contrasting a system's actual and desired performance. By lowering the exergy destruction parameters, device performance is enhanced. Calculating the exergy efficiency is as follows [134]:

$$\eta_{ex,tot} = \frac{\dot{E}x_{tot}}{\dot{E}x_{in}} \tag{3.16}$$

where $\dot{E}x_{tot}$ is the total quantity of exergy obtained, and $\dot{E}x_{in}$ is input exergy of the system, they can be obtained as [134]:

$$\dot{E}x_{in} = G\ A_{PV}\ \left(1 - \frac{4\ T_{amb}}{3T_s} + \frac{1}{3}\left(\frac{T_{amb}}{T_s}\right)^4\right) \tag{3.17}$$

$$\dot{E}x_{tot} = \dot{E}x_{th} + \dot{E}x_{PV} + \dot{E}x_{TEG} \tag{3.18}$$

where, G is solar radiation, A_{PV} is panel aperture area, T_{amb} is surrounding air temperature, and T_s is the temperature of the energy source (sun). Exergy acquired from the water, PV, and TEGs is denoted as $\dot{E}x_{th}, \dot{E}x_{PV}, \dot{E}x_{TEG}$, and they can be obtained as [135]:

$$\dot{E}x_{th} = \dot{m}_w\ c_{P_w}\ \left(T_{out_w} - T_{in_w} - T_{amb} ln\left(\frac{T_{out_w}}{T_{in_w}}\right)\right) \tag{3.19}$$

$$\dot{E}x_{pv} = \eta_{pv}\ G\ A_{pv} = \eta_{ref}\ G\ A_{pv}\ \left(1 - \beta_{ref}\left(T_{pv} - T_{amb}\right)\right) \tag{3.20}$$

$$\dot{E}x_{TEG} = P_{TEG} + Q_c\ \left(1 - \frac{T_{out_w}}{T_c}\right) \tag{3.21}$$

In these equations, $\dot{m}_w$ represents the mass flow rate of a coolant fluid, and c_{P_w} is its heat capacity. T_{out_w} and T_{in_w} are water inlet and outlet temperatures. The PV reference efficiency is denoted by η_{ref}, while the PV efficiency temperature coefficient is β_{ref} and the PV temperature is T_{pv}. P_{TEG} and Q_c represent output power and power absorbed by TEGs, respectively. Q_c can be obtained as [135] :

$$\dot{Q}_c = N\left(S_m I_{TEG} T_c - \frac{1}{2}\ I_{TEG}^2\ R + K(T_h - T_c)\right) \tag{3.22}$$

where N is the number thermocouples of the TEG, S_m is the Seebeck coefficient, I, R, and K are electric current, electrical resistance and thermal conductivity of the TEGs, respectively. The PV panel and thermoelectric generator parameters found in [66, 136-139] and those for the heat exchanger are given in section 3.5.2.4.

3.3 Uncertainty Analysis

Measurement accuracy, test system design specifics, and human error all affect the accuracy of experimental findings. Table 3-1, derived from measuring equipment, lists experimental errors that could exist in the parameters utilized.

Table 3-1 Measurement uncertainties of various devices

Measurement Instrument	Range	Accuracy	Uncertainty %
TES 132 Solar Power Meter (Datalogging)	$0-2000\ W/m^2$	$\pm$ 5 %	2.89
Pro HVAC Anemometer Handheld CFM Meter Wind Speed Meter	$0.001\sim 45\ m/s$	$\pm$ 3 %	1.73
AC/DC Digital Clamp Meter 1000A Professional Multimeter	$0-1000$ V	$\pm$0.01%	0.01
4 Channel K Type Thermometer SD Card Data Logger Thermocouple	$-200\sim1370°C$	$\pm$0.3 %	0.17
Digital and Temperature Humidity Meter, °C, RH%	$-20\sim70$ ℃	$\pm$1.0 ℃	0.58
	$0\sim100\%\ RH$	$\pm$3.0%	1.73
NTC single-end glass seal thermistor temperature sensor	$-200\sim260$ ℃	$\pm$1%	0.58
Water Flow Meter	$1\sim40\ L/min$	0.1 %	0.06

Using previously published error analysis methodology [41, 81, 140, 141], the total percentage of uncertainty *u(z)* can be calculated using Equation (3.23).

$$\boldsymbol{u(z)} = \left[\left(\frac{\partial z}{\partial y_1}\right)^2 \boldsymbol{u^2(w_1)} + \left(\frac{\partial z}{\partial y_2}\right)^2 \boldsymbol{u^2(w_2)} + \ldots\ldots\ldots + \left(\frac{\partial z}{\partial y_n}\right)^2 \boldsymbol{u^2(w_n)}\right]^{\frac{1}{2}} \qquad (3.23)$$

where $\boldsymbol{Z}$, $\boldsymbol{\Delta y_1, \Delta y_2}$, $\ldots\ldots\boldsymbol{\Delta y_n}$ are dependent variables of various inputs, in which potential errors may exist. The total percent of uncertainty in the proposed system used in these experiments is 3.87 %, which is considered allowable in the context of a study such as this.

3.4 Economic Analysis

A levelized cost of energy (LCOE) strategy was employed to analyze energy production costs for the proposed system. This strategy is often used to evaluate the economic feasibility of renewable energy facilities. It indicates the costs in a way that compares various power producing methods on a normalized basis [142, 143]. The levelized cost of energy is described as the lowest cost at which produced energy must be sold to financially break-even over the life of the project [144, 145]. Also, it assesses the average overall cost of building and running a power plant over the course of its lifespan divided by the total amount of energy produced during that period. The mathematical formulation of the LCOE is [146] :

$$\mathrm{LCOE} = \frac{\mathrm{LC_{inv}} + \mathrm{LC_{O\&M}} + \mathrm{LC_{fule}}}{\mathrm{E_{annual}}} \tag{3.24}$$

$$\mathrm{LC_{inv}} = \mathrm{CRF} \times \mathrm{C_{inv}} \tag{3.25}$$

$$\mathrm{CRF} = \frac{\mathrm{i_{eff}}.(1+\mathrm{i_{eff}})^{n}}{((1+\mathrm{i_{eff}})^{n})-1} \tag{3.26}$$

$$\mathrm{LC_{O\&M}} = \mathrm{C_{O\&M}} \times \mathrm{CELF} \tag{3.27}$$

$$\mathrm{CELF} = \left(\mathrm{K_{O\&M}} \times \frac{1-\mathrm{K_{O\&M}^{n}}}{1-\mathrm{K_{O\&M}}}\right) \mathrm{CRF} \tag{3.28}$$

$$\mathrm{K_{O\&M}} = \frac{1+\mathrm{r_n}}{1+\mathrm{i_{eff}}} \tag{3.29}$$

where investing cost is C_{inv}, n is plant lifetime, CRF is the capital recovery factor, $C_{O\&M}$ represents yearly operation and maintenance expense, CELF is the constant escalation laterization factor, i_{eff} represents the effective discount rate and r_n is the nominal escalation rate.

3.5 Materials and Methods

3.5.1 HPVTEG Hybrid System Description

A hybrid HPVTEG system paired with water-cooled heat exchangers was fabricated to study heat recovery and cooling of a PV panel and capture of a greater portion of the solar spectrum. This is one option to improve the efficiency of PV technologies [147-150]. Figure 3-2 depicts the configuration of the hybrid system, which consists of two solar panels mounted on an iron structure that is tilted at a 33° angle towards the south.

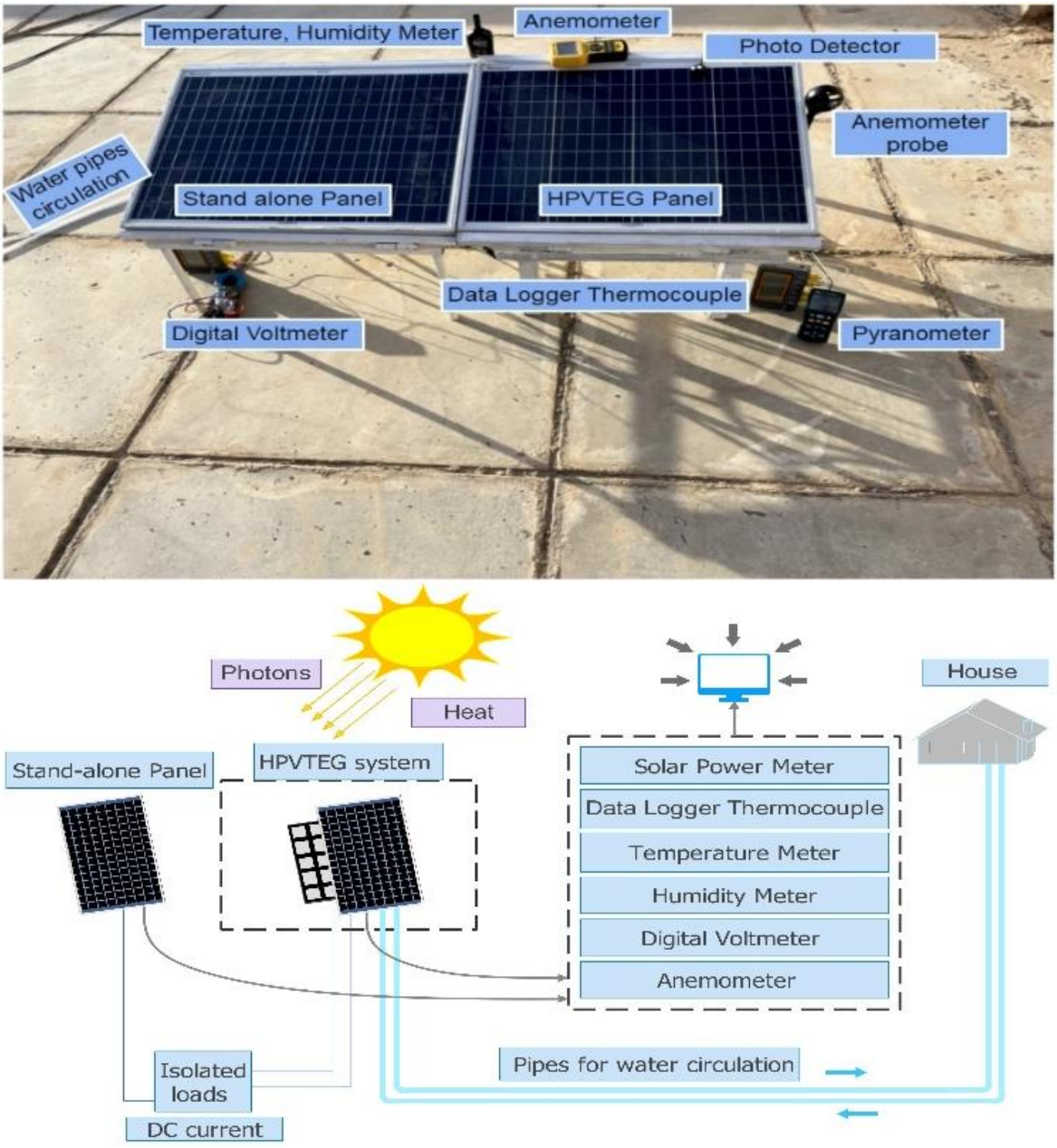

Figure 3-2 The proposed system, (a) experimental setup system with measurement devices, (b) schematic diagram of the experimental system

3.5.2 Main and Subsystem Components

3.5.2.1 PV panel

The PV plays a crucial part in determining the system's final output. Two of the polycrystalline PV panel, manufactured by Fortuner, chosen for this experiment have a nominal maximum power of 50 W, a power coefficient of 0.004/K and an efficiency of 14.51% under standard test conditions (STC:AM=1.5, 1000 W/m^2; cell temperature, 25°C). Table 3-2 highlights PV panel properties [150].

Table 3-2 PV panel properties

Property	Units	Value
Model Area ($\boldsymbol{A}$)	m^2	0.36297
Irradiance ($\boldsymbol{I_{SA}}$)	mw/cm^2	99.96
Maximum Power Voltage ($\boldsymbol{V_{mp}}$)	V	18.0352
Open-circuit Voltage ($\boldsymbol{V_{oc}}$)	V	22.4289
F.F	-	77.2
Maximum Power Current ($\boldsymbol{I_{mp}}$)	A	2.8831
Short-circuit Current ($\boldsymbol{I_{sc}}$)	A	3.003
Peak Power ($\boldsymbol{P_{mp}}$)	W	51.9975
Module eff. ($\boldsymbol{Stc}$)	%	14.51

3.5.2.2 Thermoelectric Generator (TEG Module)

A semiconductor-based device, known as a thermoelectric generator (TEG), serves as a tiny generator using the Seebeck effect when a temperature differential is applied to its surfaces. TEG modules made from bismuth-telluride (BI_2 T_3) are employed to produce the require power. These modules were created specifically for power generation. Table 3-3 lists the TEG module characteristics [110, 118] .

Table 3-3 Thermoelectric module properties

Property	Units	Value
Material	-	bismuth-telluride
Open-circuit Voltage	V	4.8
Operating Temperature	℃	0 to 150
Maximum Temperature	℃	150

3.5.2.3 Poly-methyl methacrylate (PMMA)

Generally, either the heat exchangers or the thermoelectric modules themselves are taken into consideration when optimizing thermoelectric generators [151] [152]. However, since a poor contact or a thermal bridge can undermine the performance of a perfect generator, consideration of the entire assembly of the thermoelectric generator is crucial. This is to control the pressure distribution's impact on the assembly, as well as the thermal contact resistance between the modules, the heat exchangers and the thermal bridge between the exchangers. Poly-methyl methacrylate (PMMA), an acrylic, was considered with dimensions of 142.5 × 455 mm2. It has specific qualities that make it a good material for use under a variety of applications. This thermoplastic is ideal for joining TEG pieces to aluminum sheets to sandwich a PV module, due to its excellent thermal insulation properties and high resistance to temperature changes [153].

3.5.2.4 Heat exchanger cooling

An aluminum water block was utilized to dissipate heat from the cold side of the TEG and rear PV panel. The dimensions of each piece are 40 x 240 x 10 mm^3. The heat exchanger parameters and some characteristics of water are shown in Table 3-4, where these values were extracted using numerical analysis in an ANSYS program during our earlier work [154] .

Table 3-4 Heat exchanger parameters and water properties

Parameters	Symbols	Unit	Value
Mass flow rate	$\dot{m}_w$	kg/s	0.030726
Constant gravity acceleration	g	m/s^2	9.81
Specific heat capacity of water	C_{p_w}	$kJ/\,(kg.K)$	4.187
Water-tube inner diameter	D_{tub}	m	7×10^{-3}
Channel height	a_{ch}	m	10×10^{-4}
Channel width	b_{ch}	m	9.6×10^{-3}
Channel length	l_{ch}	m	0.24×10^{-2}
Number of channels for each heat exchanger	n_{ch}	-	3
Thickness of each heat exchanger front surface	δ_{hs}	m	1×10^{-4}
Cross-sectional area of each heat exchanger front surface	A_{hs}	m^2	9.6×10^{-3}
Thermal conductivity of heat exchanger	K_{hs}	$W/\,(mK)$	200

3.5.2.5 Mathematical Modeling for Solar Cell

Due to the fall of solar radiation on the solar cell of a PV panel, electricity is created. Nevertheless, of the energy produced by solar radiation, only 47% is converted into electricity, and the rest will be the heat loss that negatively affects the solar PV panels, which decreases the lifetime of a plant. The VOC is the open-circuit voltage when the current is zero, and Isc is the short circuit current when the voltage is zero, which defines the maximum power theoretically [155]. The I-V equation of solar cell is expressed in the Equation 3.30 [156].

$$I_{total} = I_0 \left(e^{\frac{av}{nkt}} - 1 \right) - I_l \qquad (3.30)$$

here, $I_l = qAG\ (L_n + L_p + W)$ represent the light generated current that shows that the carriers produced inside the volume of cross-sectional area A as well as the length $(L_n + L_p + W)$.

Parameters such as fill factor (FF), V_{OC}, I_{SC} and efficiency (η) are used to compare solar cells. The V_{OC} depends on the PV panel's temperature, this can be seen from Equation 3.31.

$$V_{OC} = V_{OC}(T_0) - \left[\frac{E_{g0}}{e} - V_{OC}(T_0)\right]\left[\frac{T}{T_o} - 1\right] - \frac{3kT}{e} In \frac{T}{T_o} \quad (3.31)$$

When the temperature increases by 40 K and T_o = 300 K, then T = 340 K becomes the PV panel's temperature. The Boltzmann constant is k, E_{g0} is the band-gap energy. These can be ignored: $\frac{T}{T_o}$ = 0.125 and $\frac{3kT}{e} In \frac{T}{T_o}$ = 10 mV. V_{OC} varies with temperature as presented in Equation 3.27. Where E_{g0} = 1.21 eV and T = 300 K and V_{OC} = 0.55 V, which is a characteristic of a silicon solar cell, it reduces in V_{OC} with a rise in T of $\frac{dV_{OC}}{dT}$ = -2.45 mVK^{-1} at 25 ℃ [157] .

$$\frac{dV_{OC}}{dT} = -\frac{\left[\frac{E_{g0}}{e} - V_{OC}(T_0)\right]}{T_O} - \frac{3kT}{e} \quad (3.32)$$

3.6 Materials and Methods

3.6.1 Experimental Setup

This section presents the techniques and materials required to fabricate the experimental setup and techniques to record the experimental data.

3.6.1.1 Thermoelectric Module

It is necessary to take advantage of the heat produced during PV cell operation and ensure that the hybrid system performance is better than that of the non-hybrid systems. Two electrical configurations were considered for thermoelectric generators.

3.6.1.1.1 Experiment 1: Configuration-1-SP

Series and parallel array configurations (Configuration-1-SP) with twenty thermoelectric generators are suggested. This configuration used two groups of ten TEG modules connected in series. Then, the two groups were connected in parallel. Figure 3-3 shows an equivalent circuit for this configuration.

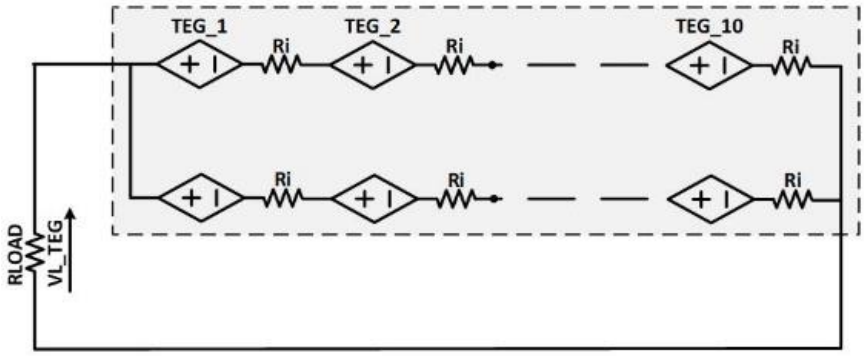

Figure 3-3 Equivalent circuit of the Configuration-1-SP thermoelectric generator

3.6.1.1.2 Experiment 2: Configuration-2-SP

In Configuration-2-SP, groups with two TEG modules are connected in series. Then, ten groups were connected in parallel. Figure 3-4 depicts the equivalent circuit of this configuration.

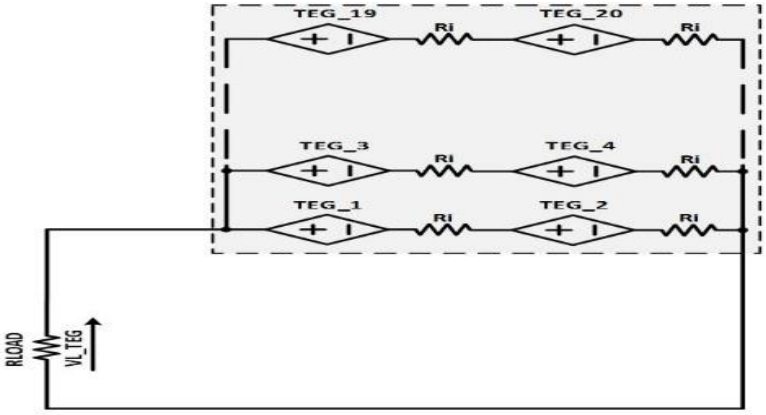

Figure 3-4 Equivalent circuit of a Configuration-2-SP of thermoelectric generators

Then, Configuration-1-SP was considered in this work. This configuration is used to make the internal resistance, R_in, approximately equal to the external load, to improve electrical performance, since the maximum power can be achieved when (Rin is R Load).

3.6.1.2 Assembly of the HPVTEG System

As shown in Figure 3-1 above, assembly used TEG modules attached to a sheet of aluminum 6061, affixed to the rear of the PV panel with thermal paste. Four heat exchangers are attached underneath each group of five TEG modules. These heat sinks are attached to the TEG modules using thermal paste to improve heat transfer. Finally, thermoplastic PMMA was used for joining the TEG to the PV module, fixing it to the frame. Silicon water tubes were used to connect the heat sinks to a tap water source. Tap

water was selected as a cooling fluid because it is readily available in homes and there is no need for a circulation pump. It is quite suitable for heat transfer due to its low cost and high heat capacity. The water was flowed with at an approximately constant flow rate (2.56 l/min) at about 23 ℃ throughout the experiment. The water circulates through the heat exchanger and is returned to the homes.

The temperature of the PV cell and TEG hot side that provides the heat input was considered equal through the experiment. The temperatures of the hot and cold sides of TEGs as well as the inlet and outlet water temperatures of their corresponding heat sink were measured using K-type thermocouples. The operating temperature of the solar panel was measured using a separate thermocouple attached to the rear of the PV panel. Measured values from multiple thermocouples are transmitted directly to a microcontroller and saved on an SD memory card.

The approach used in this study is unique and simple. In most studies, the TEGs are individually fixed of the rear side of the panel. In the current study, we attached the TEGs as groups with an electrical configuration appropriate for an individual panel.

The cooling mechanism employed in this study also allows the back of the PV panel to be cooled by the TEG panels, i.e., the cooling block water, since the TEG panels do not cover the entire back surface of the solar panel. The complete experimental setup is provided in Figure 3-5.

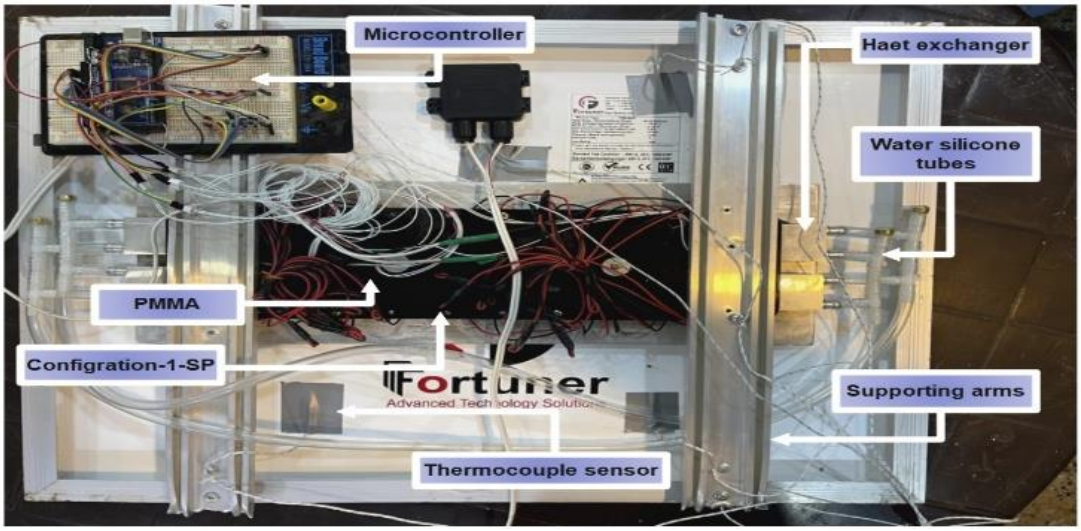

(a)

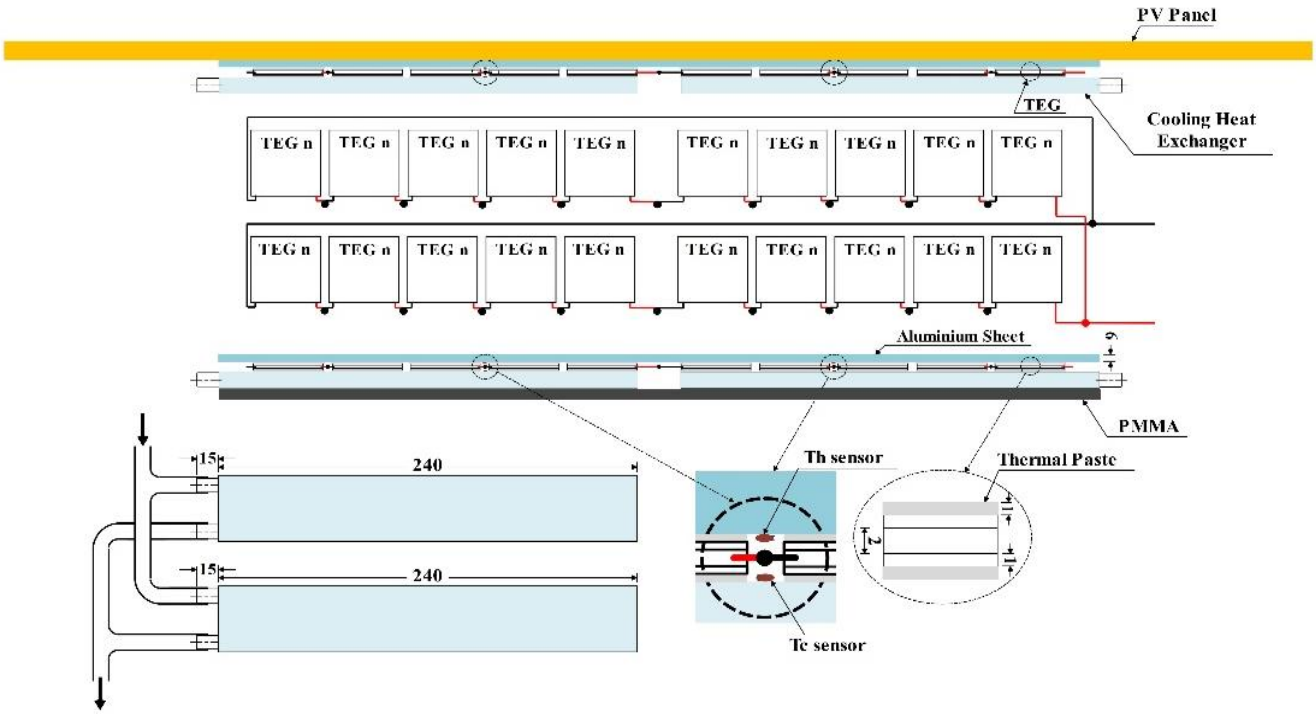

(b)

Figure 3-5 Overview of the experimental setup of the HPVTEG system, (a) final experimental setup with Configuration-1-SP, (b) schematic of the experimental setup

3.6.2 Experimental results and discussion

The experimental results of the TEG and hybrid HPVTEG systems are discussed in this section, as well as the results of the hybrid system compared with a stand-alone PV panel operated under the same conditions. The experiments were conducted in July, during the summer, at Baghdad, Iraq. The geographical coordinates were latitude 33.313o N and longitude 44.331o E. Testing was conducted from 9:00 h to 16:30 h. The measurements were done at approximately 15-minute intervals.

3.6.2.1 Environmental impact and analysis

The radiation profile, relative humidity, wind speed, and air temperature during the testing period are shown in Figure 3-6 and Figure 3-7, drawn using Origin software [158] to develop curves for radiation and temperature. The findings show that solar irradiance increases steadily over time. The average solar irradiance 783.18 W/m^2, peaked at noon with an instantaneous value of 963.07 W/m^2, and began to decline thereafter. The outside temperature, relative humidity, and wind speed averages are 42.61 ℃, 11.70% and 1.88 m/s, respectively. The wind velocity varied from approximately 1.0 to 2.2 m/s.

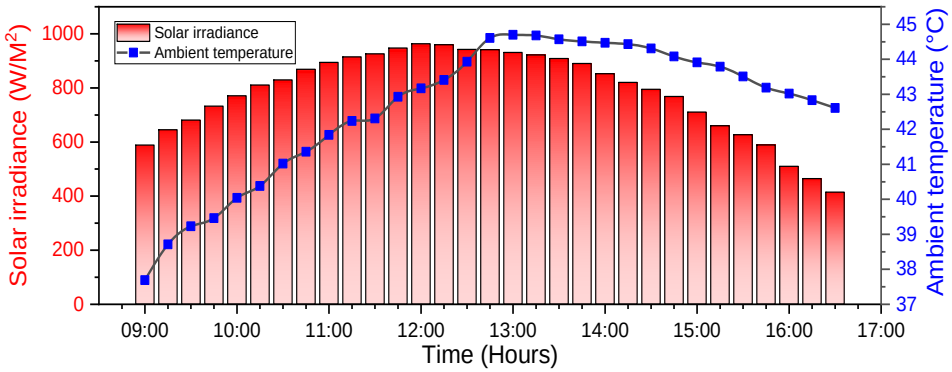

Figure 3-6 Solar radiation and air temperature during the experimental runtime

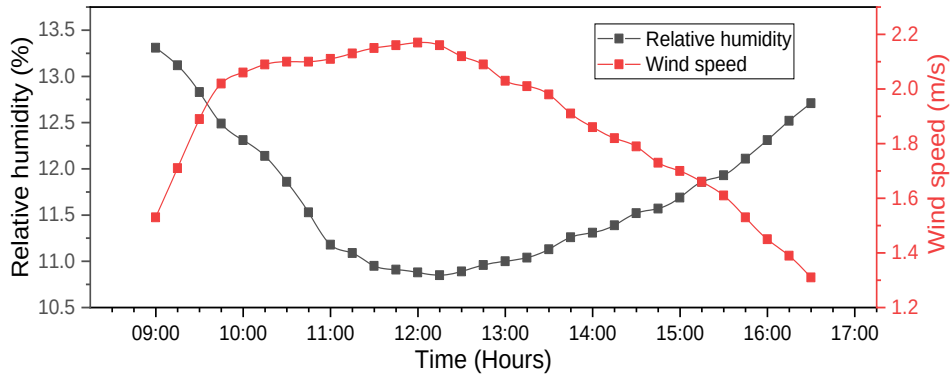

Figure 3-7 Relative humidity and wind speed during the experiments

3.6.2.2 Temperature effects

3.6.2.2.1 Analysis of thermoelectric generator temperatures profile

Since the air temperature peaks at 13:00 h, the hot and cold side temperatures, ΔT, similarly peak at this time and then fall, as illustrated in Figure 3-8. The TEG hot side (T_h) showed high and low temperatures of 51.49°C and 35.08°C, respectively, with an average temperature of 44.97°C. When the experiment first begins, (T_c) is low on the cold side. After noon, it gradually diminishes since heat has accumulated in the water and has reached equilibrium. Low and high cold side temperatures were 24.88°C and 27.55°C, respectively, with an average temperature of 26.71°C. The temperature difference (ΔT) between the hot and cold sides of the ranged between 10.21°C and 24.06°C, respectively, with an average temperature difference of 18.25 °C. These temperatures were measured using thermocouples and a microcontroller to provide more precise results.

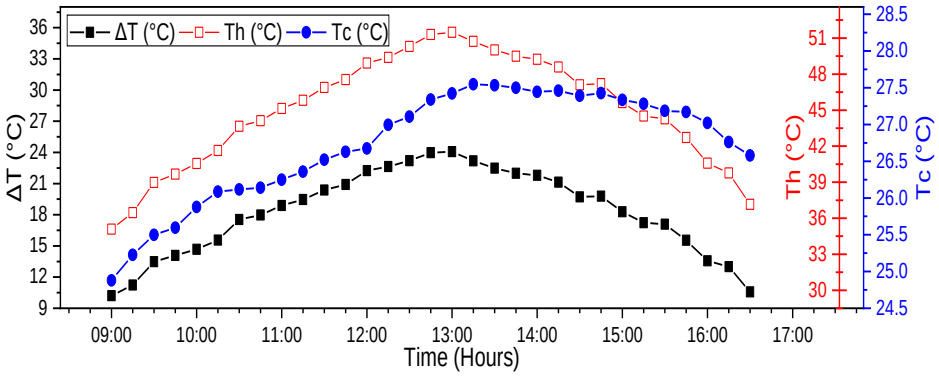

Figure 3-8 TEGs hot side and cold side temperatures, with temperature differentials at various times

3.6.2.2.2 HPVTEG System Temperature Profiles

The PV panel temperature is a crucial component since it determines system performance. Figure 3-9 displays a temperature-time curve for HPVTEG and stand-alone systems. Each PV panel has five K-type thermocouples installed in various places to provide measurements every 15 minutes.

According to Figure 3-9, the temperature of the HPVTEG system and stand-alone PV panel increased throughout the day until it reached a maximum at 13:00 hours. The HPVTEG system's maximum, minimum, and average temperatures during the testing were 51.49℃, 35.08℃, and 44.97℃ and 67.76℃, 52.86℃, and 60.98℃ for the stand-alone panel, respectively. This drop represents a 16.01℃ cooler operating temperature for the HPVTEG system compared to a stand-alone module.

This reduction is significant, especially considering that this process uses little circulation water to remove heat from the cold side of the TEGs and no electricity is used to cool the PV module. As a result, this system can be used in regions with readily accessible tap water or as geothermal technology in areas that lack water.

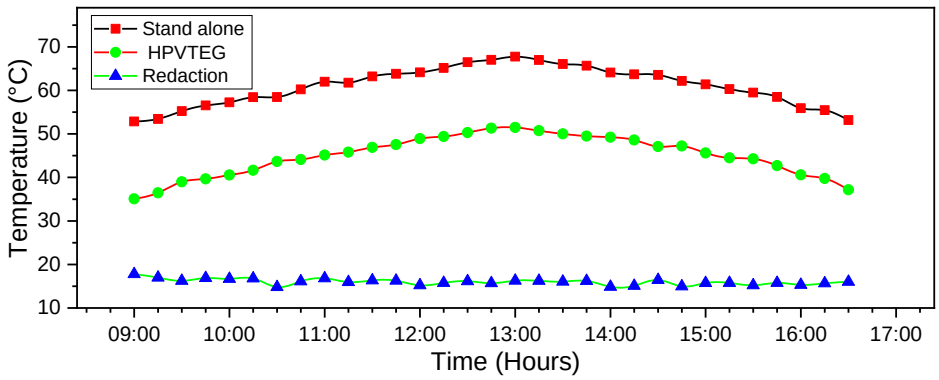

Figure 3-9 PV modified and stand-alone PV panel temperatures as a function of time

3.6.2.2.3 Heat Exchangers

The input and output water temperature profiles of the four heat exchangers are shown in Figure 3-10. Input water temperatures were approximately constant, about 23℃, during the experiment. The output water temperature is greater than its input temperature, as shown in this figure, as a result of increased TEG cold side temperatures, which averaged 25.92 ℃ with a maximum value of 26.79℃. The output water temperature peaks at 13:15 h hours, the same time as the cold-side TEG temperature, but there was a 15 minute lag in the PV panel's peak temperature since its cooling water was slower to lose heat.

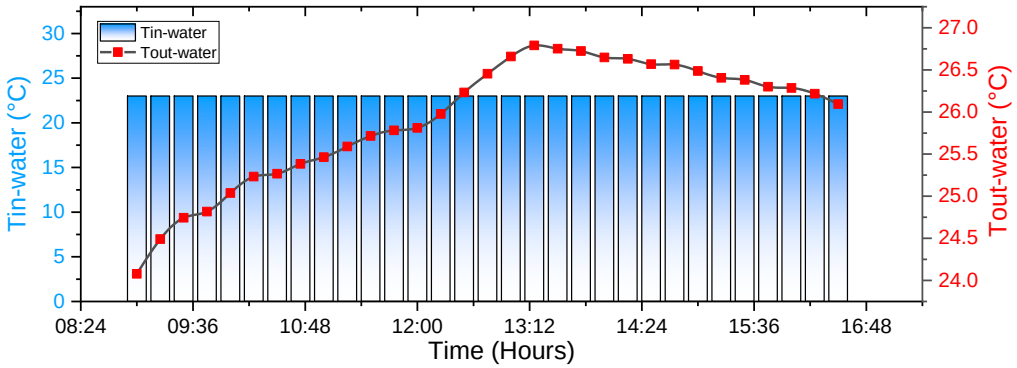

Figure 3-10 Input and output temperatures of a heat exchanger as a function of time

3.6.2.3 Electrical Energy Assessment

3.6.2.3.1 Thermoelectric Generator Configuration Analysis

Figure 3-11 shows the power and efficiency results from the two TEG electrical configurations. Since the temperature was the same for each setup during the experiment, the power extracted and efficiency varied, with Configuration-1-SP achieving the highest performance. This arose from the type of TEG electrical connections. According to the findings, the average output power and efficiency of configuration-1-SP were 1.24 W and 0.51%, while they were 0.20 W, 0.08% for Configuration-2-SP, respectively.

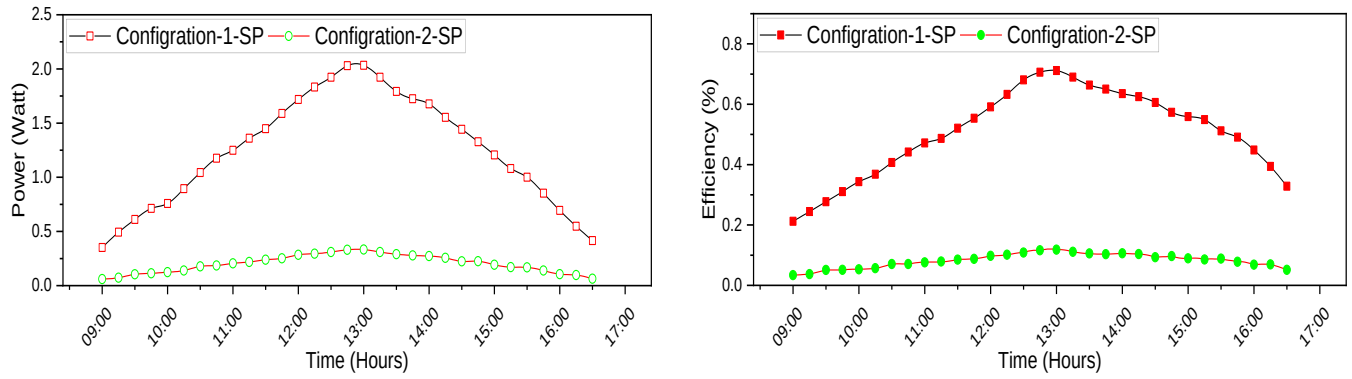

(a) (b)

Figure 3-11 Electrical configurations of TEGs, (a) output power vs. time, (b) efficiency vs. time

3.6.2.3.2 HPVTEG System

Figure 3-12 and Figure 3-13 display the output power and efficiency values for the HPVTEG system and stand-alone panel. The statistics show that at 12:00 h, the HPVTEG system maximum power output was 39.97 W, while the stand-alone panel peak power was 33.99 W. However, since the stand-alone panel operates at a relatively high temperature, it suffers a power reduction. Throughout the testing, the HPVTEG system and the standalone panel average power values were 32.76 W and 28.06 W, respectively. The HPVTEG system shows an average improvement of 16.7%.

The efficiency of the systems under test are shown in Figure 3-13. As the day progresses, both the HPVTEG system and the stand-alone panel overall efficiency values rise. Until midday, solar insulation helps both panels' efficiency rise. However, they begin to decline after noon as a result of increased panel temperatures and a decline in the intensity of solar radiation. The HPVTEG has an average efficiency of 13.86% compared to the PV stand-alone system, 11.90%. Electrical efficiency for the HPVTEG system has been improved by roughly 16.4%.

Since the hybrid system used TEGs and heat exchangers, this efficiency improvement is very significant. This resulted in a decreased panel operating temperature that enabled more power extraction from the TEGs.

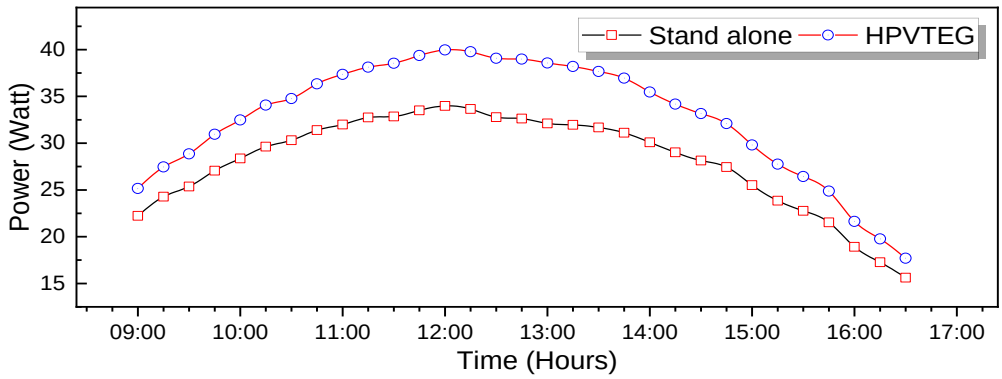

Figure 3-12 Output power of the HPVTEG and stand-alone PV systems

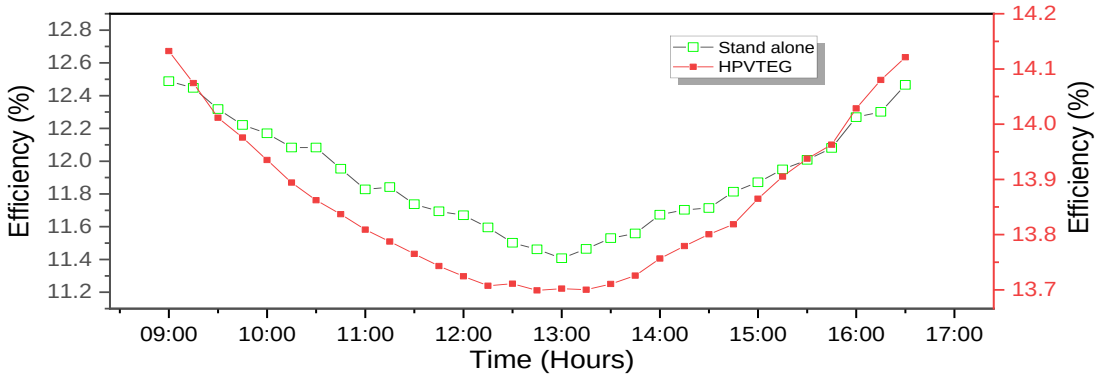

Figure 3-13 Electrical efficiency vs. time the HPVTEG and stand-alone PV systems

3.6.2.4 Exergy Efficiency Assessment Analysis

Figure 3-14 displays the exergy efficiency results from the HPVTEG system and standalone PV panel. The power output of a power plant has a negative impact on its energy efficiency. The profiles for the energy efficiency for the two systems can thus be observed from the data since they are similar to those for electrical efficiency.

Exergy efficiency decreased from the beginning of the experiment until about 13:00, when it began to rise due to increased PV module temperatures. The HPVTEG system's exergy was consistently greater throughout the testing indicating that the suggested hybrid system can be used to control PV module temperature.

As a result, the average exergy efficiencies for a HPVTEG system and a stand-alone PV panel, respectively, are 12.79% and 10.98%. It is clear from the data that the modified PV panel had higher exergy efficiency.

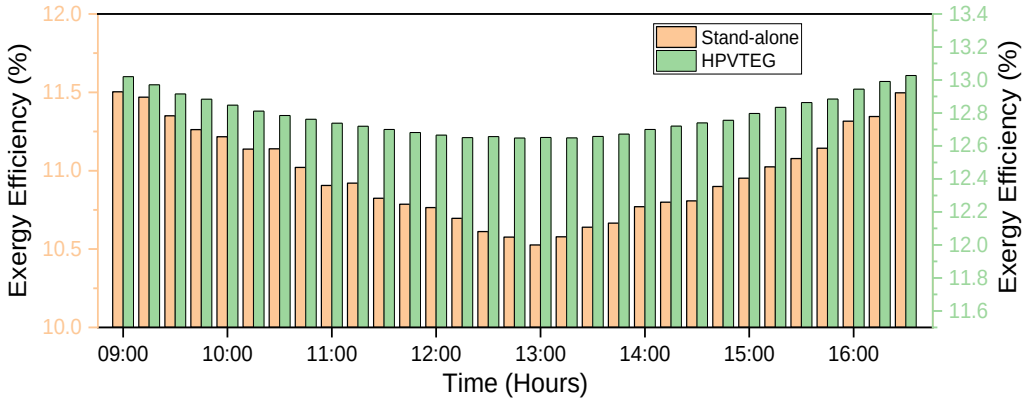

Figure 3-14 Exergy efficiency of stand-alone and HPVTEG systems vs. time

3.6.3 Examining the System in Relation to another Research

Table 3-5 compares our findings with the research discussed above and other studies. Generally, the outcomes are superior or equivalent to systems described in prior investigations.

Table 3-5 Comparison of the current system to previous studies

Ref	Improvement Mechanism, material	Study type	P_{tot} of PV-TEG, Change, W, Improvement, %	Eff_{tot} of PV-TEG, increase , Improvement, %
[115]	Concentrating PV-TEG, (Single junction GaAs Bismuth telluride)	Experiment	N/A	From 22.5% to 23.2% (Improvement, 3.11 %)
[116]	PV-TEG-Nanofluid- Phase Change Material, (Polycrystalline silicon, Bi2Te3)	Experiment	From 2.93W to 4.18W (Improvement 42%)	Improvement, 15.8%
[117]	PV-TEG-Water, (Polycrystalline silicon, Bi2Te3)	Experiment	From 8.49W to 9.56W (Improvement 12.6%)	From 13.82 % to 15.6% (Improvement, 12.8 %)
[118]	PV-TEG-Beam Splitter system, (Amorphous silicon (a-Si) solar cells, Bi2Te3)	Experiment	From 0.13W to 0.4W (Improvement 2.07%)	From 0.6% to 1.65% (Improvement, 1.75 %)
[108]	Perovskite PV-TEG, (Perovskite Cell, Bi2Te3)	Experiment	N/A	From 16.8% to 19.5% (Improvement, 16.07 %)
[65]	Non-concentrated flat plate PV-TEG, (Multi crystalline solar cell, Bi2Te3)	Simulation	increased by 8.3%	Increased by 6%
[119]	Unconcentrated photovoltaic thermoelectric generator, (Mono silicon PV-Bi2Te3)	Experiment	N/A	Increase in efficiency of 0.06%,
[120]	PV–TE hybrid module, (multi-crystalline silicon,	Simulation	N/A	Increase by 14.7% and 11%

	Bi2Te3)			
[121]	Building-integrated photovoltaic (BIPV)-TEG-PCM system (N/A, Bi2Te3)	Simulation	From 80W to 87W	Increase by 1.09%
[122]	Concentrated PV-TEG, (Multijunction, Bi2Te3)	Experiment and simulation	From 1.797 to 1.895 (Improvement 9.8 %)	From 28.95 % to 30.53% At Concentration factor 205 (Improvement, 5.45 %)
[123]	PV-TEG system, (Polycrystalline silicon, Bi2Te3)	Experiment	Improvement 19%	Increase by 17%
[124]	-PV-TE, (c-Si cell, N/A) -PV-TE, (GaAs cell, N/A)	Simulation	N/A	From 9.5% to 11.07% (Improvement, 16.5%) From 21.91% to 22.94% (Improvement, 4.7 %)
[125]	PV-TEG, (Perovskite cell & BI2TE3)	Simulation	N/A	From 17.8% to 18.6% (Improvement, 4.49 %)
[126]	PV-PCM-TE, (Single-junction GaAs, Bi2Te3)	Experiment	N/A	From 13.43% to 13.45% (Improvement, 0.14 %)
Current	Unconcentrated HPVTEG-Water, (Polycrystalline silicon , Bi2Te3)	Experiment	From 28.06 to 32.76 Improvement,16.7 %	From 11.9 to 13.86 (Improvement, 16.4 %)

3.6.4 Cost Analysis

The main production expenditures in the proposed HPVTEG system are heat exchangers and thermoelectric generators, requiring two sets of TEGs at a price of US $15.2, and four of heat exchangers at a price of US $2, based on year 2022 data. Overall, the PV-TEG system and associated equipment costs US $71.2 with a solar panel price of US $54.

This study considered two possibilities for the energy produced by the power plant.

I. The first case entails circumstances in which the power plant operates year-round with no bad weather. Every day of the year is used to produce electricity in this case.

II. The second case also considers a situation with favorable weather for only a portion of the year, such as that in Iraq. This considers Iraq's eight-month summer season, or 240 days, as productive in this case.

Assumptions were made that the panel will be exposed to solar radiation for ten hours a day for 365 and 240 days, respectively. Energy output from the HPVTEG power plant and stand-alone panel in the first and second cases was (120.09 kWh, 78.96 kWh), and (102.42 kWh and 67.34 kWh) respectively. Then, we used the information in Table 3-6 to determine the LCOE of both systems.

Table 3-6 Calculation of LCOE parameters

No.	Parameter	HPVTEG	Stand-alone
1	Investment cost (C_{inv}), \$	78.8	54
2	Annual operation and maintenance cost ($C_{O\&M}$), \$	3.5	3.5
3	Effective discount rate (i_{eff}), %	5	5
4	Lifetime of the plant (n), years	30	30
5	Nominal escalation rate (r_n), %	1	1
Calculated parameters			
6	Capital recover factor (CRF), %	6.5	6.5
7	$K_{O\&M}$	0.96	0.96
8	Levelized cost of fuel (LC_{fuel}), $\$/kWh$	0	0
9	Constant-escalation laterization factor $O\&M$, ($CELF$)	1.1	1.1

According to the calculations, the HPVTEG system LCOE in the first case, with 365 days of production, was 0.06681 US $ /kWh as opposed to 0.06741 US $/kWh for the stand alone PV panel. Additionally, the HPVTEG hybrid system showed an LCOE of 0.10160 US $/kWh for the second case with 240 days of production, opposed to 0.10251 US $/kWh for the stand-alone PV panel.

These data clearly show that the HPVTEG hybrid system outperformed the stand-alone PV panel in terms of cost under both scenarios, despite the additional costs associated with integrating TEG with PV panel. This implies that adding the suggested TEG mechanism to a PV module will increase its cost-effectiveness in addition to improving its electrical and exergy efficiency.

3.6.5 Conclusion for Chapter Three

TEGs and heat exchangers were used to improve the functionality and lower the operating temperature of a PV panel while using the whole solar spectrum to in an HPVTEG system. The current research enables the following conclusions to be drawn:

I. Efficiency and output power are significantly improved using the HPVTEG system. This results from the HPVTEG system's use of water as a cooling medium, rather than unstable and variable cooling sources. This system is independent, economical, and has no complicated mechanisms.

II. The use of poly-methyl methacrylate (PMMA) board serves three functions, cohesion as well as good pressure distribution and insulation. This led to improved power from the TEG modules.

III. There was an average temperature difference (ΔT) of 18.25 °C between the hot and cold sides of the TEGs.

IV. During experimentation, the average HPVTEG system temperature was 44.97 °C, compared to 60.98 °C for the standalone PV panel. Thus, using the TEG module with cooling resulted in an average temperature that was 16.01 °C lower for the HPVTEG system.

V. During the experiments, the water average temperature at the exit of the heat exchanger was 25.92 ^{o}C.

VI. Among the TEG configurations, the average power and efficiency for Configuration-1-SP were 1.24 W W and 0.51% whereas those for Configuration-2-SP were 0.20 W and 0.08 %, respectively.

VII. The average power output for the HPVTEG system was 32.76 W, whereas that of the stand-alone PV panel was 28.06 W. The increase in electricity generation is 4.7 W total, an average improvement of 16.7%.

VIII. The average efficiency of the HPVTEG system was 13.86 %, while the efficiency for a stand-alone PV panel was 11.90 %. The increase in electricity generation is 1.96% total, an improvement of roughly 16.4 %.

IX. There is a 1.81 % average difference in exergy efficiency between a standalone PV panel and HPVTEG system.

X. Financially, in the first scenario (365 days of production), the HPVTEG system had an LCOE equivalent to 0.06681 US $/kWh compared to 0.06741 US $/kWh for the stand-alone PV panel.

Additionally, the HPVTEG system showed an LCOE of 0.10160 US $/kWh for the second case (240 days of production) compared to 0.10251 US $/kWh for the standalone PV panel.

In practice, the HPVTEG mechanism has shown to be technologically and economically better. The proposed hybrid mechanism shows the lowest LCOE due to its high efficiency, even if when its modifications came at an additional cost.

According to the findings of this study, it is possible to use the suggested cooling mechanism and the TEG module in hot climates, like that in Iraq, to improve solar PV panel performance and produce more power.

More TEGs might be utilized to cover the back of the solar panel, but future research should also consider the financial implications of this action. Future research may look towards using a nano-fluid rather than water to dissipate more heat from the PV panel.

CHAPTER FOUR: MODELING AND NUMERICAL ANALYSIS

4.1 Preface

The numerical simulation techniques have prevailed for their excellence in solving differential equations and ease of use as long as the formulations for equation discretization and iteration methods are determined. A variety of numerical models were presented in the literature to design, investigate, evaluate, and enhance the TEG performance. These models were split into different categories, some are one dimensional built to seek the characterized nonlinear TE material properties based on regression analysis of TEMs [159]. The others are a three-dimensional models based on commercial software, such as the ANSYS and COMSOL. They make a reliable calculation possible for its easy coupling of nearly all related TEG effects and factors simultaneously. For instant, Wang, Huang [160] introduced a sophisticated 3-D TEG model to assess two common assumptions of constant and variable TEG properties. With these techniques, the TEG geometric optimization and performance improving become an easy, practical, and more cost effective task.

This chapter employs a computational fluid dynamics (CFD) model is developed for a thermoelectric generator consists of five TEG modules embedded between two aluminum blocks. The upper block collects the solar energy and heats the hot side of the modules. The lower block has an internal M-shaped water channel to cool the cold side of the module.

4.2 Numerical Approach

Numerical analysis provides an approximation for real life problems that is hard to solve mathematically. It finds an increasing application in TEG system due to their reasonable approximation of engineering problems that do not has analytical solution. It also provides significant reduction in the time and cost of designing and investigating a real system.

Ruan, Xie [161] developed a fluid-thermal-electric multiphysics coupled model to investigate the performance enhancements of the TEG system using nonfluid. The study simultaneously considered the thermodynamic and thermoelectric performances in the developed model. The nanofluid effects on heat transfer, TEG's electricity generation, and TEC's cooling capability were investigated for varying Reynolds numbers (Re). The analysis demonstrated the validity of the performance improvements, also showed that the enhancement effect increases with the nanoparticle concentration but reduces with Re.

It has been proven that the use of variable area pins (VAPs), and nanomaterials, in place of traditional bulk semiconductor materials, has improved the performance of TEGs. In this regard, Maduabuchi [162] modeled a full nano-enhanced VAP TEG module with a 127 thermoelectric pairs in three-dimensions using ANSYS 2020 R2. The shortcomings of the previous studies on VAP TEGs are also discussed and addressed in this study. Results indicate that the power density and efficiency of the nano VAP TEG are 12x and 6x higher than that of the traditional bulk semiconductor VAP TEG, respectively.

Chen, Wang [42] provided a three-dimensional fully numerical simulation technique to investigate the heat transfer and power generation of a thermoelectric module installed with fin to harvest vehicle exhaust waste heat. The study considers a TEG in a hot channel without fins as well as with plate fins and square pin fins, while a cold channel is used to cool the TEM. The results revealed that installing plate fins or square pin fins can significantly increase the waste heat harvest. Moreover, the optimal number of the square pin fins is 78 which increase the output power of the TEM by 24.14% compared to the plate fins.

4.2.1 Analysis Using Finite Elements Method

Finite Element Method (FEM) is a numerical technique, based on minimization of energy, developed to solve complex engineering problems by converting the governing differential equations of the physical phenomenon into algebraic equations that can be numerically solved [163]. To analyze the human wrist heat harvesting using bismuth telluride-based TEG, [164] used the finite element method to investigate the performance of the TEG. The actual heat harvesting environment from the human wrist was developed during the simulation. Based on the analysis, an output voltage and power of 40.7 mV and 4.245 mW, respectively, were obtained from the proposed TEG module at a temperature gradient of 12.5 K. Besides, the generator was able to produce a maximum power efficiency factor of 0.66 $\mu Wmm^{-2} K^{-2}$. The output of the developed wearable TEG could be improved by employing more thermocouples.

Selimefendigil, Öztop [165] used the finite element method to provide an assessment for the shape effects of TEG performance characteristic during alumina-water nanofluid convection. Triangular, rectangular, different configurations were modeled in the study where the interface temperatures of hot and cold side are varied by changing the cavity shape, opening ratio (OR) and Reynolds number (*Re*). The results showed that the highest hot side temperature is obtained with l-shaped cavity followed by U, T and R-shaped cavities. Further, by using the T, L and U shaped cavities, the increase in the power are determined as 38%, 78% and 76% at *Re*=1000 compared to the rectangular cavity.

Potirniche and Barannyk [166] presented a coupled thermoelectricity nonlinear model model and implemented it in the finite element method. The model considered the Seebeck, Peltier and Thomson effects in thermoelectric materials within the framework of the coupled thermal and electrical behaviors governed by the Fourier and Ohm's laws. The model is verified by comparing its predictions with analytical results obtained from the system of ordinary differential equations that represent the simplified model for the one-dimensional case. Then, the finite element model is applied to estimate the energy conversion performance of nanostructured thermoelectric materials compared with that of traditional bulk materials. The study showed the excellent behavior of nanostructured materials in terms of their power output and conversion efficiency. The analysis also demonstrated the advantages of developing nanostructured thermoelectric materials for increased performance and miniaturization.

4.2.2 Analysis using Computational Fluid dynamics (CFD)

Eldesoukey and Hassan [167] developed a three-dimensional model of thermoelectric generators (TEGs) by using CFD modeling. The solution of the model was performed using three-dimensional (3D) numerical solution and User defined function (UDF) of the ANSYS-Fluent software. The model was used to investigate the effect of the performance of the TEG mounted on a chimney wall, and the velocity of the hot flow gasses and coolant air on the heat transfer and generated output power. The results showed good agreement between the presented 3D model and the experimental results. Further, increasing the hot gases inlet velocity without increasing cooling air velocity or vice versa did not affect the TEG output power. Also, the heat transfer of the cold side of the TEG was found to be more effective on the TEG output power compared to the hot side.

Chen, Lin [168] developed an advanced simulation method by integrating CFD and a thermoelectric module (TEM) where the TEM is modeled as a heat sink to absorb waste heat from flue gases. The study evaluated the influences of the convection heat transfer coefficient at the cold surface, Reynolds number, dual TEM, gas inlet temperature, and channel geometry on the TEM system performance. The study findings provided a measure in increasing the performance with rising the Reynolds number, flue gas inlet temperature, and convection heat transfer coefficient at the cold surface. Moreover, the results showed that the dual TEM can produce an additional 43% power when compared with the single TEM. Modifying the channel geometry raises the flue gas velocity at Re = 1,000 can increase the output power and efficiency by 53.5% and 25.2%, respectively.

Shen, Gou [169] built a three-dimensional TEG dynamics solver (TEGFoam) based on the open-source CFD software. The TEGFoam is able to define the complete process of flow, electricity conversion, and heat transfer in detail. TEG solver and the proposed model were verified with experimental date. The verification process results revealed that the numerical model can reproduce the TEG system characteristics. Compared with the low-dimensional model, the 3D numerical simulation modeling using the TEGFoam solver can obtain more accurate system characteristics, and can deliver useful basic data of the TEG structure and its operation mode. Also, the TEGFoam is applicable for TEG structural designing, and TEG optimization operation.

Qing, Chen [170] proposed a high- and medium-temperature coupled TEG system operated by a combustion heat source. A novel burner with baffle is also proposed to augment the heat transfer between the hot side of TEG and the fired gas. A 2D CFD model was used to optimize the geometrical dimensions of the new burner. The model comprises the flow, combustion reactions, and heat transfer in simplified TEGs. The results showed 73K increase in the inner-wall temperature of the high-temperature TEG module. Further, an improvement of 42.48% and 3.38% were reported for the TEG system's power generation and conversion efficiency, respectively. The 2D model was further developed, during the study, using an equivalent thermoelectric effects model of segmented high-temperature TEG for further improvement for the high temperature TEG performance.

Montserrat, Cózar [171] studied the influences of design parameters of finned heat sinks on the TEG net output power. The design comprises a cooling fan; therefore the net output power is equal to the power generated by the TEG minus the power absorbed by the fan that supplies air into the forced convection system. The study was conducted using the CFD simulations in the multi-physics commercial software ANSYS. An experimental data was used to validate the model prediction; the results showed that, for a constant heat sink exchange area, a better performance is achieved with fin thicknesses greater than 1 mm.

Qasim, Velkin [154] developed a CFD model for a TEG system consists of five TEG modules embedded between two aluminum blocks. The upper block collects solar energy and heats the hot side of the modules, while the lower block has an internal M-shaped water channel to cool the cold side of the modules. The model was validated by comparing it outcome with previously published experimental data. The model was then used to investigate the effects of various solar collector block thicknesses and different water flow velocities on the TEG-generated voltage and efficiency. The study concluded an inverse relationship between the thickness of the solar-collecting mass, the efficiency of the system, and the heat flux. However, the relationship was proportional to the velocity of water flow.

4.3 CFD Modeling of the TEG for Power Generation

4.3.1 Model Design and Theoretical Background

Thermoelectrics are solid-state devices that perform energy conversion using the Seebeck effect. According to Zhao, Wang [102], the temperature difference between the hot and cold junctions is the driving force of the Seebeck effect to produce a potential difference across the load. Figure 4-1a illustrates use of a TEG module, and Figure 4-1b demonstrates its fundamental design, where heat flux, αIT_h, is collected by the hot junction, and αIT_c is ejected at the cold junction. The TEG process is also associated with the Joule effect, heat leakage, and Thomson effect. The latter exhibits the lowest impact on the TEG output compared to the others. Therefore, it is usually neglected in modeling. Table 4-1 provides the basic specifications of the considered TEG module.

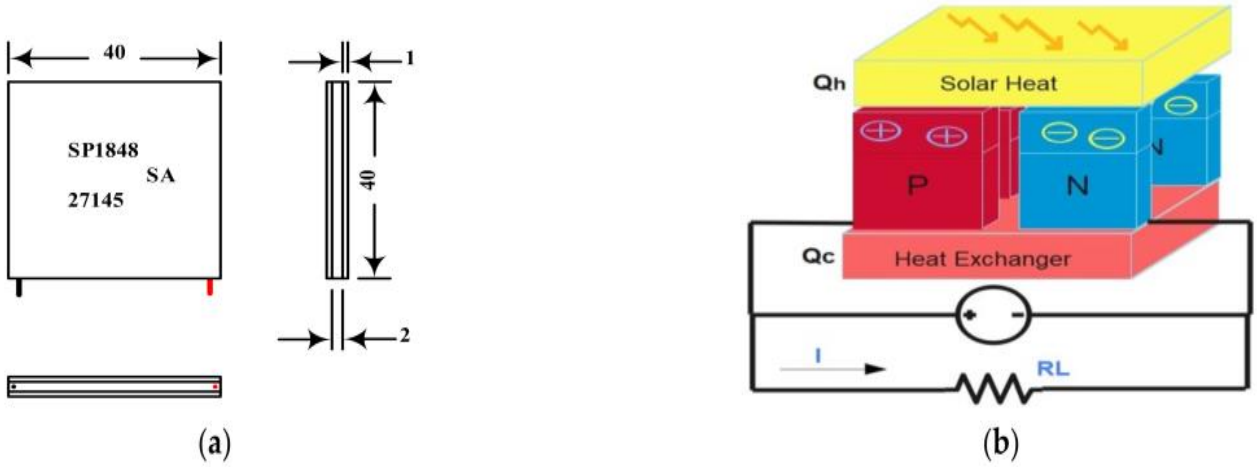

Figure 4-1 (a) Geometry of the module, (b) the basic structure of a TEG

Table 4-1 Specifications of the TEG SP1848-27145 module as given by [41, 172]

Specification	Value
Material	Ceramic/Bismuth Telluride
Color	White
Temperature (^oC)	150
Open-circuit voltage (V)	4.8
Short-circuit current (mA)	20/0.97/225; 40/1.8/368; 60/2.4/469; 80/3.6/559; 100/4.8/669
Module size (L × W × H)	40 × 40 × 4 mm^3
Weight	25 gm

4.3.2 Model Design

To generate power, the hot surface of a TEG must absorb enough heat while the cold surface remains at a lower temperature. A temperature difference triggers the Seebeck effect to convert heat into electricity. The Workbench ANSYS program was used in this study to build a TEG model. It consists of a solar-heat-collecting plate, 5-TEG modules, and a water-cooled aluminum block heat sink (Figure 4-2). The upper part of the device is a block made of aluminum alloy 6063 with dimensions of 240 mm × 40 mm × 16 mm (L, W, H), and it acts as a solar collector. The middle part contains the TEG modules, evenly distributed with 5 mm spacing between the modules. The lower part is a cuboid block made of an aluminum alloy with dimensions of 240 mm × 40 mm × 10 mm (L, W, H). It has an internal M-shaped water flow channel to maximize the heat exchange area for a better cooling effect.

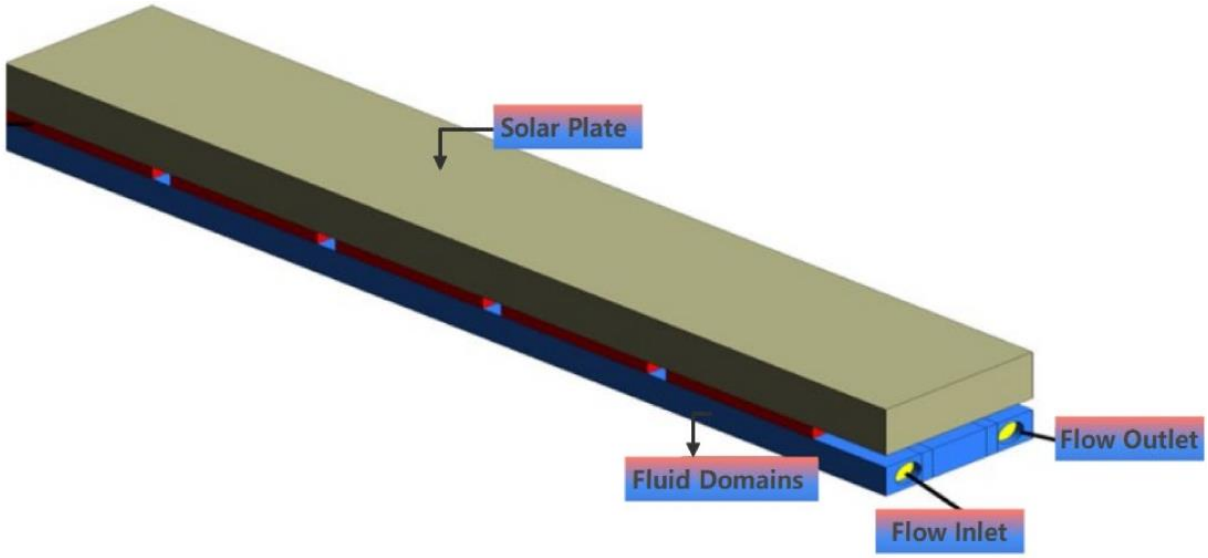

Figure 4-2 The geometry of proposed design

The physical properties of the aluminum alloy used in the design are given in Table 4-2, and the configuration of the cooling block is illustrated in Figure 4-3.

Table 4-2 Physical properties of the aluminum alloy 6063

Property	Value
Density	2.70 kg/m^3
Thermal expansion	23.5 × 10^{-6}/K
Thermal conductivity	200 W/m·K
Electrical resistivity	0.035 × 10−6 Ω· m

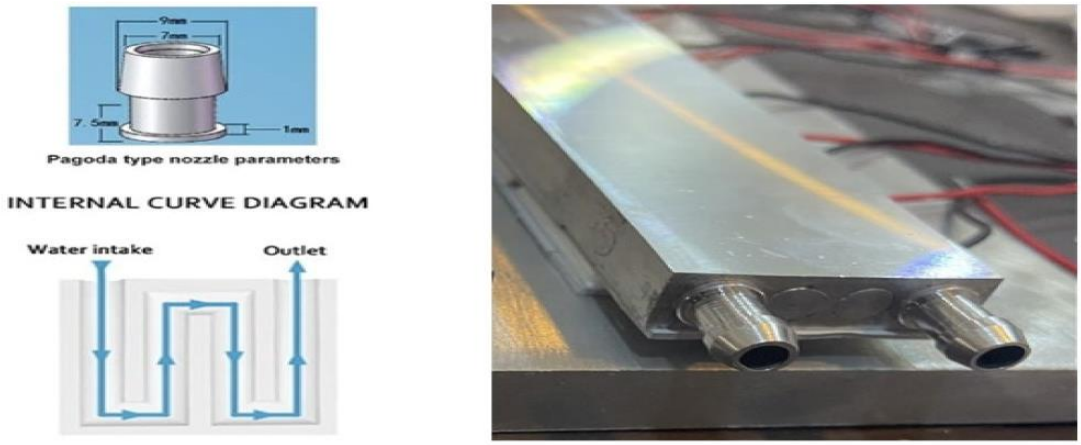

Figure 4-3 The practical configuration of the lower aluminum block with an M-shaped water channel

A 1 mm-thick thermal paste layer was used between both hot and cold surfaces of the TEG module. It provides improved surface contact to ensure good heat transfer from the hot plate to the module, and from the module to the heat sink block.

4.4 Governing Equations

Steady-state flow is assumed in the M-shaped channel with a laminar and incompressible characteristic assumed for the flow field. The governing equations are solved simultaneously. They include the continuity, momentum, and energy equations, as follows [168].

Continuity equation:

$$\nabla.\left(\rho\vec{V}\right) = 0 \qquad 4.11$$

Momentum equation:

$$\rho\vec{V}.\nabla\vec{V} = -\nabla P + \nabla\left[\mu\left(\nabla\vec{V}\right) + \left(\nabla\vec{V}\right)^{T}\right] \qquad 4.12$$

Energy equation:

$$\rho C_P\vec{V}\nabla T = \nabla.(k\nabla T) \qquad 4.13$$

4.5 Boundary Conditions

The simulation adopted the same boundary conditions employed earlier by Qasim, Velkin [41]. Various inlet fluid flow velocities (0.2, 0.4, 0.6, and 0.8 m/s) were used for the cooling block. The temperature was

set to (300 K) with the default viscosity ratio and turbulence intensity. Radiation was the heat transfer process at the solar collection plate surface. Mass and energy conservation were adopted at the outlet. A fixed 1 atm pressure was set at the outlet with a no-slip condition at the channel walls.

4.6 Numerical Approach and Validation

A finite volume method was used to solve the governing Equations 4.12 – 4.14 to calculate the water flow velocity. Thermo-flow numerical analysis was conducted using ANSYS FLUENT CFD code. The energy and momentum equations were solved using a second-order upwind scheme to eliminate potential numerical errors. The momentum and continuity equations were solved first, before flow determination. Then, the energy equation was solved to determine the thermal field in the domain. The procedure continued until the sum of the residuals of the continuity and energy equations reached the converging criteria.

4.6.1 Mesh Study

The analyzed model was entirely discretized with the hexahedral mesh shown in Figure 4-4. This includes the upper solar-collecting plate, the TEG modules, and the lower heat sink block (flow domain).

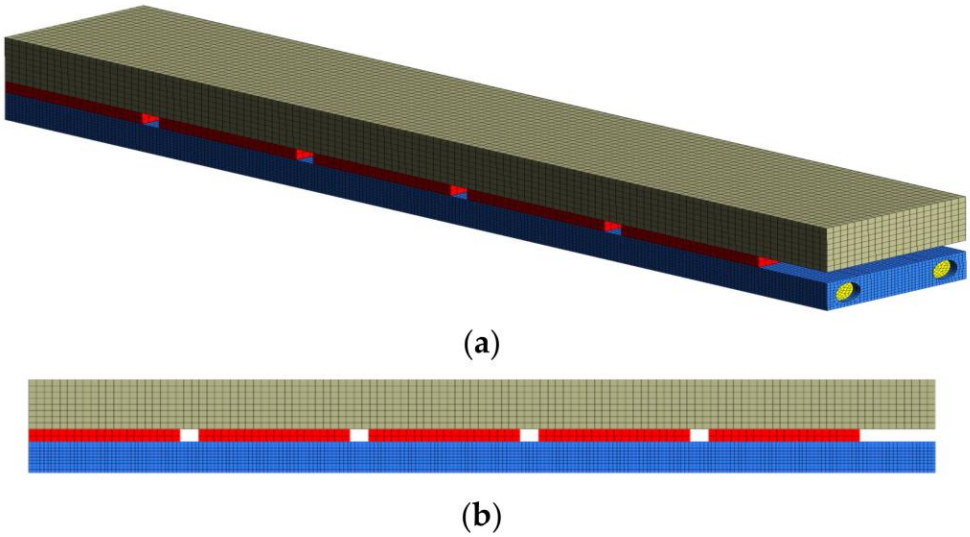

Figure 4-4 (a) Top and (b) side views of structural hexahedral mesh of the CFD model used in this study.

A mesh independence study was performed to determine that the predicted results were independent of mesh size. There was no significant change in the temperature obtained when solving the energy equation. So, pressure and velocity results were chosen instead. Two points were chosen before the outlet to obtain independent mesh values for the velocity and pressure. Figure 4-5 shows the effect of the cell size on

pressure and velocity. Independent pressure and velocity values were obtained for all cell sizes. Here, mesh cell sizes of 1 and 2 mm both reached steady state. However, the solution used a cell size of 1 mm because it reached steady state earlier than the 2 mm cells, as shown in Figure 4-5.

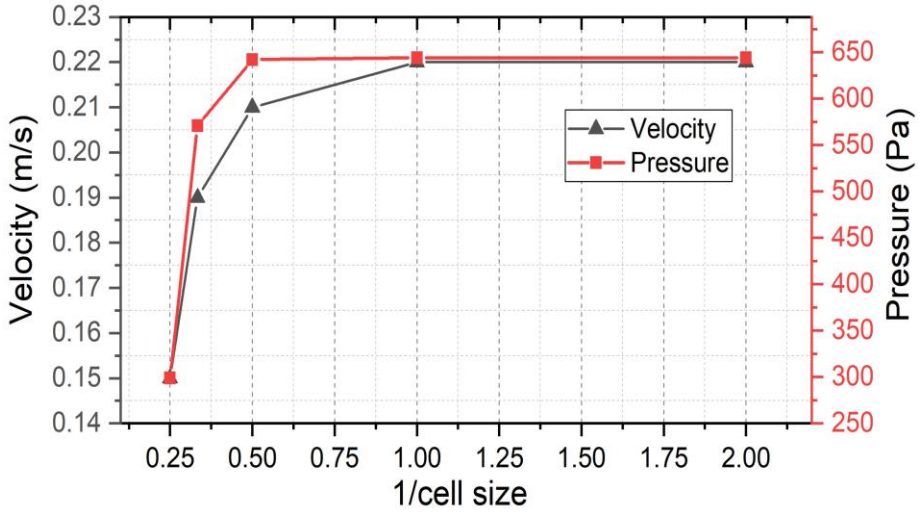

Figure 4-5 The mesh convergence study results

The number of cells corresponding to each examined mesh size is given in Table 4-3 below.

Table 4-3 Number of cells for each cell size

Cell Size	Total number of cells
4.00	4861
3.00	6759
2.00	19,551
1.00	128,474
0.50	964,572

4.6.2 Model Validation

Once the optimum cell size and mesh density were determined, verification processes were performed to confirm the accuracy and reliability of the model. Validation processes were carried out using previously published experimental results [41]. A many-TEG modules, arranged in 30 sections, was investigated in the experimental system. However, using symmetry considerations to simplify the model, only one section was considered in this study. Figure 4-6 shows the experimental model that was validated. The current simulation used the same design and process parameters considered in the experiment. Therefore, this work can be considered valid and has achieved its aim.

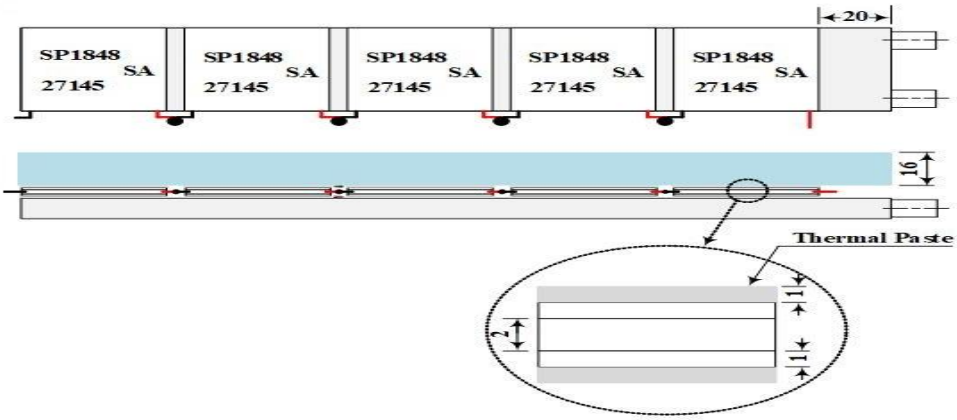

Figure 4-6 A schematic view of one row of the TEG board consisting of two sections, each with 5 modules.

A weighted average area method was used to obtain the temperature values at the TEG hot and cold surfaces. Table 4-4 provides a comparison of the current model predictions and the corresponding experimental data obtained at different times of the day.

Table 4-4 Experimental data and model predictions obtained at different times of the day

Qasim, Velkin [41]				Predicted			
Time	T_h (°C)	T_c (°C)	∇T (°C)	T_h (°C)	T_c (°C)	∇T (°C)	Diff. (%)
11:30 a.m.	51	27	24	51	29	22	8.3
12:30 p.m.	62	32	30	62	31	31	3.3
1:30 p.m.	72	37	35	72	35	37	5.7
3:30 p.m.	63	32	31	63	31	32	3.2

4.7 Results and Discussion

The effects of the solar plate thickness and the flow velocity on the temperature difference, ΔT, between the hot and cold surfaces of the TEG module are presented in this section.

4.7.1 Solar Plate Thickness

Figure 4-7 depicts the effects of four different solar plate thicknesses on the TEG module surface temperatures. No significant variation in T_h or T_c due to changes in plate thickness was seen.

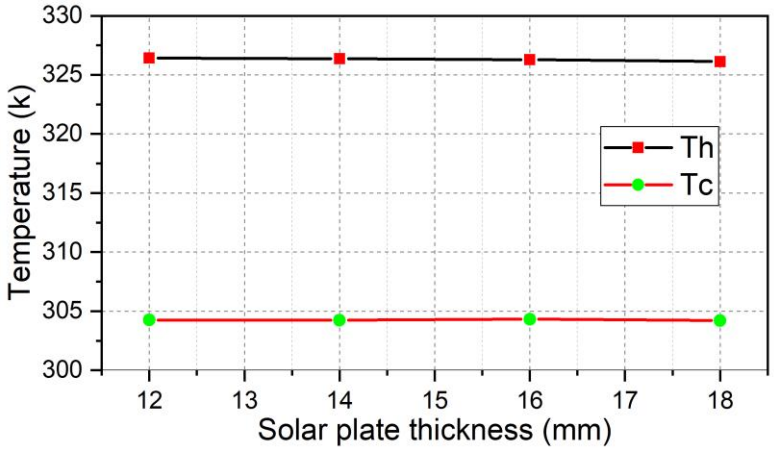

Figure 4-7 The effects of the solar plate thickness on the temperature of the module's hot and cold surfaces

Figure 4-8 demonstrates a significant effect of the plate thickness on the heat flux difference across the module's hot and cold surfaces. Greater plate thickness resulted in higher heat flux. This is attributed to the increased heat capacity of the thicker solar plate compared to the cold plate.

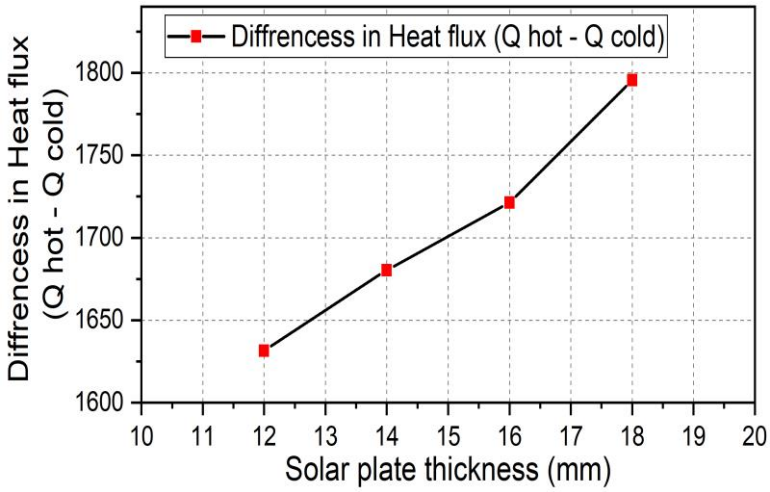

Figure 4-8 The relation between the solar plate thickness and the heat flux between the module's hot and cold surfaces

Figure 4-9 demonstrates the effect of the solar plate thickness on the efficiency, η, of the TEG. Equation 3.12 was used for calculation of this efficiency. The results indicate significant effects of plate thickness on TEG efficiency. Increasing the plate thickness had a slight adverse effect on efficiency. This is due to the dependence of efficiency upon the temperatures of the two sides of the TEG module according to Equation 3.12.

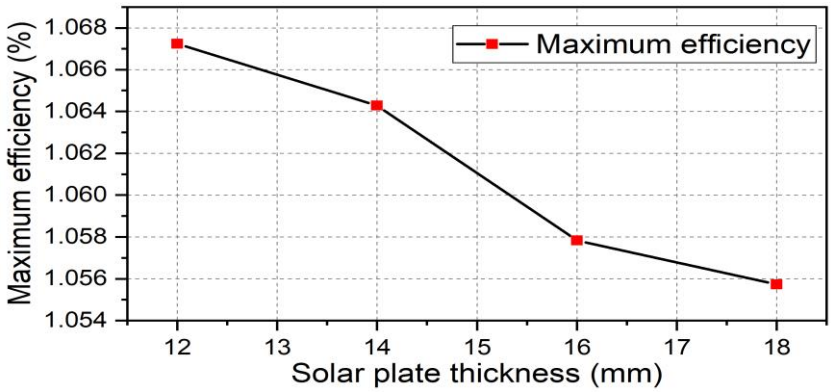

Figure 4-9 The relation between solar plate thickness and TEG efficiency

4.7.2 Flow Velocity

The effect of the cooling water flow velocity on the temperature of the module surfaces is shown in Figure 4-10. The results show a more prominent effect of the flow velocity on the cold surface than the hot one. Accordingly, larger temperature differences were achieved for higher flow velocities, as is illustrated in Figure 4-11.

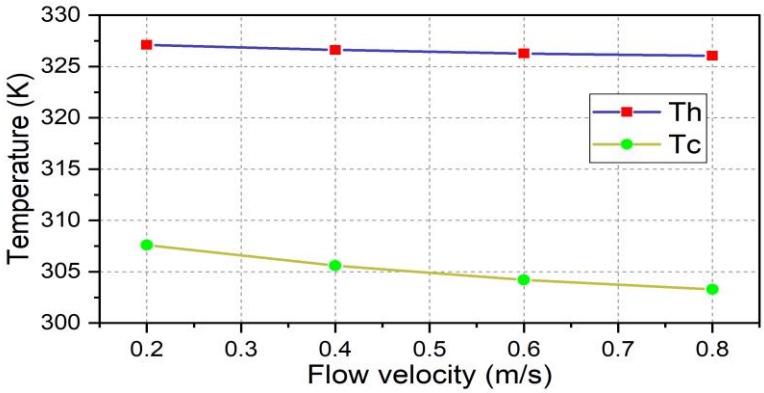

Figure 4-10 The relation between the flow velocity and the module's hot and cold surface temperatures

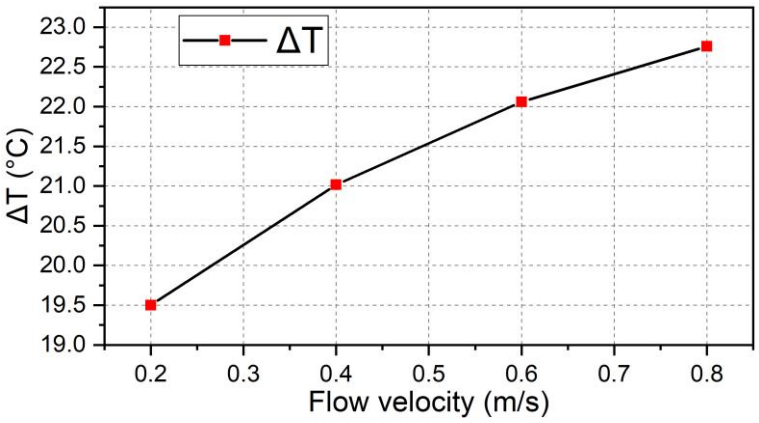

Figure 4-11 The effect of flow velocity on the temperature difference between the TEG module's hot and cold surfaces

The effect of the flow velocity on the output voltage and efficiency of the TEG is presented in Figure 4-12 and Figure 4-13, respectively. The results indicate a positive effect of the flow velocity on the output voltage and efficiency. Comparing these results to earlier research [87, 173], it was found that using stripe-shaped surfaces on the cooling cold side of a TEG module is better than plate-shaped or diamond-shaped surfaces. In these earlier studies, temperature increases in the cooling fluid from the inlet-to-outlet conditions were 8.5, 6.2, and 10.5 ◦C, respectively, for stripe-, plate-, and diamond-shaped surfaces. In the current study, the cooling system employed an M-shaped channel through a block of an aluminum alloy, and the inlet-to-outlet temperature rise was about 2 ◦C with a flow rate of 0.8 m/s, as shown in Figure 4-14d. These results demonstrate better efficiency using an M-shaped channel rather than other shapes. It allows for maintenance of a higher temperature differential for heat transfer and therefore a higher output voltage [87, 173, 174].

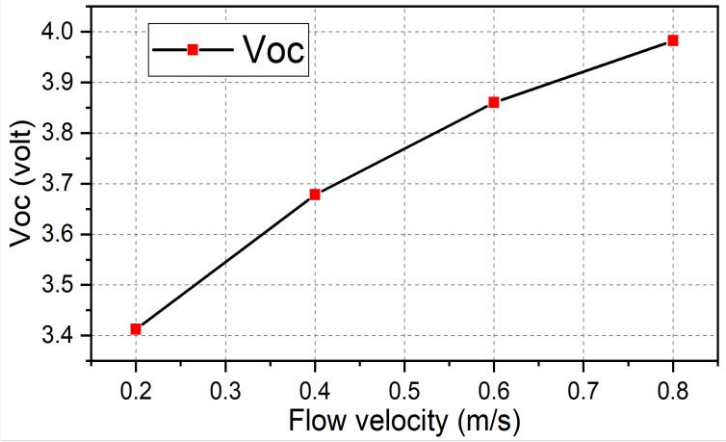

Figure 4-12 The relation between the flow velocity and output voltage

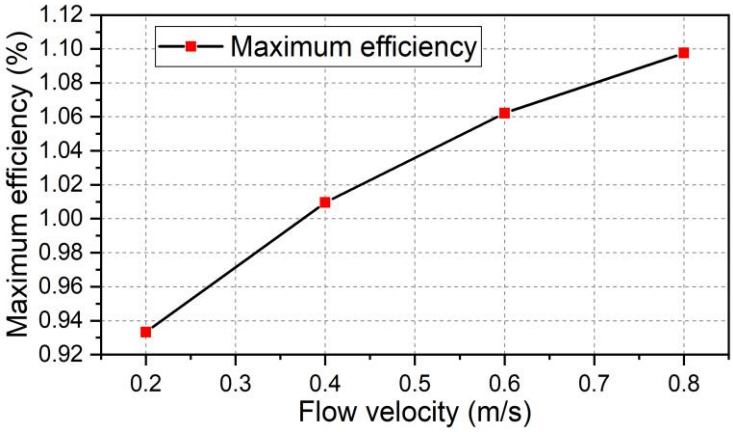

Figure 4-13 The relation between flow velocity and TEG efficiency

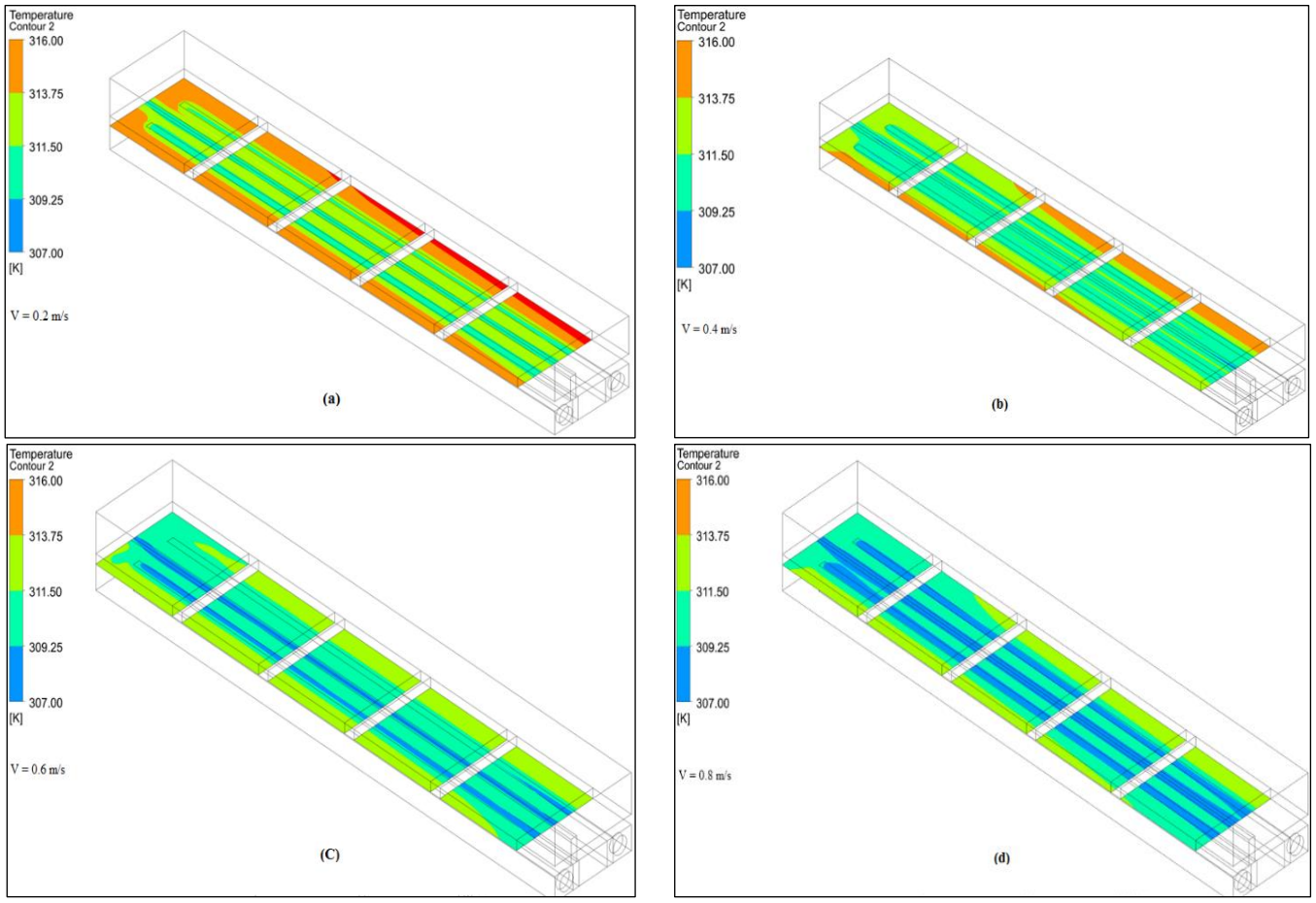

Figure 4-14 Temperature distribution contours at a plane just below the cold surface of the TEG for flow velocity: (a) 0.2 m/s, (b) 0.4 m/s, (c) 0.6 m/s, and (d) 0.8 m/s.

In Figure 4-14, contour plots of the temperature distribution at a plane just below the cold surface of the TEG, for different inlet flow velocities, are presented. (The results indicate a reduction in the temperature near the fluid channel that was proportional to the inlet flow velocity. The reason for this is to reduce the heat gain time between the entry and exit of aluminum block, and this leads to a high cooling rate. Hence, a larger ΔT for two surfaces of (TEG) is anticipated when the inlet flow velocity is increased). Figure 4-14shows the flow velocity contours at the same plane as the temperature contours. Velocity contours are presented in Figure 4-15. The highest flow velocity was at the inlet. However, due to turns in the channel, high-pressure regions were generated, which resulted in a velocity reduction at the channel outlet.

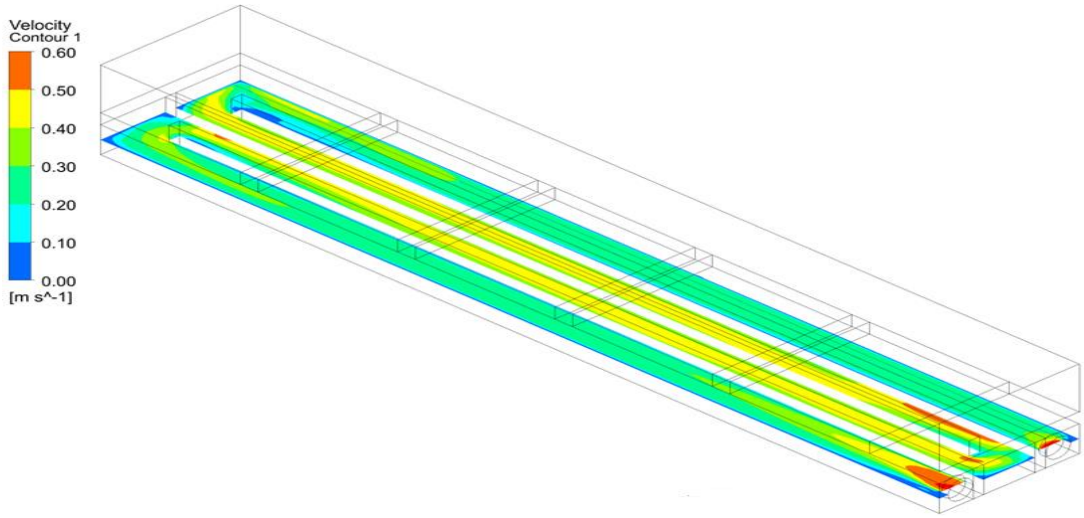

Figure 4-15 Flow velocity contours

4.8 Conclusion for Chapter Four

A successful, new CFD model was developed in this study to analyze the performance of a solar power–thermoelectric power generation system. The system comprises five TEG modules embedded between two aluminum blocks. A single block functions as a solar power collector to heat one side of the modules, while the other side has an internal M-shaped channel cooled with ordinary tap water. The model was first validated with experimental data available in the literature. Then, it was employed to conduct a parametric study to investigate the effect of different solar block thicknesses and water flow velocities on power generation and efficiency. The results show that the optimum cell size for the best results is 1 mm. Additionally, the model output showed excellent agreement with the experimental data, which makes it a powerful tool for TEG system design. Cooling water flow velocity had a positive effect on the temperature difference between the TEG module surfaces, which consequently produced higher voltage and efficiency. Moreover, the proposed M-shaped water flow provided even heat distribution along the cold side of the TEG system, which is essential for constant voltage generation. Additionally, greater plate thickness resulted in higher heat flux between the hot and cold sides of the TEGs. For further investigations and improvement, nanofluids can be investigated as alternatives to cooling water. It is anticipated that they can enhance heat dissipation from the cold surface and consequently increase power output.

CHAPTTER FIVE: MODELING, ANALYSIS, AND SIMULATION OF HYBRID PV-TEG SYSTEM

5.1 Preface

The numerical simulation techniques have prevailed for their excellence in solving differential equations and ease of use as long as the formulations for equation discretization and iteration methods are determined. SIMULINK is a multi-domain simulation and Model-Based Design block diagram environment. It enables embedded systems, system-level design, simulation, automatic code generation, and continuous testing and verification. It includes a graphical editor, block libraries that can be customized, and solvers for modeling and simulating dynamic systems. It is also integrated with MATLAB software, so users can incorporate MATLAB algorithms into models and export simulation results to MATLAB for further analysis [174].

It is well known that renewable energy systems such as photovoltaic (PV), thermoelectric generators (TEG) have recently become in high demand for cleaner energy production. Due to the fact that during the normal operation of PV panels, it dissipate high amount of heat. On the other hand, TEG modules could be attached to hot areas that dissipate heat to generate electricity. Since PV panels dissipate high amount of heat during their normal operation, it is possible to attach them to the hot side of PV panels, to generate an electric current [175]. In this chapter, a single PV panel is connected in series with a thermoelectric generator (TEG) panel as a hybrid PV-TEG system.

In recent years, many researchers developed several technologies to enhance the hybrid TEG and PV system. They investigated conversion of the wasted heat from the PV panels into useful electricity utilizing various Maximum Power Point Tracking (MPPT) methods. Kwan and Wu [176] used a Lock-On Mechanism (LOM) as an MPPT method. Their proposed MPPT provided the required pulses for a twin SEPIC DC/DC converter. Here, each input source is independent. The PV panel and TEG feed electrical voltage from each side of the converter. A LOM is used to reduce oscillations under steady state operation with improved MPPT. Tawil and Zainal [107] used a selector switch to choose the power source, either a PV or TEG system. Each source is joined to a separate DC/DC step-up converter to increase voltage levels for the loads. Their design is made to operate small power applications such as a cooling fan. Shatar, Rahman [177] developed a hybrid PV-TEG device for a precision agriculture system. A PV is used to supply loads and charge a battery bank with an appropriate MPPT. The TEG is only used for charging batteries. Belkaid, Colak [178] developed a combination PV TEG system. Electricity is supplied via solar

radiation and the waste heat is recovered to attain optimal performance. For each source, a boost converter is used to perform an MPPT and each converter is connected to a load. The MPPT is based on an algorithm called a 'sliding mode'. The aim of their design is to achieve smart grid requirements. Ibrahim, Rezk [179] fabricated a hybrid PV-TEG device for pumping applications. One synchronous reluctance motor (SRM) is used as a load. The entire system is controlled in two ways. The first way is operation at the maximum torque per Ampere, while the second is running the system so that that it produces the maximum power under specified environmental conditions. To accomplish this strategy, a three-leg inverter is used instead of a DC/DC converter. Mirza, Mansoor [180] developed an Arithmetic Optimization Algorithm (AOA), which is an MPPT algorithm, to control this hybrid PV-TEG system. They used a single DC/DC boost converter driven by an AOA to reach a Maximum Power Point (MPP) with high stability. A similar hybrid PV-TEG was made by Kanagaraj [181]. For the MPPT, a Fractional Order Fuzzy Logic Controller (FOFLC) was used. Performance of his proposed system was examined under various electrical and thermal operating conditions in a MATLAB Simulink environment. Ejaz [182] examined a hybrid PV-TEG device under Generalized Particle Swarm Optimization (GEPSO), an MPPT method. He compared it with the performance of Perturb and Observe (P&O), Cuckoo Search (CS), Incremental Conductance (INC), and normal PSO techniques for cases requiring tracking speed and accuracy.

Generally, previous studies neglected some issues. Choosing the appropriate electrical connections and assembly of TEG modules to obtain the appropriate voltage such issues. Where most PV-TEG systems link many thermoelectric modules in a series and parallel array to achieve the necessary power level. Also, most of the studies was about generating electricity for applications with low amount of power consumption. Expansion of the hybrid system to obtain more power or its exposure to unstable conditions is not considered. Therefore, creation of a hybrid system that addresses these issues is extremely important.

In this chapter, the numerical approach is about seeks to develop a hybrid PV-TEG device. The dissipated heat from a PV panel during its normal operation is converted into electricity, enhancing power generation as well as overall system effectiveness. For this purpose, a TEG panel is used that is made from several TEG modules that are connected both in series and parallel. These TEGs are subsequently attached to a PV panel. Then, they are connected electrically in series. The hybrid PV-TEG panel is modeled, analyzed, & simulated by MATLAB SIMULINK environment. Practically, it is possible that the upper side of the TEG panel receives the heat from the rear side of the PV panel and the cold side of the TEG is cooled by a

water heat exchanger (aluminum blocks), where the normal tap water flows through it. Furthermore, four MPPT algorithms were tested to examine the system. The most effective one was chosen to achieve optimal system performance under stable and unstable conditions. Also, the expansion study of the proposed system to increase power and capacity was addressed.

5.2 Hybrid PV-TEG System

The proposed hybrid system is comprised of a single PV panel and TEG panel which are electrically connected in series. The TEG panel has two surfaces. The first is a high-temperature side while the other is at a lower temperature. Its hot side is mounted on the back of a PV panel. The cooled side maintains its temperature using tap water flowing through aluminum radiator elements [110]. The details of each panel are discussed below:

5.2.1 The PV Panel

Normally, a photovoltaic (PV) panel is modeled as a PN diode with parallel and series resistances and a source of current, as depicted in Figure 5-1. The PV panel generates an electrical current (I_{PV}) when light strikes the PN junction where electron-hole pairs are formed [183-185]. IPV can be calculated using Equations 5.1 and 5.2 can be used to mathematically represent an ideal PV cell model ,

$$I_{PV} = I_{ph} - I_s - I_{rs} \tag{5.1}$$

$$I_{PV} = I_{ph} - I_s \tag{5.2}$$

where I_s, I_{rs} are diode saturation current and resistance current, respectively, and I_{Ph} is current from incoming photons, denoted as [123],

$$I_{Ph} = (I_{sc} + K_i(T - T_o))\left(\frac{G}{G_o}\right) \tag{5.3}$$

I_{sc} , K_i , T , G are short-circuit current, current conductivity, module temperature, solar irradiance, respectively. T_o and G_o are the ambient temperature and solar intensity under standard test conditions (STC), respectively. Resistance current can be expressed as [123]:

$$I_{rs} = I_{scr}\left[\exp\left(\frac{q\,V_{oc}}{N_s\,KAT}\right) - 1\right] \tag{5.4}$$

I_{scr} denotes short circuit current, V_{oc} is open circuit voltage, q represents the electron charge, N_s denotes cells number of PV model, k is the Boltzmann constant ($1.38 \times 10^{-23}\, J$), and A is the diode ideality factor. The diode current can be determined by [123]

$$I_s = I_{rs} \left(\frac{T}{T_o}\right)^3 \exp\left[\frac{qE_g}{AK}\left(\frac{1}{T_o} - \frac{1}{T}\right)\right] \quad (5.5)$$

E_g denotes bandgap energy. Then Equation 5.2 is rewritten as [123, 185],

$$I_{PV} = N_p I_{ph} - N_p I_{rs}\left[\exp\left(\frac{q\,V_{pv}+I_{pv}R_s}{N_s KAT}\right) - 1\right] - \frac{V_{pv}+I_{pv}\,R_s}{R_{sh}} \quad (5.6)$$

where R_s denotes series resistance, R_{sh} is parallel resistance, and N_p represents the number of PV cells connected in parallel. It is possible to show the input power caused by solar irradiance as [186]

$$p_{in} = G\,A_{pv} \quad (5.7)$$

where, A_{pv} is the area of the photovoltaic module, PV panel efficiency expressed as [158]

$$\eta_{PV} = \frac{I_{mp}\,V_{mp}}{G\,A_{p_v}} \quad (5.8)$$

where I_{mp}, V_{mp} are the maximum current and voltage of the photovoltaic module.

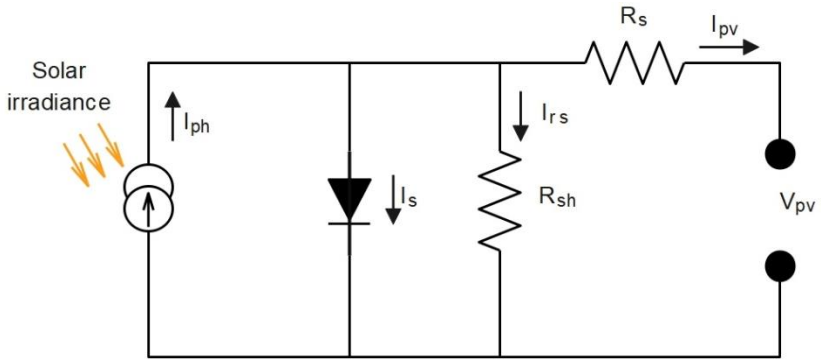

Figure 5-1 Equivalent circuit of PV cell

5.2.2 The TEG Panel

A thermoelectric generator (TEG) transforms heat directly into electrical energy [187]. It has two surfaces; one is a hot surface while the other is cold. From the Seebeck phenomenon, a difference in temperature (ΔT) is established across these two surfaces. This difference results in an energy flow from a

higher to lower level that finally produces a voltage across the TEG module. In most cases, these modules are manufactured from ceramic/bismuth telluride materials [188]. A TEG is simulated as single voltage source that is connected in series. This arrangement has an internal resistance, depicted in Figure 5-2 [189].

Heat that is absorbed Q_h and dissipated Q_c by a TEG, where the sides are at different temperatures, are determined as [74]:

$$Q_h = \left(K_p + k_n\right)(\Delta T) + \left(\alpha_p - \alpha_n\right)IT_h - \frac{I^2R}{2} \quad (5.9)$$

$$Q_c = \left(K_p + k_n\right)(\Delta T) + \left(\alpha_p - \alpha_n\right)IT_c + \frac{I^2R}{2} \quad (5.10)$$

where K_p and k_n are the thermal conductivity values of the p-type and n-type TEG materials, α_p and α_n values are the Seebeck coefficients for p-type and n-type TEG materials, respectively. I represents the current and R is the resistance at the terminals of a TEG module. This is shown in Figure 5-3 $\Delta T = (T_h - T_c)$, where T_h and T_c are the hot and cold temperatures on opposite sides of a TEG, respectively. From the input-output power balance equation then [74]:

$$W = Q_h - Q_c = V.I \quad (5.11)$$

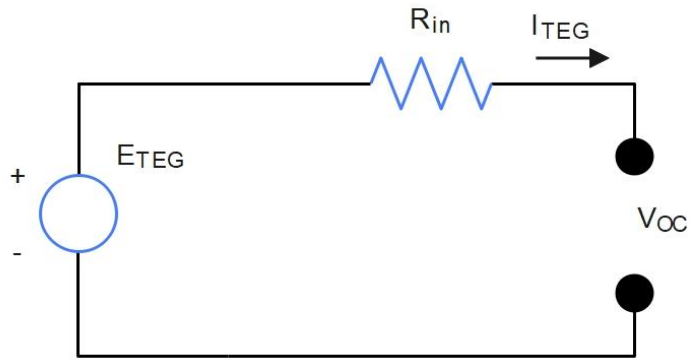

Figure 5-2 Equivalent circuit of a TEG module

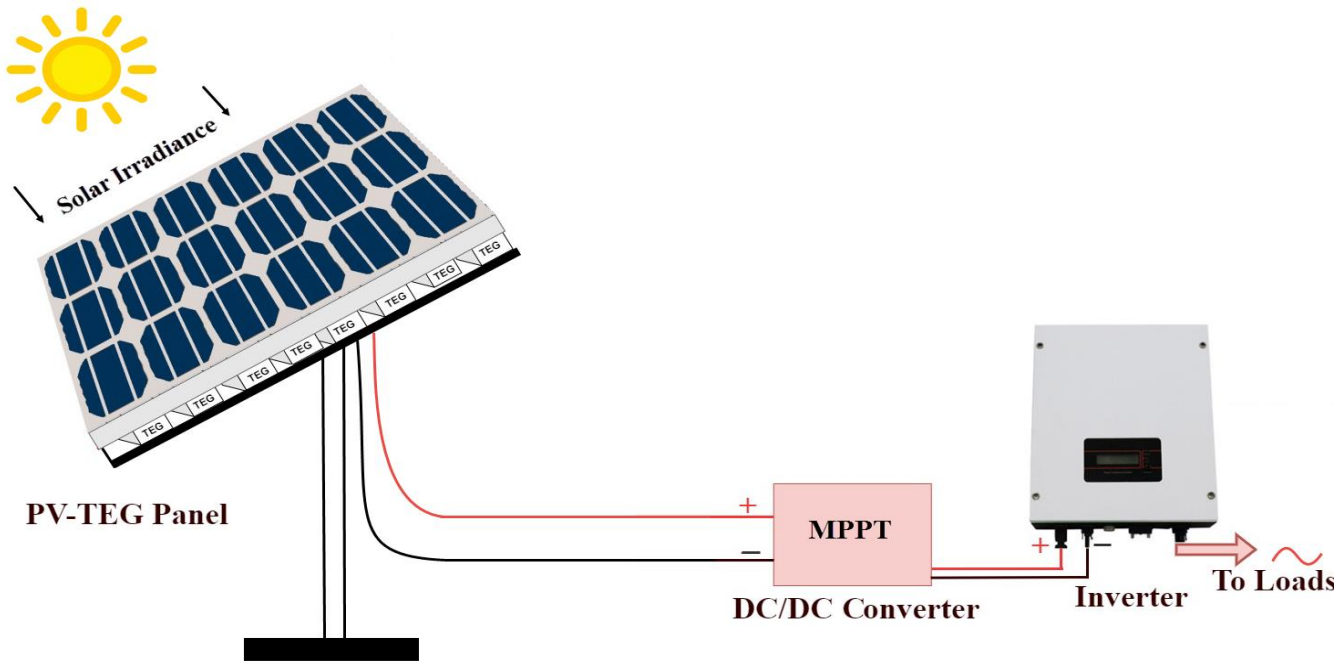

Figure 5-3 The proposed hybrid PV-TEG system

Rearranging of Equations 5.9 and 5.10, the terminal voltage is expressed by:

$$V = (\alpha_p - \alpha_n)(T_h - T_c) - IR \tag{5.12}$$

Substituting $\alpha = (\alpha_p - \alpha_n)$ and $\Delta T = (T_h - T_c)$, Equation 5.12 becomes

$$V = \alpha \times \Delta T - IR \tag{5.13}$$

The open circuit voltage (V_{oc}) is determined by

$$V_{oc} = \alpha \times \Delta T \tag{5.14}$$

Maximal efficiency of a TEG is represented as [92]

$$TEG\ \eta_{max} = \frac{T_h - T_C}{T_h} \frac{\sqrt{1+Z\bar{T}}-1}{\sqrt{1+Z\bar{T}}+\frac{T_C}{T_h}} \tag{5.15}$$

where $Z\bar{T}$ is the 'figure of merit' [131]. Voltage of a TEG can be increased by employing a greater number of TEG modules used.

When heat from radiation is transferred to the hot side of TEGs, it is transformed into additional electrical power, even though it is not converted to electricity by the PV panel. Finally, the system overall electrical

efficiency can be representing as follows in Equation 5.16, were the P_L is load output power of the system [90, 91, 133, 190]

$$\eta_{overall} = \frac{P_L}{G\,A_{pv}} \quad (5.16)$$

The proposed hybrid PV-TEG device is illustrated in Figure 5-3. Heat generated from the PV panel during its normal operation is absorbed at the TEG hot side, mounted adjacent to the opposite surface of the PV panel. This generated thermal energy can be converted into electrical energy by the TEG panel. Since the panels are connected in series, generated voltages at the terminals of TEG panels are summed to yield the system voltage. Using more TEG modules will increase the overall system voltage and power.

5.2.3 DC/DC Boost Converter

DC/DC converter functions to regulate the DC link voltage at the desired level and to track the MPP from the renewable energy generating system. The most common DC/DC converter circuit used for this purpose is the DC/DC boost converter. A DC/DC boost converter was used with an output voltage (V_o) that is higher than its input voltage (V_i). It consists of an inductor, a switch that is nominally an IGBT or MOSFET, a diode, and a capacitor at its output terminals. When the switch is ON, the inductor works as an energy saving element to store electrical energy. When the switch is OFF, the inductor releases this energy as a current flowing to the load. Thus, at this state, the output voltage equals the sum of inductor and the input side voltages. The diode maintains forward feed to the load. The role of the capacitor is as a filter of the output DC voltage. For a loss-less system, the output voltage is determined using Equation 5.17 [191, 192]:

$$V_o = \frac{1}{1-D} V_i \quad (5.17)$$

where D represents the duty cycle. The duty cycle is defined as the ratio between the period when the switch is at ON state (T_{ON}) to the overall switching period ($T_{ON} + T_{OFF}$) as shown in Figure 5-4. An MPPT technique is used to modify the D value to control the power and voltage that is supplied to the load or DC bus.

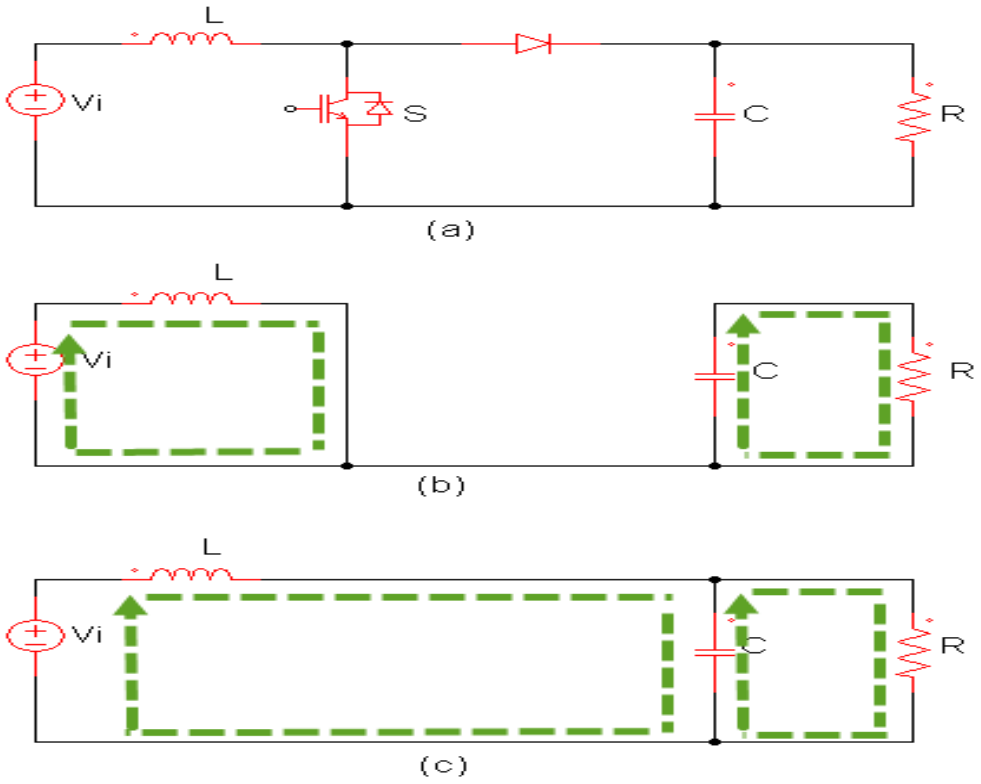

Figure 5-4 DC/DC boost converter: (a) Main circuit, (b) S is ON , and (C) S is OFF

5.3 Maximum Power Point Tracking (MPPT) Methods

The PV solar and TEG characteristics should be known first to understand the need for applying MPPT techniques. In a PV solar system, the MPP comes from its I-V curve, where (I) represents the output current of the panel and (V) represents its output voltage. An I-V curve can be drawn at various levels of solar irradiation, change in ambient temperature of PV panel, and the amount of change in temperature of both sides of the TEG panel (ΔT). This curve can be plotted at any particular radiation, such as 1000 W/m^2. At no load, the panel has the greatest voltage, while with a short circuit, it has the greatest current. Additionally, at a no load or short circuit, the power of the PV panel is zero. Each intermediate power point appears in the P-V curve. At each level of solar irradiation, or TEG panel ΔT, there is a particular P-V curve with a maximum point representing the MPP of the hybrid PV-TEG panel. At this point, the panel can generate the greatest voltage during normal operation. A P-V curve is shown in Figure 5-5.

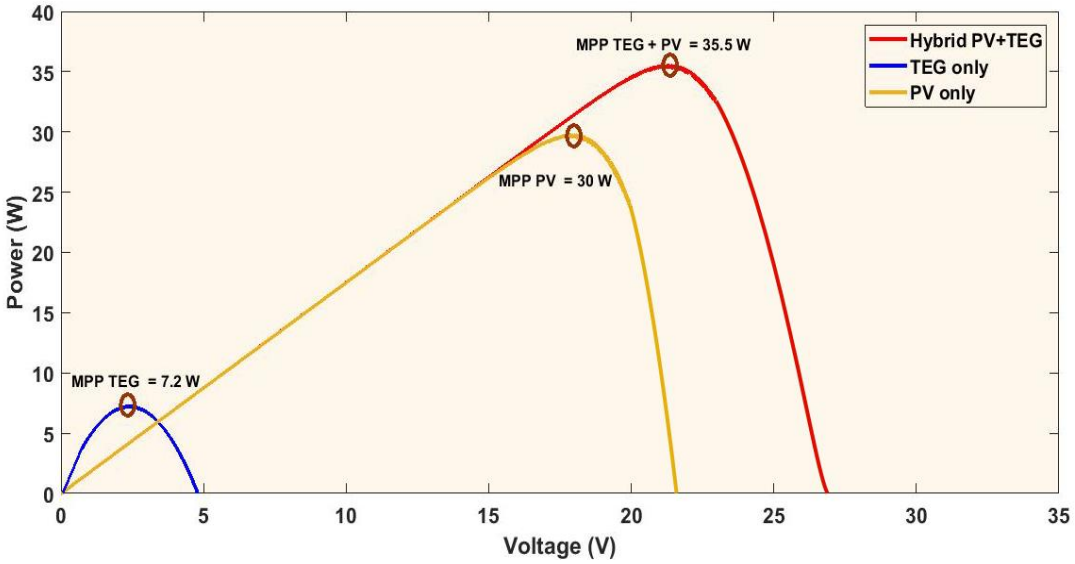

Figure 5-5 PV curves for the TEG panel, PV panel, and hybrid PV-TEG system

In this figure, it can be noted that the MPP of TEG panel is 7.2 W when $\Delta T = 30$ °C. Also, the MPP of the PV panel is 30 W when the solar irradiance is 1000 W/m^2 at 25 °C. Thus, due to the series connection of PV and TEG panels, the total power at the MPP is increased to 35.5 W for each the PV and TEG panel under the same operating conditions.

5.3.1 Purtrb & Observe (P & O) Algorithm

The P & O algorithm operates iteratively to either increase or decrease the voltage at the output terminals of a PV panel. It also takes the power of the current cycle and compares it with its corresponding value in a former cycle. When the voltage changes and power value is increasing, the controller moves the current operating point to a forward orientation. Otherwise, it is moved to a backward orientation. At an instant when the movement of current direction is known, then the current (I) changes by a fixed amount. This will lead to an increase of the speed of parameters that need to be controlled to balance this faster response with less variation in stability. A flow chart for this algorithm is shown in Figure 5-6. If the steps, which depend on the maximum power point distance, are changed, then a modified version will be determined to improve efficiency. A common problem of the P & O method is that even if the controller reaches the MPPT, the PV pannel output voltage will fluctuate over each MPPT cycle. This may lead to energy losses [129, 193, 194]. Problems arise with the conventional perturb and observe algorithm. It cannot be performed when solar irradiance and temperature suddenly change.

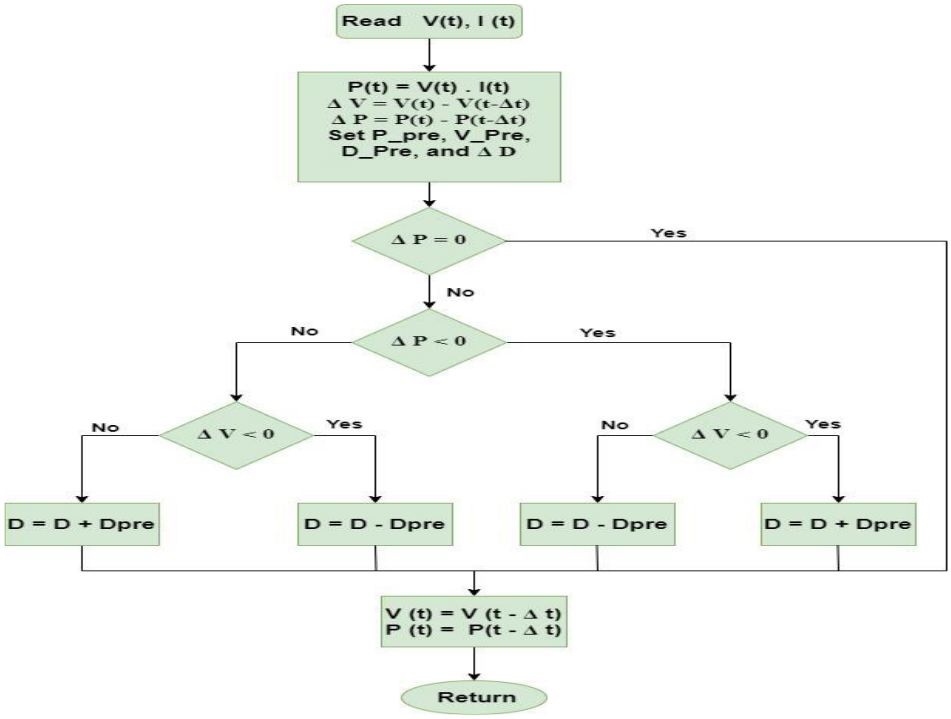

Figure 5-6 Flowchart of the perturb and observe (P&O) algorithm

5.3.2 Incremental Conductance (IC) Algorithm

The term conductance refers to a ratio between current and voltage (I/V). The incremental conductance (IC) algorithm shows that the slope, ΔP/ΔV, for a PV panel is zero at the MPP. It also has positive values to the left of this point and negative values to the right, as can be seen in Figure 5.7. In this way, the MPP can be determined by examining incremental conductance. Mathematically, Equation 5.18 is used to find the conditions necessary for the IC algorithm, which are presented by Equations (19a, b and c) [193, 195-197].

$$\frac{dp}{dv} = \frac{d(v,i)}{dv} = i + v\frac{di}{dv} = 0 \tag{5.18}$$

$$\frac{\Delta i}{\Delta v} = -\frac{i}{v} \tag{5.19a}$$

$$\frac{\Delta i}{\Delta v} > -\frac{i}{v} \tag{5.19b}$$

$$\frac{\Delta i}{\Delta v} < -\frac{i}{v} \tag{5.19c}$$

Here, Equation 5.19a is the status at the MPP, Equation 5.19b is the status to the left of the MPP, and Equation 5.19c is the status at the right of the MPP. A flow chart of this algorithm is given in Figure 5.7. This algorithm seeks the MPP in a similar manner as the P&O algorithm.

5.3.3 Fuzzy Logic Controller (FLC)

The term fuzzy refers to something that is ambiguous or does not have a clear interpretation. Fuzzy logic employs sets of logical values that range between 0 and 1. This logic deals with situations that involve incomplete truth. The true value may lie anywhere ranging from fully true to fully false [198]. Fuzzy logic control is done by fuzzification, use of an inference engine, and defuzzification. A block diagram depicting this is given in Figure 5-9. Fuzzification is an operation that identifies linguistic variables, E and CE in Figure 5-8

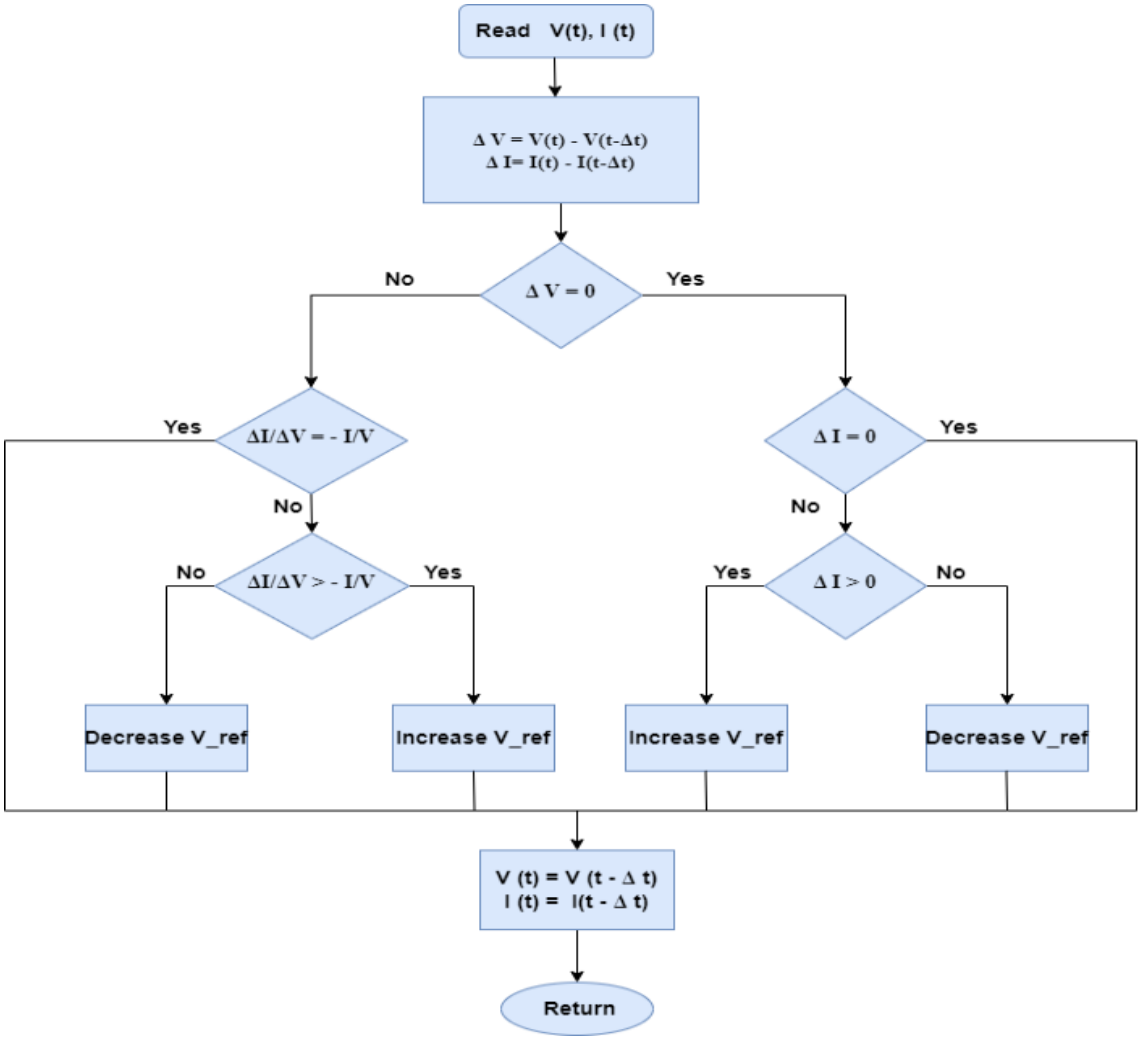

Figure 5-7 Flow chart of the incremental conductance (IC) algorithm

The inference engine takes the linguistic variables and applies rules based on knowledge of the systems. Finally, the defuzzification process take places, converting the linguistic variables into numerical form. The range of input for each of the linguistic variables is called the universe of discourse. In this universe, the membership functions of all the linguistic variables are formed so that the values of each membership function range between 0 and 1 [199].

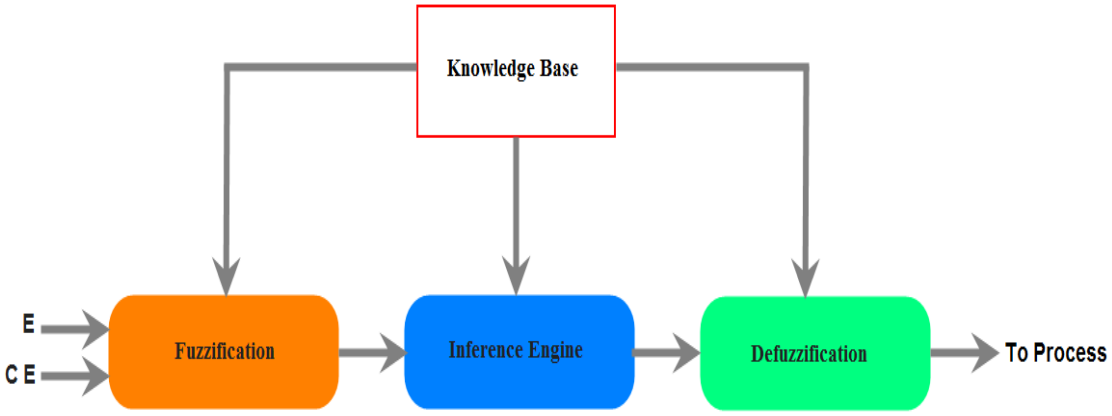

Figure 5-8 Block diagram of a fuzzy logic controller

In FLC, there are two inputs based on membership functions (MFs) which are “change in current “and “change in power”. The output represents the “duty cycle”. Figure 5-9 represents the two input of the proposed FLC as MPPT method.

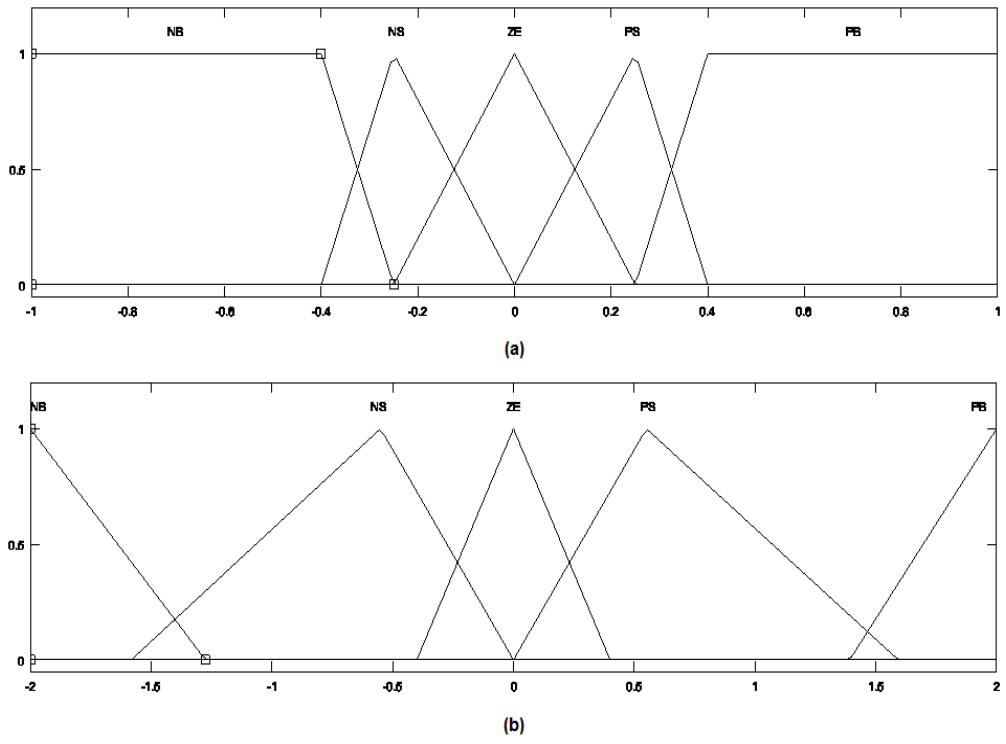

Figure 5-9 FLC MFs of inputs: (a) change in current, (b) change in power

The x-axis is called univese of discorse where its range from -1 to +1 for change of current and -2 to +2 for change of power. There are five MFs for each input named as (Negative Big (NB), Negative Small(NS), Zero (ZE), Positive small (PS) and Positive Big (PB). The height of each MFs is from 0 to 1. For this purpose, there are 25 rules as listed in Table 5-1.

Table 5-1 Rules of FLC

Change (P)					
Change (I)	NB	NS	ZE	PS	PB
NB	PB	PM	NM	NM	NB
NS	PB	PS	NS	NS	NB
ZE	NB	NS	ZE	PS	PB
PS	NB	NS	PS	PS	PB
PB	NB	NM	PM	PM	PB

The defuzzification is based on Mamdani type. The output is made of from 5 MFs as shown in Figure 5-10.

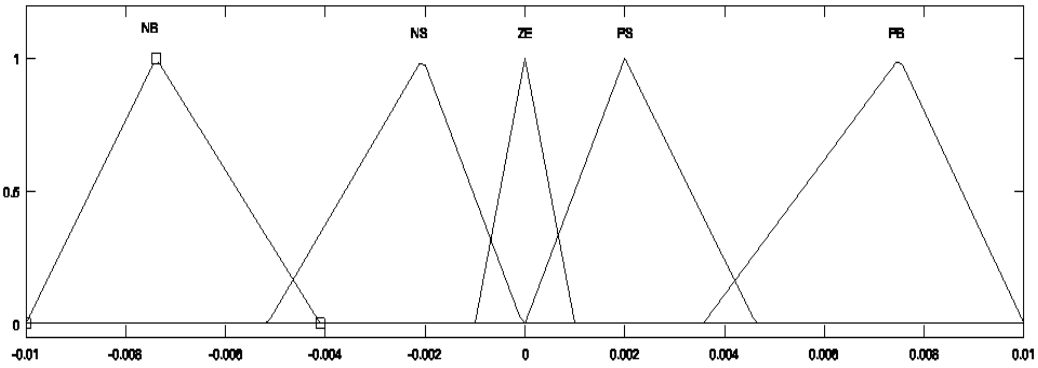

Figure 5-10 FLC MFs of output

5.3.4 Interval Type 2 Fuzzy Logic Controller (IT2FLC)

A new method is applied as MPPT for hybrid PV-TEG system. The IT2FLC can work as an MPPT technique based on (P&O) algorithm. Each MF is split into two parameters upper and lower. For MPPT purposes, there are two inputs and one output. The two inputs are the change in power and the change in current. The output represents the duty cycle (D). The MFs of the inputs are shown in Figure 5-11 (a) and (b) respectively. The number of MFs for each input has similar structure of the MFs of the proposed FLC as MPPT method.

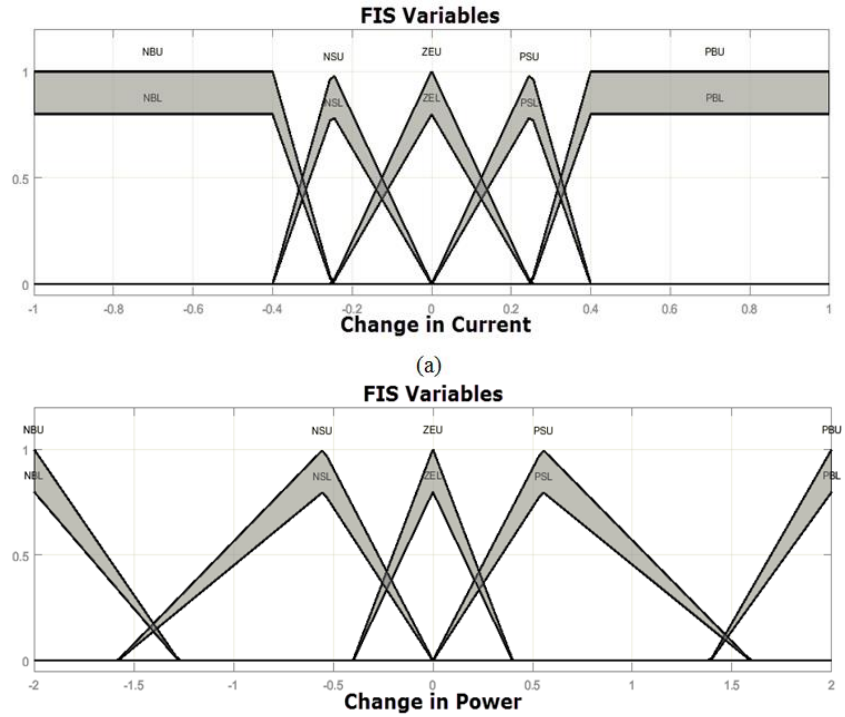

Figure 5-11 MFs of IT2FLC inputs (a) Change in Current, (b) Change in Power

For each input, the MFs have upper parameters represented by (U) and lower parameters represented by (L). For (U), the maximum degree of membership is 1. For (L) the maximum degree of membership is 0.8. There are 5 MFs for the input (Change in Power), and their names are NB (Negative BIG), NS (Negative Small), ZE (Zero), PS (Positive Small), and PB (Positive Big). All the MFs are in the range between -2 to +2. Also, there are 5 MFs for the input (Change in Current) which their names are NB, NS, ZE, PS, and PB and have been put in a range between -1 to +1. The Fuzzy interference system of IT2FLC is based on the Sugeno type. So, the output MFs are identified in linear vector as listed in the Table 5-2.

Table 5-2 Output FIS variables

FIS Variable	Values (Linear)
NB	[0 0 -0.0075]
NS	[0 0 -0.001667]
ZE	[0 0 -2.385e-19]
PS	[0 0 0.001667]
PB	[0 0 0.0075]

Due to that fact that there are 5 MFs for the input (Change in Power) and 5 MFs for the input (Change in Current) then there are 25 rules that should be defined. Those rules are given in the Table 5-1. The defuzzification is based on Karnik-Mendel algorithm (KM) [200]. All the MFs and rules are implemented in MATLAB through an open source Interval Type 2 Fuzzy Logic system [201]. The output of the MPPT

method is used to modulate a high frequency carrier to achieve the required pulse duty cycle for a DC/DC converter, such as a boost converter [202-206]. Figure 5-12 represents the surface of the relationship between each input of an FLC and IT2FLC as well as their corresponding outputs, which is the duty cycle.

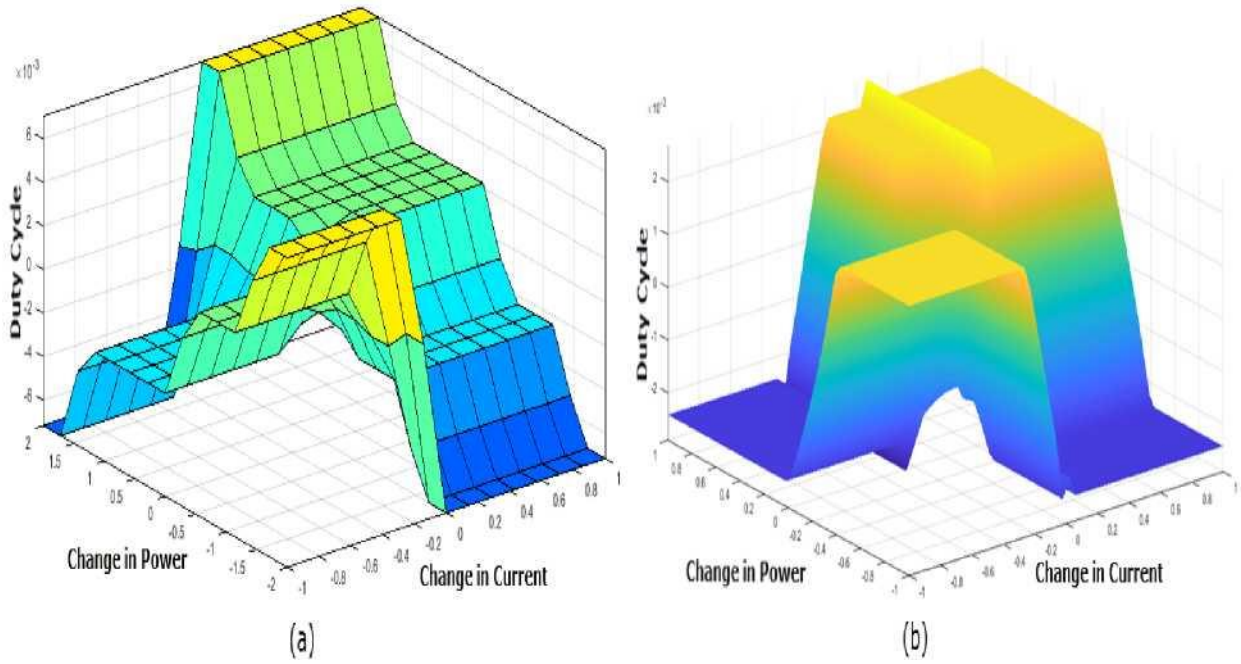

Figure 5-12 Surface of inputs and outputs of (a) FLC as MPPT and (B) IT2FLC as MPPT

5.4 Results and Discussion

The proposed system consists of a 30 W PV panel connected in series with a TEG panel. The TEG panel has been built from a 32 TEG module connected. Each four TEG modules are connected in series representing a TEG line. There are eight TEG lines are connected in parallel to form a 4×8 TEG panel. Both panels are modelled and connected in series as shown in Figure 5-13. There is a bypass diode connected between both panels for protection in case of defect or malfunctioning of the TEG panel. The specifications of the system are listed in Table 5-3. The simulation is made for P & O algorithm, IC algorithm, FLC, and IT2FLC MPPT methods.

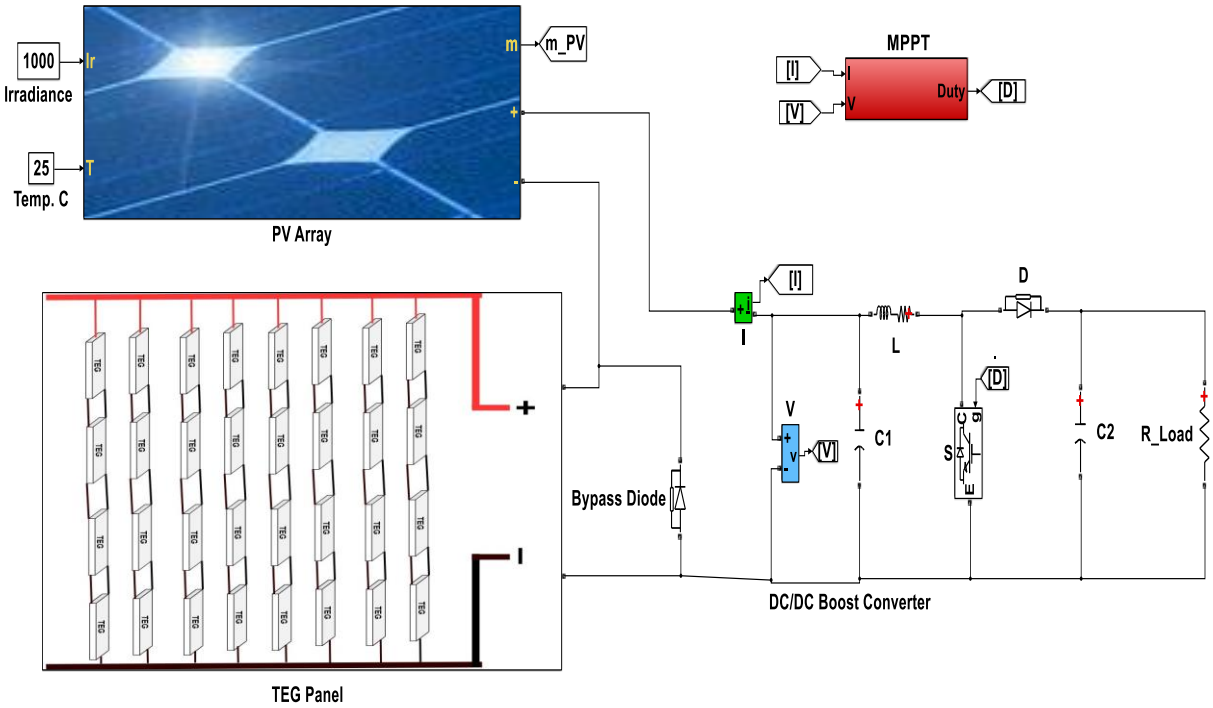

Figure 5-13 Simulink model of the proposed PV-TEG system

The PV panel is made based on 30W "AMERESCO SOLAR" PV module with code "30J" [207, 208]. It is made of 36 crystalline silicon cut cells in series.

Table 5-3 Specifications of the proposed hybrid PV-TEG system

System Portion	Component	Specifications
PV Panel	Maximum Power	30 W
	Open Circuit Voltage	22.1 V
	Voltage at MPP	17.9 V
	Short Circuit Current	1.7 A
	Rated solar irradiation and temperature	1000 W/m^2 at 25 ^{0}C
C.B. DC/DC converter	S	IGBT
	L	1 mH
	C_1	4000 µF
	C_2	2000 µF
TEG panel	No. of TEG modules	32 (4 TEGs in series × 8 parallel)
	Materials	Ceramic/Bismuth Telluride

5.4.1 System Startup

During system startup, it is assumed that the amount of solar irradiance is 1000 W/m2 and ΔT is 30 0C. The reason behind selecting such value of ΔT and solar irradiance since the normal value of T_h is (60 ~ 65) 0C and T_c is (25 ~ 30) 0C based on other experimental measurements for solar irradiance at mid-day and the temperature value of PV panel and normal tap water respectively. Figure 5-14 shows the response of system startup for each MPPT method. It can be noted that the fastest response for the system is when the IT2FLC MPPT method is followed by FLC, P & O algorithm, and finally IC algorithm. Also, at a steady state, the smooth response of input power (P_i) for the whole system is the best for the IT2FLC MPPT method followed by FLC, IC algorithm, and finally P & O algorithm. For each method, the selected load value is 30 Ω. The total MPP is 35.45 W which is higher by 18.16 % than the MPP of the used PV panel.

Figure 5-15 shows the simulation results of the output voltage of the boost converter. In this figure, it can be seen that the best stability in the output voltage value is made during the operation of for IT2FLC MPPT method followed by FLC, IC algorithm, and finally P & O algorithm. At the same load, it can be noted that the value of the output voltage in the proposed hybrid system is 32 V which is higher by 9.21% that in the case when only PV panel is used. If only PV panel is used then the output voltage will be 29.3 V. Table 5-4 lists a comparison between the change in input power (ΔP_i), change in output voltage (ΔV_o) and input power (P_i) and output power (P_o) with the value of efficiency percentage of the converted DC/DC power.

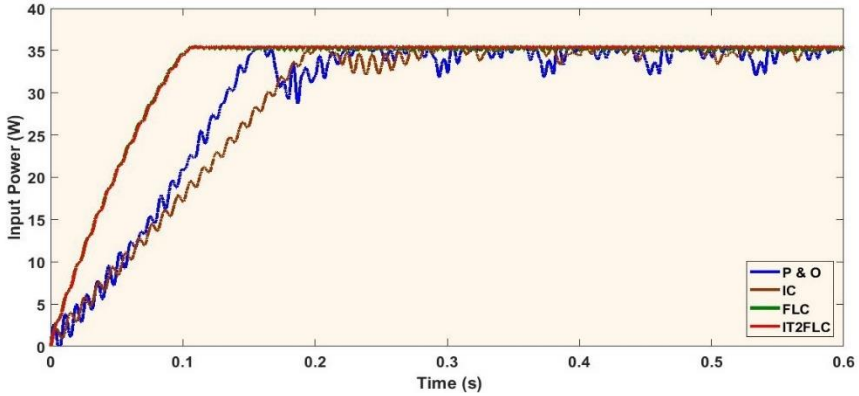

Figure 5-14 Input Power of hybrid PV-TEG system at different MPPT Methods

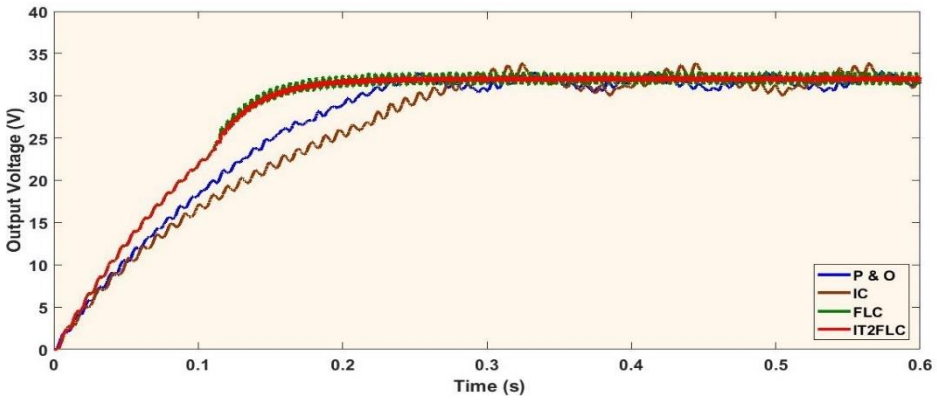

Figure 5-15 Output voltage of hybrid PV-TEG system at different MPPT Methods

Table 5-4 Performance comparison of different MPPT methods at a load of 30 Ω

MPPT Methods	ΔP_i (W)	ΔV_o (V)	P_i (W)	P_o (W)	Efficiency (%)
P & O	3.5	2.8	33.65	31.32	93.1
IC	1.7	2.74	34.55	32.89	95.2
FLC	0.3	1.43	35.19	33.78	96
IT2FLC	0.07	0.66	35.4	34.12	96.4

5.4.2 Effect of Change in solar irradiance and ΔT

In Figure 5-16 when the simulation time is 0.4 s, the solar irradiance is changed from 1000 W/m2 to 700 W/m2. Even if the value of input power is decreased to 25.4 W, the power is still higher than in the case if only PV panel is used where the power will be 20.9 W. In comparison with the steady state case in Figure 5-16 and Figure 5-17 the MPPT by IT2FLC method is still superior to the other MPPT methods. Figure 5-17represents the change in output voltage during the change in the solar irradiance. In this figure, due to the decrease in the amount of falling irradiance then the output voltage is decreased from 32 V to 27.1 V. In both Figure 5-16 and Figure 5-17, it is assumed that the system is working at 30 0C of ΔT.

In Figure 5-18, the value of solar irradiance is kept at 1000 W/m^2, the value of ΔT is changed from zero to 40 ^{0}C.As made experimentally in [11], it can be seen that there is a linear relationship between the increase of ΔT to the value of input power. In this figure, when ΔT is 40 ^{0}C then the input power is 38.1 W which is higher by 27% than the case in only PV panel is used. The estimated linear equation of between the input power and ΔT can be gotten by making regression analysis. The estimated mathematical expression for the data of Figure 5-18 is:

$$Input\ power = 27.44 + 0.26\ \Delta T \quad (5.18)$$

This equation means that if ΔT is zero then the input power is 27.44 W whereas it should be 30 W. This decrease from 30 W to 27.44 W is due to the existence of the TEG inner resistance since when ΔT is zero then the voltage of TEG panel is zero V as well which

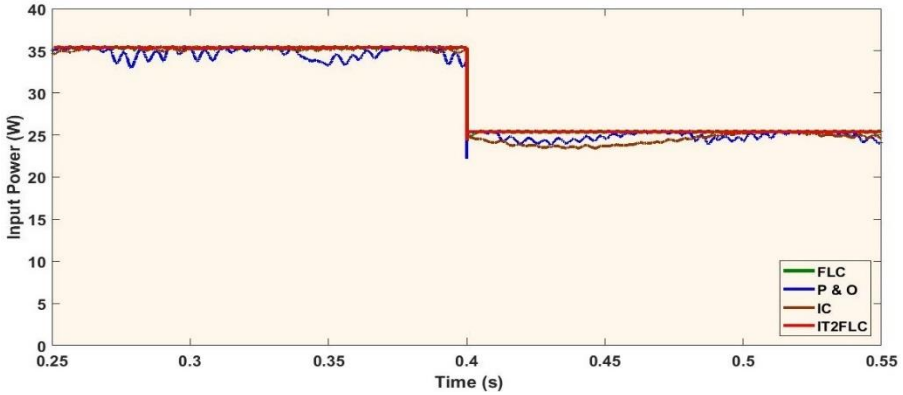

Figure 5-16 Input Power of hybrid PV-TEG system at sudden change in solar irradiance from (1000 to 700) W/m^2

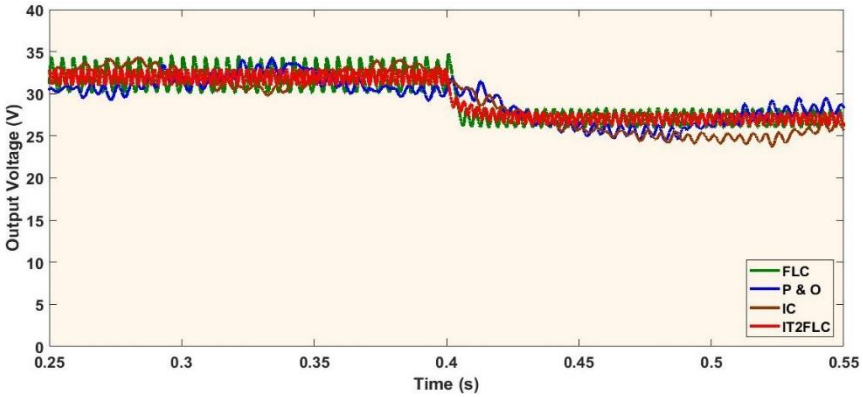

Figure 5-17 Output Voltage of hybrid PV-TEG system at sudden change in solar irradiance from (1000 to 700) W/m^2

means that the TEG is working as short circuit. If there is cut in the + branch of the TEG panel, due to the existence of the bypass diode then the input power will become 29.1 W instead of 30 W due to losses in the bypass diode itself. The state of this diode is shifted from OFF state to ON state only when the + branch of the TEG panel is disconnected.

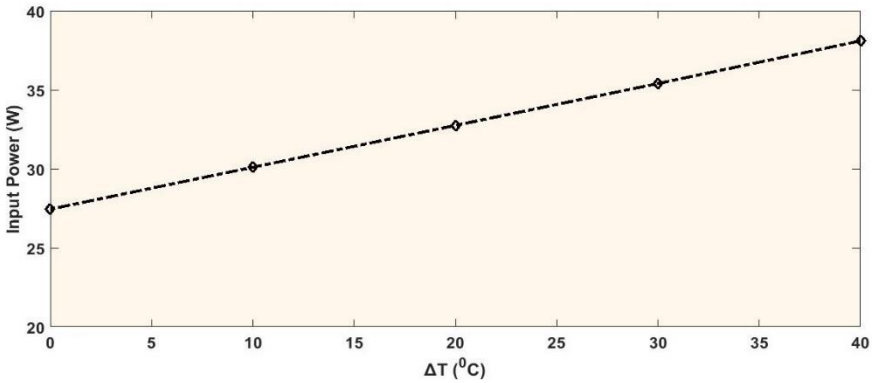

Figure 5-18 Input Power of hybrid PV-TEG system different ΔT values (0 to 40) 0C

At the same operating conditions of section 5.4.1 and applying Equation 5.15, the $TEG\ \eta_{max}$ is 1.42 % where $Z\bar{T}$ is taken from [110]. Also, photovoltaic panel efficiency η_{PV} can be determined using Equation 5.8. At 1000 W/m^2 and (0.358 × 0.796) m^2 of A_p, η_{PV} is 10.53%. Using Equation 5.16, the overall efficiency for the proposed hybrid PV-TEG is 12.44 %. This indicates an increased efficiency of 18.167 %. At various operating conditions, both η_{PV} and $TEG\ \eta_{max}$ will have different values, so the total efficiency will be different as well.

5.4.3 Effect of System Expansion

At the same operating condition of section 5.4.1, let's suppose that there are many items of the proposed hybrid PV-TEG systems that are made as one unit. Each unit is connected in parallel and there is only one central DC/DC boost converter for MPPT purposes. The aim is to make system expansion to increase the input power. It is required now to check the benefit and gain from the hybrid system over connecting PV panels in parallel individually i.e. not as a hybrid system. Figure 5-19 reveals the effect of the increase in the total input power of the hybrid system rather than connecting PV panels only. In this figure, it can be seen that at each number of PV panels there is an 18.16 % of power increase for the PV-TEG than using PV panels. Also, as the number of hybrid units increases, the input power is increasing widely.

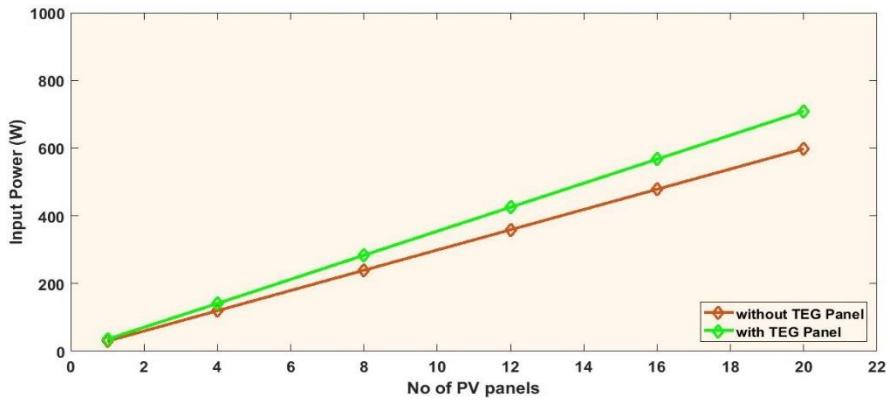

Figure 5-19 The difference between the input power at many PV panels weather they are alone or connected with TEG panels

5.5 Conclusion for Chapter Five

The current work presents a hybrid renewable PV-TEG system. A 30 W PV panel is connected in series with a (4×8) TEG panel. The system is simulated under various changes in solar irradiance and ΔT values with different MPPT methods. It can be concluded:

1. The efficiency of the proposed system is 18.16 % greater than for only a PV panel alone when the solar irradiance and ΔT are 1000 W/m^2 and 30 °C , respectively. Also, the proposed hybrid system showed a 9.215 % increased voltage over a PV panel alone.

2. With sudden change in solar irradiance from 1000 to 700 W/m^2 after 0.4 seconds of operation, the efficiency of PV-TEG system is 12.73 %. This is still higher than in the case where only a PV panel is used, with a resulting efficiency of 10.48 % and this mean improvement in efficiency of 21.53 % in comparison with PV panel alone. Also, the hybrid system showed a 4.5 W increased in power over a PV panel alone.

3. With changes in deferent temperatures from 0 to 40 ℃, and solar irradiance held to 1000 W/m^2. The power of PV-TEG system and PV panel alone are 38.1 W, 30 W respectively, at ΔT 40 ℃. This means increase of 8.1 W. Also, the PV-TEG system records an improvement in efficiency of 27 %. Here, the positive effect of improving the system appears when the different temperatures are increased.

4. Additionally, the expansion of the hybrid system to 20 PV-TEG hybrid panels has positive effects. The outcomes support the suggested hybrid system's superior robustness to a PV panel alone.

5. Furthermore, four MPPT methods are examined. IT2FLC has superior performance to other examine algorithms for transient behavior as well as in steady-state operation. The IT2FLC MPPT method can be practically applied, but it requires a high-performance microprocessor to function properly. Otherwise, the system response will suffer in reaching the correct MPP with changing operational conditions.

General Conclusion:

In conclusion, the main results of the work are presented .

In this study, TEGs were used for power generation based on solar energy combined with solar cells as a hybrid system to improve overall efficiency. Calculations and demonstration tests show that:

1. In the L-TEG system, the change in ΔT is uneven, since the Fresnel lens concentrates solar radiation in a small area. This creates an uneven temperature distribution on the hot side of the panel. Thus, the output power of NL-TEG is 35.52% higher than that of L-TEG.

2. The efficiency of the system without the use of Fresnel lenses (NL-TEG) is 16.09% higher than the systems using Fresnel lenses (L-TEG). Efficiency can be increased by more efficient cooling.

3. In the panels (2×10 TEG and 15×10 TEG), an active cooling method using a two-way water flow is used, which has led to an increase in TEG efficiency up to 2.1% and is promising due to the use of simple tap water and solar energy.

4. The use of TEG with active cooling of the heat exchanger to reduce the temperature of the solar cell made it possible to lower the temperature of the panel by 16 ℃, which led to an increase in the efficiency of the solar cell by 16.4% and is promising due to the low cost of the system.

5. The use of a hybrid HPVTEG system (TEG combination on the back surface of a solar cell) was more cost effective (LCOE) compared to a stand-alone solar cell, where the cost of kWh was 0.06681 US $/kWh, and for a stand-alone solar cell - 0.06741 US $/ kWh, based on 365 days of electricity production.

6. The results of the CFD code demonstrate that the flow rate of the cooling water heat exchanger (M-shaped) had a positive effect on the temperature difference between the surfaces of the TEG module, which led to an increase in voltage and efficiency by 0.4 - 0.6%

7. Increasing the plate thickness by more than 12 mm resulted in a higher heat flux between the hot and cold sides of the TEG.

8. As a result of applying the MPPT algorithm in the MATLAB SIMULINK program for the PV-TEG hybrid system, the following were registered: power 35.5 W and efficiency 12.44%. Thus, the efficiency of the PV-TEG system increased by 18.13% in comparison with the autonomous PV system.

Recommendations for the use of Research Materials:

The following is recommended to reduce the gap between supply and demand of energy in Iraq and increase the use of renewable energy sources by more than 2%:

1- Generating electricity from the hybrid system PV-TEG. The proposed designs are suitable for the climatic conditions of Iraq and countries with hot climates. The research materials enable investors and the Government to assess the potential development opportunities of various sectors of renewable energy in Iraq.

2- Creating a favorable investment environment to facilitate the transition of the private sector to the production and use of renewable energy sources. It is also necessary to provide various investment incentives, competitive preferential tariffs, and tax incentives for the purchase of equipment for the development of renewable energy sources.

3- In the conditions of an operating photovoltaic power plant in the Republic of Iraq, it is necessary to carry out a study that can be used to reduce the cost of electricity and increase electricity generation by 8-10 MW, as well as to reduce the cost of electricity production, carbon dioxide emissions, and the use of fossil fuels.

4- The research materials can be used to illuminate streets, roads, and bridges where connections to the power grid are impossible. The Department of Roads and Bridges of Diyala Province in Iraq has authorized the materials for use in a real-case scenario in accordance with the Law on Renewable Energy Sources (Electricity Law No. 53 of 2017), adopted by the Ministry of Energy of Iraq. The law is aimed at the active use of renewable energy sources, environmental protection, and mitigation of the effects of climate change. **Appendix A**

NOMENCLATURE:

Symbols	Description	Symbols	Description
E	Electric field $[V/m]$	$u(z)$	Function number of different inputs
I	Electric current $[A]$	V	Voltage $[V]$
J	Current density $[A\ m^{-2}]$	Voc	Open circuit voltage $[V]$
$k^{'}$	Thermal conductivity $[W/m\ K\ ]$	$Z_{p,n}$	Figure of merit of p-type and n-type junctions $[1/K]$
K_n	n-type Thermal conductivity [$W\ m^{-1}K^{-1}$]	$Z\bar{T}$	Figure of merit, Dimensionless [unit Less]
K_p	p-type Thermal conductivity [$W\ m^{-1}K^{-1}$]	α	Seebeck coefficient $[V\ K^{-1}]$
Q_c	Dissipated heat of TEG $[W]$	α_n	Seebeck coefficient of n-type thermoelements $[V\ K^{-1}]$
Q_h	Absorbed heat of TEG [W]	α_p	Seebeck coefficient of p-type thermoelements $[V\ K^{-1}]$
R	Electrical resistance $[\Omega]$	ΔT	Temperature difference$[K]$
$\bar{T}$	Mean temperature	ΔV	voltage difference $[V]$
T_c	Cold side temperature $[K]$	λ	Thermal conductivity $[W/m\ K\ ]$
TEG	Thermoelectric generator	σ	Electrical conductivity [$\Omega^{-1}\ m^{-1}$]
T_h	Hot side temperature $[K]$	η_{max}	Maximum efficiency [%]
u_n	Standard uncertainty	$y_1, \Delta y_2$	Potential errors

Appendices: Appendix A

The possibility of applying the results of the research in Diyala Governorate in Iraq Using the study materials in practice according to the Renewable Energy Sources Law (Electricity Law No. 53 of 2017)

جمهورية العـــراق
محافظة ديالى
مديرية الطرق والجسور

بسم الله الرحمن الرحيم

Diyala Governarate

العدد : ٢٨٩٤
التاريخ: ٥/٦/٢٠٢٢م
١٤٤٣هـ

إلى / جامعة الاورال الفيدرالية (UrFU) ، ايكاترينبرغ ، روسيا

الموضوع/ تأييد

استنادا الى الطلب المقدم من قبل طالب الدكتوراه السيد (محمد عبد الخالق قاسم/ قسم إدارة محطات الطاقة النووية ومصادر الطاقة المتجددة) الى مديرية طرق وجسور ديالى المرفق ربطا، وبعد دراسة الفكرة المقدمة من قبله والخاصة باستخدام منظومة كهربائية تعتمد على الطاقة الشمسية والمبين تفاصيلها ادناه، والتي تعتمد على استخدام (Thermoelectric Power Generation and Photovoltaic Panel) ، لا مانع لدينا من امكانية استخدام المنظومة المذكورة انفا، بإنارة الشوارع والطرق العامة والجسور في المناطق النائية والتي يصعب وصول الطاقة الكهربائية اليها ، خاصة بعد زيادة الطاقة الاستيعابية لها وذلك لا عتمادها على مصادر الطاقة المتجددة (الطاقة الشمسية) وهي متوفرة بشكل مجاني على مدار العام ، حيث يمكن تطوير الفكرة حسب راي الكادر الهندسي لدينا . كذلك تقدم هذه المنظومة تخفيضا كبيرة في استهلاك الطاقة لاعتمادها على طاقة مجانية على عكس مصادر الطاقة الأخرى المعتمدة على طاقة الوقود الاحفورية (fossil fuels) الشائعة الاستخدام.

للتفضل بالاطلاع مع التقدير..

تفاصيل المنظومة:

-The Experimental Investigation of a New Panel Design for Thermoelectric Power Generation to Maximize Output Power Using Solar Radiation.
- New Panel Design for Thermoelectric Power Generation integrated with Photovoltaic Panel

المرفقات:
- الطلب

المهندس
هاني غازي فكري
مدير طرق وجسور محافظة ديالى
/ ٢٠٢٢ /

نسخة منه إلى:
- الأرشفة الالكترونية .
- الإضبارة المختصة .

Diyala Governarate

Figure A-1: An Arabic version of an official letter received from the Diyala governorate / Republic of Iraq indicating their desire to install the thermoelectric power generation and photovoltaic panel systems for roads lightening in rural areas

Перевод с арабского/английского языков на русский язык.

Республика Ирак
Провинция Дияла
Управление дорог и мостов

Во имя Аллаха, Милостивого и Милосердного!
/Герб провинции Дияла/
Провинция Дияла

Номер: 2892
Дата: 05.06.2022 г.
1443г. по Х.

Кому: Уральский федеральный университет (УрФУ), г. Екатеринбург, Россия

Тема: Подтверждение.

На основании запроса, прикрепленного ниже, от аспиранта г-на Мухаммеда Абдулхалика Касима / Департамент атомных электростанций и возобновляемых источников энергии в Управлении дорог и мостов провинции Дияла, и после изучения представленных им идей использования электрической системы на основе солнечной энергии, детали которой указаны ниже, и которая основывается на использовании фотоэлектрических панелей для производства термоэлектрической энергии,

мы не возражаем против использования вышеупомянутой системы исключительно для освещения улиц, дорог общего пользования и мостов в отдаленных районах, где затруднен доступ к электроэнергии, в частности, после увеличения ее поглощающей способности, поскольку это не зависит от возобновляемых источников энергии и солнечная энергия доступна бесплатно в течение всего года. В соответствии с экспертным мнением нашего инженерного персонала, данная идея вполне может быть реализована. Эта система также обеспечивает значительное снижение потребления электроэнергии и разработана по принципу использования бесплатной энергии в отличие от других энергетических источников, которые зависят от использования ископаемого топлива.

С глубоким уважением.

Детали проекта:

- Экспериментальное исследование новой конструкции панели для производства термоэлектрической энергии для максимизации выходной мощности с использованием солнечного излучения.
- Новая конструкция панели для производства термоэлектрической энергии, интегрированная с фотоэлектрической панелью.

Приложения:
- запрос

Инженер */подпись/*
Хани Гази Фаджри
Начальник Управления дорог и мостов провинции Дияла
_____2022

Печать: Провинция Дияла // Управление дорог и мостов

Копия:
- электронный архив
- специальное дело

Настоящий перевод с арабского/английского языков на русский язык выполнен мной, переводчиком Швецовой Юлией Сергеевной. Идентичность перевода подтверждаю.

Швецова Юлия Сергеевна г.Екатерин-

Figure A-2: A Russian version of an official letter received from the Diyala governorate / Republic of Iraq indicating their desire to install the thermoelectric power generation and photovoltaic panel systems for roads lightening in rural areas

-бург

Российская Федерация

Город Екатеринбург Свердловской области

Двадцать второго июня две тысячи двадцать второго года

Я, Филиппова Ольга Владимировна, нотариус города Екатеринбурга, свидетельствую подлинность подписи переводчика Швецовой Юлии Сергеевны.

Подпись сделана в моем присутствии.

Личность подписавшего документ установлена.

Зарегистрировано в реестре: **№ 66/201-н/66-2022-7-1080**.

Уплачено за совершение нотариального действия: 730 руб. 00 коп.

О.В. Филиппова

НОТАРИУС О.В. ФИЛИППОВА
МЕСТО НАХОЖДЕНИЯ НОТАРИАЛЬНЫЙ ОКРУГ: ГОРОД ЕКАТЕРИНБУРГ

НОТАРИУС О.В. ФИЛИППОВА
МЕСТО НАХОЖДЕНИЯ НОТАРИАЛЬНЫЙ ОКРУГ: ГОРОД ЕКАТЕРИНБУРГ

Компьютерная система "Экспресс"

References

1. Stern, D.I., P.J. Burke, and S.B. Bruns. The impact of electricity on economic development: a macroeconomic perspective //. 2019. URL: https://escholarship.org/uc/item/7jb0015q.
2. F., B. Electricity Market Report - January 2022 //. 2022. URL: https://www.iea.org/reports/electricity-market-report-january-2022.
3. Jamal, M., et al. Iraqi Electricity Sector Overview //. 2021. URL: https://kapita.iq/storage/app/media/Research/Iraqi%20Electricity%20sector%20overview%20final%20March.pdf.
4. Agency, I.E. Iraq's Energy Sector: A Roadmap to a Brighter Future //. 2019. URL: https://www.iea.org/reports/iraqs-energy-sector-a-roadmap-to-a-brighter-future.
5. Ersoy, S.R. Sustainable transformation of Iraq's energy system: development of a phase model //. 2021. URL: https://library.fes.de/pdf-files/bueros/amman/18460.pdf.
6. Al-Khafaji, H. Electricity generation in Iraq Problems and solutions // Al-Bayan Center for Planning and Studies. Available at www. bayancenter. org. 2018. URL: https://www.bayancenter.org/en/wp-content/uploads/2018/09/786543454657687.pdf.
7. Al-Maleki, Y., R. Tollast, and H. Istepanian. 2018 Annual Report: Riding the Oil Markets, Iraq's Economy in Transition //. 2019. URL: https://iraqenergy.org/2019/02/18/2018-annual-report-riding-oil-markets-iraq-economy-in-transition/
8. Agyekum, E.B., et al. A bird's eye view of Ghana's renewable energy sector environment: A Multi-Criteria Decision-Making approach // Utilities Policy, 2021. Vol. P. 101219.
9. Al-Amri, F., et al. Innovative technique for achieving uniform temperatures across solar panels using heat pipes and liquid immersion cooling in the harsh climate in the Kingdom of Saudi Arabia // Alexandria Engineering Journal, 2022. Vol. № 2. P. 1413-1424.
10. Al-Kayiem, H.H. and S.T. Mohammad. Potential of renewable energy resources with an emphasis on solar power in Iraq: An outlook // Resources, 2019. Vol. № 1. P. 42.
11. Bashaer, M., O.I. Abdullah, and A.I. Al-Tmimi. Investigation and analysis of wind turbines optimal locations and performance in Iraq // FME Transactions, 2020. Vol. № 1. P. 155-163.
12. Darwish, A.S., et al. A methodology for improving wind energy production in low wind speed regions, with a case study application in Iraq // Computers & Industrial Engineering, 2019. Vol. P. 89-102.
13. Al-Hussieni, A.J.M. A prognosis of wind energy potential as a power generation source in Basra City, Iraq State // European Scientific Journal, 2014. Vol. № 36. P. 163-176.
14. Kazem, H.A. and M.T. Chaichan. Status and future prospects of renewable energy in Iraq // Renewable and Sustainable Energy Reviews, 2012. Vol. № 8. P. 6007-6012.
15. Darwish, A. and A. Sayigh. Wind energy potential in Iraq // Journal of Wind Engineering and Industrial Aerodynamics, 1988. Vol. № 1-3. P. 179-189.

16. Dihrab, S.S. and K. Sopian. Electricity generation of hybrid PV/wind systems in Iraq // Renewable energy, 2010. Vol. № 6. P. 1303-1307.

17. Ali, S., A. Mahdi, and A.H. Shaban. Wind speed estimation for Iraq using several spatial interpolation methods // Environ. Prot, 2012. Vol. № 2.

18. Solar GIS Map. . URL: https://solargis.com/maps-and-gis-data/download/iraq.

19. Istepanian, H.H. Solar energy in Iraq: From outset to offset // Iraq Energy Institute, 2018. Vol.

20. Al-Maleki. Overview of Iraq's Renewable Energy Progress in 2019 //. 2020.

21. Istepanian, H. 2018 Annual Report: Riding the Oil Markets, Iraq's Economy in Transition //. 2018. URL: https://iraqenergy.org/2019/02/18/2018-annual-report-riding-oil-markets-iraq-economy-in-transition/.

22. Abbood, A.A., M.A. Salih, and H.N. Muslim. Management of electricity peak load for residential sector in Baghdad city by using solar generation // International Journal of Energy and Environment, 2017. Vol. № 1. P. 63.

23. Muslim, H.N., A.A. Alkhazraji, and M.A. Salih. Electrical load profile management based on storage energy scenarios for residential PV storage system // International Journal of Energy and Environment, 2017. Vol. № 5. P. 427-440.

24. Muslim, H.N., A. Alkhazraji, and M.A. Salih. Feasibility study of using 2kWp residential PV system comparing with 2.5 kVA gasoline generator (Case study: Baghdad city) // International Journal of Energy and Environment, 2018. Vol. № 1. P. 57-62.

25. Abbood, A.A., M.A. Salih, and A.Y. Mohammed. Modeling and simulation of 1mw grid connected photovoltaic system in Karbala city // International Journal of Energy and Environment, 2018. Vol. № 2. P. 153-168.

26. Muslim, H.N. Solar tilt angle optimization of PV systems for different case studies // EAI Endorsed Transactions on Energy Web, 2019. Vol. № 23. P. e7-e7.

27. Alhassany, H.D., et al. Review of Bioenergy Potential from the Agriculture Sector in Iraq // Energies, 2022. Vol. № 7. P. 2678.

28. Saleh, A.M. and M.T. Chaichan. The effect of alcohol addition on the performance and emission of single cylinder spark ignition engine // proceeding to Najaf Technical collage international scientific conference, Najaf, Iraq, 2010.

29. Alwash, A., et al. Towards sustainable water resources management in Iraq // Iraq Energy Institute: London, UK, 2018. Vol.

30. The Electrical Law No. (53) of 2017. URL: https://www.moj.gov.iq/upload/pdf/4443.pdf.

31. Risseh, A. and H.-P. Nee. Design of a thermoelectric generator for waste heat recovery application on a drivable heavy duty vehicle // SAE International Journal of Commercial Vehicles, 2017. Vol.

32. Børset, M.T., et al. Exploring the potential for waste heat recovery during metal casting with thermoelectric generators: On-site experiments and mathematical modeling // Energy, 2017. Vol. P. 865-875.

33. Jouhara, H., et al. Thermoelectric generator (TEG) technologies and applications // International Journal of Thermofluids, 2021. Vol. P. 100063.

34. Enescu, D. Thermoelectric energy harvesting: basic principles and applications // Green energy advances, 2019. Vol. P. 1.

35. Chen, J., et al. Enhanced efficiency of thermoelectric generator by optimizing mechanical and electrical structures // Energies, 2017. Vol. № 9. P. 1329.

36. Luo, D., et al. A novel optimization method for thermoelectric module used in waste heat recovery // Energy Conversion and Management, 2020. Vol. P. 112645.

37. Kraemer, D., et al. Concentrating solar thermoelectric generators with a peak efficiency of 7.4% // Nature Energy, 2016. Vol. № 11. P. 1-8.

38. Maduabuchi, C., et al. Overall performance optimisation of tapered leg geometry based solar thermoelectric generators under isoflux conditions // Journal of Power Sources, 2021. Vol. P. 229989.

39. Weng, Z., et al. Performance improvement of variable-angle annular thermoelectric generators considering different boundary conditions // Applied energy, 2022. Vol. P. 118005.

40. Alahmer, A., et al. An Experimental Investigation into Improving the Performance of Thermoelectric Generators // Journal of Ecological Engineering, 2022. Vol. № 3.

41. Qasim, M.A., V.I. Velkin, and S.E. Shcheklein. The Experimental Investigation of a New Panel Design for Thermoelectric Power Generation to Maximize Output Power Using Solar Radiation // Energies, 2022. Vol. № 9. P. 3124.

42. Chen, W.-H., et al. Performance evaluation and improvement of thermoelectric generators (TEG): Fin installation and compromise optimization // Energy Conversion and Management, 2021. Vol. P. 114858.

43. Saleh, U.A., et al. Analysis of the Performance of Thermoelectric Generators for Ambient Energy Generation through ANSYS Software // Proceedings of the 11th Annual International Conference on Industrial Engineering and Operations Management Singapore, 2021. P. 3460-3472.

44. Wodołażski, A., et al. CFD Numerical Modelling of a PV–TEG Hybrid System Cooled by Air Heat Sink Coupled with a Single-Phase Inverter // Materials, 2021. Vol. № 19. P. 5800.

45. Bayendang, N.P., M.T. Kahn, and V. Balyan. Simplified thermoelectric generator (TEG) with heatsinks modeling and simulation using Matlab and Simulink based-on dimensional analysis // AIMS Energy, 2021. Vol. № 6. P. 1213-1240.

46. Selimefendigil, F. and H.F. Öztop. Performance of TEG integrated channel with area expansion by using advanced passive techniques // International Journal of Mechanical Sciences, 2021. Vol. P. 106210.

47. Mohammadnia, A., et al. Fan operating condition effect on performance of self-cooling thermoelectric generator system // Energy, 2021. Vol. P. 120177.

48. Hilmin, M.N.H.M., et al. Thermoelectric power generations from vehicle exhaust gas with TiO2 nanofluid cooling // Thermal Science and Engineering Progress, 2020. Vol. P. 100558.

49. Lekbir, A., et al. Improved energy conversion performance of a novel design of concentrated photovoltaic system combined with thermoelectric generator with advance cooling system // Energy Conversion and Management, 2018. Vol. P. 19-29.

50. Selimefendigil, F. and H.F. Öztop. Identification of pulsating flow effects with CNT nanoparticles on the performance enhancements of thermoelectric generator (TEG) module in renewable energy applications // Renewable energy, 2020. Vol. P. 1076-1086.

51. Karthick, K., et al. Experimental investigation of solar reversible power generation in Thermoelectric Generator (TEG) using thermal energy storage // Energy for Sustainable Development, 2019. Vol. P. 107-114.

52. Borhani, S., et al. Performance enhancement of a thermoelectric harvester with a PCM/Metal foam composite // Renewable energy, 2021. Vol. P. 1122-1140.

53. Naderi, M., B.M. Ziapour, and M.Y. Gendeshmin. Improvement of photocells by the integration of phase change materials and thermoelectric generators (PV-PCM-TEG) and study on the ability to generate electricity around the clock // Journal of Energy Storage, 2021. Vol. P. 102384.

54. Huang, K., et al. Improving transient performance of thermoelectric generator by integrating phase change material // Energy, 2021. Vol. P. 119648.

55. Wang, Y., et al. Experimental investigation on performance improvement of thermoelectric generator based on phase change materials and heat transfer enhancement // Energy, 2021. Vol. P. 120676.

56. Wang, J., S. Liu, and L. Li. Experiments and modeling on thermoelectric power generators used for waste heat recovery from hot water pipes // Energy Procedia, 2019. Vol. P. 1052-1058.

57. Susanto, F., et al. Application of Thermoelectric Generator TEG Type Parallel Series Electric Circuit Produces Electricity from Heat Rocket Stove // Journal of Physics: Conference Series. 1845 IOP Publishing, 2021. P. 012036.

58. Hoang, A.T., et al. Power generation characteristics of a thermoelectric modules-based power generator assisted by fishbone-shaped fins: Part II–Effects of cooling water parameters // Energy Sources, Part A: Recovery, Utilization, and Environmental Effects, 2021. Vol. № 3. P. 381-393.

59. Garmejani, H.A. and S. Hossainpour. Single and multi-objective optimization of a TEG system for optimum power, cost and second law efficiency using genetic algorithm // Energy Conversion and Management, 2021. Vol. P. 113658.

60. Karana, D.R. and R.R. Sahoo. Effect of Design Parameters on the Performance of a New Modified Annular TEG System // International Journal of Energy for a Clean Environment, 2019. Vol. № 4.

61. Zarifi, S. and M.M. Moghaddam. Utilizing finned tube economizer for extending the thermal power rate of TEG CHP system // Energy, 2020. Vol. P. 117796.

62. Saleh, U.A., et al. Evaluation of a PV-TEG Hybrid System Configuration for an Improved Energy Output: A Review // International Journal of Renewable Energy Development, 2021. Vol. № 2. P. 385-400.

63. Shittu, S., et al. Advancements in thermoelectric generators for enhanced hybrid photovoltaic system performance // Renewable and Sustainable Energy Reviews, 2019. Vol. P. 24-54.

64. Daghigh, R. and Y. Khaledian. A novel photovoltaic/thermoelectric collector combined with a dual–Evaporator vapor compression system // Energy Conversion and Management, 2018. Vol. P. 156-167.

65. Babu, C. and P. Ponnambalam. The theoretical performance evaluation of hybrid PV-TEG system // Energy Conversion and Management, 2018. Vol. P. 450-460.

66. Lamba, R. and S. Kaushik. Solar driven concentrated photovoltaic-thermoelectric hybrid system: Numerical analysis and optimization // Energy Conversion and Management, 2018. Vol. P. 34-49.

67. Yin, E., Q. Li, and Y. Xuan. Experimental optimization of operating conditions for concentrating photovoltaic-thermoelectric hybrid system // Journal of Power Sources, 2019. Vol. P. 25-32.

68. Riahi, A., et al. Performance investigation of a concentrating photovoltaic thermal hybrid solar system combined with thermoelectric generators // Energy Conversion and Management, 2020. Vol. P. 112377.

69. Wu, S.-Y., et al. Performance evaluation and parametric analysis of AMTEC/TEG hybrid system // Energy Conversion and Management, 2017. Vol. P. 118-126.

70. Wu, S.Y., Y.C. Zhang, and L. Xiao. Conceptual design and performance analysis of concentrated solar-driven TIC/AMTEC/TEG hybrid system // International Journal of Energy Research, 2018. Vol. № 15. P. 4674-4686.

71. Al-Widyan, M. and Q. Al-Oweiti. A hybrid TEG/Thermal radiator system for space heating and electric power generation // Journal of Building Engineering, 2021. Vol. P. 102364.

72. Zoui, M.A., et al. A review on thermoelectric generators: Progress and applications // Energies, 2020. Vol. № 14. P. 3606.

73. Qasim, M., V. Velkin, and A. Hassan. Seebeck Generators and Their Performance in Generating Electricity // Journal of Operation and Automation in Power Engineering, 2022. Vol. № 3. P. 200-205.

74. Hsu, C.-T., et al. An effective Seebeck coefficient obtained by experimental results of a thermoelectric generator module // Applied energy, 2011. Vol. № 12. P. 5173-5179.

75. Clyxgs Aluminum Water Cooling Block. Available online: https://www.newegg.com/p/2YM-0045-00255 (accessed on 17 April 2022).

76. Wu, Y., et al. Experimental characterisation of a Fresnel lens photovoltaic concentrating system // Solar Energy, 2012. Vol. № 1. P. 430-440.

77. Rajkrishna, A. Solar Geyser using spot Fresnel lens // J. Fundam. Renewable Energy Appl, 2016. Vol. № 2. P. 1-8.

78. BETHESDA, M., *Handbook of magnetic compass adjustment*, 2004, Defense Mapping Agency Hydrographic/Topographic Center Washington, DC, USA.

79. Amin, S.H., J.; Stenhouse, K.; Yyelland, B.; Donev, J. Energy Education—Solar Panel Orientation, 2018. Available online: https://energyeducation.ca/encyclopedia/Solar_panel_orientation (accessed on 17 April 2022).

80. Chandrika, V., et al. Experimental analysis of solar concrete collector for residential buildings // International Journal of Green Energy, 2021. Vol. № 6. P. 615-623.

81. Kline, S.J. Describing uncertainty in single sample experiments // Mech. Engineering, 1953. Vol. P. 3-8.

82. Gaurav, K. and S.K. Pandey. Efficiency calculation of thermoelectric generator by extracting waste heat, for practical applications // J. Renew. Sustain. Energy, 2017. Vol. P. 1-4.

83. Yan, Z., et al. Effects of interfacial properties on conversion efficiency of Bi2Te3-based segmented thermoelectric devices // Applied Physics Letters, 2021. Vol. № 23. P. 233902.

84. Qian, D., et al. The mechanical and thermoelectric properties of Bi2Te3-based alloy prepared by constrained hot compression technique // Metals, 2021. Vol. № 7. P. 1060.

85. Memon, S. and K.N. Tahir. Experimental and analytical simulation analyses on the electrical performance of thermoelectric generator modules for direct and concentrated quartz-halogen heat harvesting // Energies, 2018. Vol. № 12. P. 3315.

86. Tritt, T.M. and M. Subramanian. Thermoelectric materials, phenomena, and applications: a bird's eye view // MRS bulletin, 2006. Vol. № 3. P. 188-198.

87. Pfeiffelmann, B., A.C. Benim, and F. Joos. Water-Cooled Thermoelectric Generators for Improved Net Output Power: A Review // Energies, 2021. Vol. № 24. P. 8329.

88. Hendricks, T.J., S. Yee, and S. LeBlanc. Cost scaling of a real-world exhaust waste heat recovery thermoelectric generator: A deeper dive // Journal of Electronic Materials, 2016. Vol. № 3. P. 1751-1761.

89. Lv, S., et al. Study of different heat exchange technologies influence on the performance of thermoelectric generators // Energy Conversion and Management, 2018. Vol. P. 167-177.

90. Esen, D.O., E. Balta, and A. Kaman. An experimental investigation of thermoelectric cooling with solar panel // 2012 International Conference on Renewable Energy Research and Applications (ICRERA) IEEE, 2012. P. 1-6.

91. Nejad, A.R., et al. Production of electrical power in very extreme-temperature environmental conditions: a new implementation of thermoelectric generators // 2017 IEEE 6th International Conference on Renewable Energy Research and Applications (ICRERA) IEEE, 2017. P. 468-472.

92. Tritt, T.M., H. Böttner, and L. Chen. Thermoelectrics: Direct solar thermal energy conversion // MRS bulletin, 2008. Vol. № 4. P. 366-368.

93. Shayan, M.E. and G. Najafi. Energy-economic optimization of thin layer photovoltaic on domes and cylindrical towers // International Journal of Smart Grid, 2019. Vol. № 2. P. 84-91.

94. Awan, M.M.A., et al. Economic Integration of Renewable and Conventional Power Sources—A Case Study // Energies, 2022. Vol. № 6. P. 2141.

95. Nararom, M. and P. Bamroongkhan. A Study on Thermoelectric Power Generator by Solar Energy Using Fresnel Lens // 2018 International Electrical Engineering Congress (iEECON) IEEE, 2018. P. 1-4.

96. Goswami, R. and R. Das. Waste heat recovery from a biomass heat engine for thermoelectric power generation using two-phase thermosyphons // Renewable energy, 2020. Vol. P. 1280-1291.

97. Xie, K., et al. A new seafloor hydrothermal power generation device based on waterproof thermoelectric modules // IEEE Access, 2020. Vol. P. 70762-70772.

98. Byon, Y.-S. and J.-W. Jeong. Annual energy harvesting performance of a phase change material-integrated thermoelectric power generation block in building walls // Energy and Buildings, 2020. Vol. P. 110470.

99. Luo, D., et al. Parametric study of a thermoelectric module used for both power generation and cooling // Renewable energy, 2020. Vol. P. 542-552.

100. Gou, X., H. Xiao, and S. Yang. Modeling, experimental study and optimization on low-temperature waste heat thermoelectric generator system // Applied energy, 2010. Vol. № 10. P. 3131-3136.

101. Kadohiro, Y., S. Cheng, and J.S. Cross. All-Day Energy Harvesting Power System Utilizing a Thermoelectric Generator with Water-Based Heat Storage // Sustainability, 2020. Vol. № 9. P. 3659.

102. Zhao, Y., et al. Energy and exergy analysis of thermoelectric generator system with humidified flue gas // Energy Conversion and Management, 2018. Vol. P. 140-149.

103. Gou, X., et al. A dynamic model for thermoelectric generator applied in waste heat recovery // Energy, 2013. Vol. P. 201-209.

104. Li, G., X. Zhao, and J. Ji. Conceptual development of a novel photovoltaic-thermoelectric system and preliminary economic analysis // Energy Conversion and Management, 2016. Vol. P. 935-943.

105. Liu, G., et al. Progress in thermoplasmonics for solar energy applications // Physics Reports, 2022. Vol. P. 1-50.

106. Hao, D., et al. Solar energy harvesting technologies for PV self-powered applications: A comprehensive review // Renewable energy, 2022. Vol.

107. Tawil, S.N.M. and M.Z. Zainal. Energy harvesting using TEG and PV cell for low power application // AIP Conference Proceedings. 1930 AIP Publishing LLC, 2018. P. 020041.

108. Lorenzi, B., et al. Practical development of efficient thermoelectric–Photovoltaic hybrid systems based on wide-gap solar cells // Applied energy, 2021. Vol. P. 117343.

109. Jaziri, N., et al. A comprehensive review of Thermoelectric Generators: Technologies and common applications // Energy Reports, 2020. Vol. P. 264-287.

110. Qasim, M.A., V.I. Velkin, and S.E. Shcheklein. Experimental and Implementation of a 15× 10 TEG Array of a Thermoelectric Power Generation System Using Two-Pass Flow of a Tap Water Pipeline Based on Renewable Energy // Applied Sciences, 2022. Vol. № 15. P. 7948.

111. Chen, X., Y. Huang, and Z. Chen. Energy and exergy analysis of an integrated photovoltaic module and two-stage thermoelectric generator system // Applied Thermal Engineering, 2022. Vol. P. 118605.

112. Bjørk, R. and K.K. Nielsen. The performance of a combined solar photovoltaic (PV) and thermoelectric generator (TEG) system // Solar Energy, 2015. Vol. P. 187-194.

113. Pang, W., et al. Empirical study on thermal performance through separating impacts from a hybrid PV/TE system design integrating heat sink // International Communications in Heat and Mass Transfer, 2015. Vol. P. 9-12.

114. Zhang, Y., et al. Integrated energy-harvesting system by combining the advantages of polymer solar cells and thermoelectric devices // The Journal of Physical Chemistry C, 2013. Vol. № 47. P. 24685-24691.

115. Kil, T.-H., et al. A highly-efficient, concentrating-photovoltaic/thermoelectric hybrid generator // Nano energy, 2017. Vol. P. 242-247.

116. Rajaee, F., et al. Experimental analysis of a photovoltaic/thermoelectric generator using cobalt oxide nanofluid and phase change material heat sink // Energy Conversion and Management, 2020. Vol. P. 112780.

117. Fini, M.A., D. Gharapetian, and M. Asgari. Efficiency improvement of hybrid PV-TEG system based on an energy, exergy, energy-economic and environmental analysis; experimental, mathematical and numerical approaches // Energy Conversion and Management, 2022. Vol. P. 115767.

118. Mahmoudinezhad, S., et al. Experimental investigation on spectrum beam splitting photovoltaic–thermoelectric generator under moderate solar concentrations // Energy, 2022. Vol. P. 121988.

119. Mohd Shatar, N., et al. Performance evaluation of unconcentrated photovoltaic-thermoelectric generator hybrid system under tropical climate // Sustainability, 2019. Vol. № 22. P. 6192.

120. Van Sark, W. Feasibility of photovoltaic–thermoelectric hybrid modules // Applied energy, 2011. Vol. № 8. P. 2785-2790.

121. Ko, J. and J.-W. Jeong. Annual performance evaluation of thermoelectric generator-assisted building-integrated photovoltaic system with phase change material // Renewable and Sustainable Energy Reviews, 2021. Vol. P. 111085.

122. Beeri, O., et al. Hybrid photovoltaic-thermoelectric system for concentrated solar energy conversion: Experimental realization and modeling // Journal of Applied Physics, 2015. Vol. № 11. P. 115104.

123. Khan, M.A.I., et al. An Experimental and Comparative Performance Evaluation of a Hybrid Photovoltaic-Thermoelectric System // Frontiers in Energy Research, 2021. Vol. P. 722514.

124. Li, G., et al. Inconsistent phenomenon of thermoelectric load resistance for photovoltaic–thermoelectric module // Energy Conversion and Management, 2018. Vol. P. 155-161.

125. Zhang, J., Y. Xuan, and L. Yang. A novel choice for the photovoltaic–thermoelectric hybrid system: the perovskite solar cell // International Journal of Energy Research, 2016. Vol. № 10. P. 1400-1409.

126. Cui, T., et al. Experimental investigation on potential of a concentrated photovoltaic-thermoelectric system with phase change materials // Energy, 2017. Vol. P. 94-102.

127. Shoeibi, S., et al. A review on using thermoelectric cooling, heating, and electricity generators in solar energy applications // Sustainable Energy Technologies and Assessments, 2022. Vol. P. 102105.

128. PraveenKumar, S., et al. Experimental assessment of thermoelectric cooling on the efficiency of PV module // Int. J. Renew. Energy Res.(IJRER), 2022. Vol. P. 1670-1681.

129. Qasim, M.A. and V.I. Velkin. Maximum power point tracking techniques for micro-grid hybrid wind and solar energy systems-A review // International Journal on Energy Conversion, 2020. Vol. № 6. P. 223-234.

130. A. Qasim, M., et al. A New Maximum Power Point Tracking Technique for Thermoelectric Generator Modules // Inventions, 2021. Vol. № 4. P. 88.

131. Shittu, S., et al. Comprehensive study and optimization of concentrated photovoltaic-thermoelectric considering all contact resistances // Energy Conversion and Management, 2020. Vol. P. 112422.

132. Ouyang, Z. and D. Li. Modelling of segmented high-performance thermoelectric generators with effects of thermal radiation, electrical and thermal contact resistances // Scientific reports, 2016. Vol. № 1. P. 1-12.

133. Ruzaimi, A., et al. Performance analysis of thermoelectric generator implemented on non-uniform heat distribution of photovoltaic module // Energy Reports, 2021. Vol. P. 2379-2387.

134. Nazri, N.S., et al. Exergy and improvement potential of hybrid photovoltaic thermal/thermoelectric (PVT/TE) air collector // Renewable and Sustainable Energy Reviews, 2019. Vol. P. 132-144.

135. Soltani, S., et al. Exergetic and enviromental assessment of a photovoltaic thermal-thermoelectric system using nanofluids: Indoor experimental tests // Energy Conversion and Management, 2020. Vol. P. 112907.

136. Yin, E., Q. Li, and Y. Xuan. One-day performance evaluation of photovoltaic-thermoelectric hybrid system // Energy, 2018. Vol. P. 337-346.

137. Gu, W., et al. Mathematical modelling and performance evaluation of a hybrid photovoltaic-thermoelectric system // Energy Conversion and Management, 2019. Vol. P. 111800.

138. Chooplod, K. and P. Kittisupakorn. Devise of Thermoelectric Generator Incorporated of a Heat Exchanger for Power Generation and Heat Recovery // International Journal of Mechanical Engineering and Robotics Research, 2020. Vol. № 1.

139. Witting, I.T., et al. The thermoelectric properties of bismuth telluride // Advanced Electronic Materials, 2019. Vol. № 6. P. 1800904.

140. Holman, J.P. Experimental methods for engineers //, 2012. Vol.

141. Sudhakar, P., et al. Performance augmentation of solar photovoltaic panel through PCM integrated natural water circulation cooling technique // Renewable energy, 2021. Vol. P. 1433-1448.

142. Agyekum, E.B., et al. Effect of two different heat transfer fluids on the performance of solar tower csp by comparing recompression supercritical co2 and rankine power cycles, China // Energies, 2021. Vol. № 12. P. 3426.

143. Boddapati, V. and S.A. Daniel. Design and feasibility analysis of hybrid energy-based electric vehicle charging station // Distributed Generation & Alternative Energy Journal, 2022. Vol. P. 41–72-41–72.

144. Lai, C.S. and M.D. McCulloch. Levelized cost of energy for PV and grid scale energy storage systems // arXiv preprint arXiv:1609.06000, 2016. Vol.

145. Amjad, F., et al. Site location and allocation decision for onshore wind farms, using spatial multi-criteria analysis and density-based clustering. A techno-economic-environmental assessment, Ghana // Sustainable Energy Technologies and Assessments, 2021. Vol. P. 101503.

146. Baloch, A.A., et al. Experimental and numerical performance analysis of a converging channel heat exchanger for PV cooling // Energy Conversion and Management, 2015. Vol. P. 14-27.

147. Khan, M.K., et al. Green energy extraction for sustainable development: A novel MPPT technique for hybrid PV-TEG system // Sustainable Energy Technologies and Assessments, 2022. Vol. P. 102388.

148. Chandan, D., U. Arunachala, and K. Varun. Improved energy conversion of a photovoltaic module-thermoelectric generator hybrid system with different cooling techniques: Indoor and outdoor performance comparison // International Journal of Energy Research, 2022. Vol. № 7. P. 9498-9520.

149. Cotfas, D., et al. Critical factors and parameters for hybrid photovoltaic-thermoelectric systems; review // Applied Thermal Engineering, 2022. Vol. P. 118977.

150. Fortuner Poly Crystalline Products. URL: https://www.fortuners.net/p-2127/poly-crystalline.

151. Ali, U., K.J.B.A. Karim, and N.A. Buang. A review of the properties and applications of poly (methyl methacrylate)(PMMA) // Polymer Reviews, 2015. Vol. № 4. P. 678-705.

152. Saxena, P. and P. Shukla. A comparative analysis of the basic properties and applications of poly (vinylidene fluoride)(PVDF) and poly (methyl methacrylate)(PMMA) // Polymer Bulletin, 2021. Vol. P. 1-31.

153. Chen, Y., L. Zhang, and G. Chen. Fabrication, modification, and application of poly (methyl methacrylate) microfluidic chips // Electrophoresis, 2008. Vol. № 9. P. 1801-1814.

154. Qasim, M.A., V.I. Velkin, and S.E. Shcheklein. Development of a Computational Fluid Dynamics (CFD) Numerical Approach of Thermoelectric Module for Power Generation // Crystals, 2022. Vol. № 6. P. 828.

155. Shastry, D. and U. Arunachala. Thermal management of photovoltaic module with metal matrix embedded PCM // Journal of Energy Storage, 2020. Vol. P. 101312.

156. Rajvikram, M., et al. Experimental investigation on the abasement of operating temperature in solar photovoltaic panel using PCM and aluminium // Solar Energy, 2019. Vol. P. 327-338.

157. Bhargava, A.K., H. Garg, and R.K. Agarwal. Study of a hybrid solar system—solar air heater combined with solar cells // Energy Conversion and Management, 1991. Vol. № 5. P. 471-479.

158. Qasim, M.A. and V. Velkin. Experimental investigation of power generation in a microgrid hybrid network // Journal of Physics: Conference Series. 1706 IOP Publishing, 2020. P. 012065.

159. Högblom, O. and R. Andersson. A simulation framework for prediction of thermoelectric generator system performance // Applied energy, 2016. Vol. P. 472-482.

160. Wang, X.-D., et al. A three-dimensional numerical modeling of thermoelectric device with consideration of coupling of temperature field and electric potential field // Energy, 2012. Vol. № 1. P. 488-497.

161. Ruan, H., et al. Numerical investigation and comparative analysis of nanofluid cooling enhancement for TEG and TEC systems // Case Studies in Thermal Engineering, 2021. Vol. P. 101331.

162. Maduabuchi, C. Improving the performance of a solar thermoelectric generator using nano-enhanced variable area pins // Applied Thermal Engineering, 2022. Vol. P. 118086.

163. Prajwal, K. and P. Bhat. Thermal analysis of a Thermoelectric Generator (TEG) using FEM technique // IOP Conference Series: Materials Science and Engineering. 1045 IOP Publishing, 2021. P. 012018.

164. Hasan, M.N., et al. Finite Element Analysis of Thermoelectric Power Generation from Human Wrist // 2021 IEEE Symposium on Industrial Electronics & Applications (ISIEA) IEEE, 2021. P. 1-5.

165. Selimefendigil, F., H.F. Öztop, and M. Afrand. Shape effects of TEG mounted ventilated cavities with alumina-water nanofluids on the performance features by using artificial neural networks // Engineering Analysis with Boundary Elements, 2022. Vol. P. 79-97.

166. Potirniche, G.P. and L.L. Barannyk. A nonlinear finite element model for the performance of thermoelectric bulk and nanostructured materials // Energy, 2019. Vol. P. 262-273.

167. Eldesoukey, A. and H. Hassan. 3D model of thermoelectric generator (TEG) case study: Effect of flow regime on the TEG performance // Energy Conversion and Management, 2019. Vol. P. 231-239.

168. Chen, W.-H., et al. A computational fluid dynamics (CFD) approach of thermoelectric generator (TEG) for power generation // Applied Thermal Engineering, 2020. Vol. P. 115203.

169. Shen, R., X. Gou, and J. Zhong. A Three-dimensional Dynamic Analysis CFD Tool for Thermoelectric Generators // International Journal of Thermophysics, 2020. Vol. № 2. P. 1-19.

170. Qing, S., et al. *Design, experiment and modelling optimization for a high-temperature and medium-temperature coupled TEG system driven by direct combustion heat source* //, 2019. Vol.

171. Montserrat, G., et al. Effect of the air cooled forced convection finned heat sinks on the TEG net power: experimental and simulation results //, 2018. Vol.

172. Nagaraj, N.N.A. and L.S. Kumar. Electrical Energy Harvesting Using Thermo Electric Generator for Rural Communities in India // International Journal of Energy and Power Engineering, 2019. Vol. № 10. P. 663-667.

173. Su, C., et al. Optimization of cooling unit design for automotive exhaust-based thermoelectric generators // Journal of Electronic Materials, 2015. Vol. № 6. P. 1876-1883.

174. Simulink, Simulation, and Model-Based Design. URL: Mathworks website https://www.mathworks.com/help/simulink/.

175. Qasim, M.A., et al. Conversion of heat generated during normal PV panel operation into useful energy via a hybrid PV-TEG connection // International Journal of Renewable Energy Research (IJRER), 2022. Vol. № 4. P. 1779-1786.

176. Kwan, T.H. and X. Wu. The Lock-On Mechanism MPPT algorithm as applied to the hybrid photovoltaic cell and thermoelectric generator system // Applied energy, 2017. Vol. P. 873-886.

177. Shatar, N.M., et al. Design of photovoltaic-thermoelectric generator (PV-TEG) hybrid system for precision agriculture // 2018 IEEE 7th international conference on power and energy (PECon) IEEE, 2018. P. 50-55.

178. Belkaid, A., et al. Maximum power extraction from a photovoltaic panel and a thermoelectric generator constituting a hybrid electrical generation system // 2018 International Conference on Smart Grid (icSmartGrid) IEEE, 2018. P. 276-282.

179. Ibrahim, M.N., et al. Hybrid photovoltaic-thermoelectric generator powered synchronous reluctance motor for pumping applications // IEEE Access, 2019. Vol. P. 146979-146988.

180. Mirza, A.F., et al. High-efficiency hybrid PV-TEG system with intelligent control to harvest maximum energy under various non-static operating conditions // Journal of Cleaner Production, 2021. Vol. P. 128643.

181. Kanagaraj, N. Photovoltaic and thermoelectric generator combined hybrid energy system with an enhanced maximum power point tracking technique for higher energy conversion efficiency // Sustainability, 2021. Vol. № 6. P. 3144.

182. Ejaz, M. Optimal Control of Hybrid Photovoltaic-Thermometric Generator System Using GEPSO // Journal of Power and Energy Engineering, 2022. Vol. № 3. P. 1-21.

183. Qasim, M., et al. MPPT FOR HYBRID WIND, SOLAR AND THERMOELECTRIC POWER GENERATION SYSTEMS FOR OFF-GRID APPLICATIONS // Вестник Южно-Уральского государственного университета. Серия: Энергетика, 2022. Vol. № 2. P. 56-68.

184. Qasim, M.A. PWM effect on MPPT for hybrid PV solar and wind turbine generating systems at various loading conditions // Periodicals of Engineering and Natural Sciences (PEN), 2021. Vol. № 2. P. 581-592.

185. Belkassmi, Y., et al. Modeling and simulation of photovoltaic module based on one diode model using Matlab/Simulink // 2017 International Conference on Engineering & MIS (ICEMIS) IEEE, 2017. P. 1-6.

186. Zainal, N.A. and A.R. Yusoff. Modelling of photovoltaic module using matlab simulink // IOP Conference Series: Materials Science and Engineering. 114 IOP Publishing, 2016. P. 012137.

187. Ni, L.-x., et al. A power conditioning system for thermoelectric generator based on interleaved Boost converter with MPPT control // 2011 International Conference on Electrical Machines and Systems IEEE, 2011. P. 1-6.

188. Tan, G., M. Ohta, and M.G. Kanatzidis. Thermoelectric power generation: from new materials to devices // Philosophical Transactions of the Royal Society A, 2019. Vol. № 2152. P. 20180450.

189. Siouane, S., S. Jovanović, and P. Poure. Equivalent electrical circuit of thermoelectric generators under constant heat flow // 2016 IEEE 16th international conference on environment and electrical engineering (EEEIC) IEEE, 2016. P. 1-6.

190. Syahputra, R. and I. Soesanti. Performance improvement for small-scale wind turbine system based on maximum power point tracking control // Energies, 2019. Vol. № 20. P. 3938.

191. Spice for power electronics and electric power. / Rashid, M.H.: CRC press, 2005.

192. Power conversion and control of wind energy systems. / Wu, B., et al.: John Wiley & Sons, 2011.

193. De Brito, M.A., et al. Comparative analysis of MPPT techniques for PV applications // 2011 International Conference on Clean Electrical Power (ICCEP) IEEE, 2011. P. 99-104.

194. Ali, U.S., et al. Stateflow based incremental conductance MPPT of a photovoltaic system using Z-source DC-DC converter // 2016 Biennial International Conference on Power and Energy Systems: Towards Sustainable Energy (PESTSE) IEEE, 2016. P. 1-6.

195. Bulle, S.S., S. Patil, and V. Kheradkar. Implementation of incremental conductance method for MPPT using SEPIC converter // 2017 International Conference on Circuit, Power and Computing Technologies (ICCPCT) IEEE, 2017. P. 1-6.

196. Ahmadzadeh, S. and G.A. Markadeh. Incremental conductance based MPPT using a high step-up Y-source DC-DC Converter // 2017 8th Power Electronics, Drive Systems & Technologies Conference (PEDSTC) IEEE, 2017. P. 543-548.

197. El Telbany, M.E., A. Youssef, and A.A. Zekry. Intelligent techniques for MPPT control in photovoltaic systems: A comprehensive review // 2014 4th International Conference on Artificial Intelligence with Applications in Engineering and Technology IEEE, 2014. P. 17-22.

198. MATLAB and its applications in engineering. / Bansal, R.K., A.K. Goel, and M.K. Sharma: Pearson Education India, 2009.

199. Gomide, F. Uncertain rule-based fuzzy logic systems: introduction and new directions-Jerry M. Mendel; Prentice-Hall, PTR, Upper Saddle River, NJ, 2001, 555pp., ISBN 0-13-040969-3 // Fuzzy Sets and Systems, 2003. Vol. № 133. P. 133-135.

200. Taskin, A. and T. Kumbasar. An open source Matlab/Simulink toolbox for interval type-2 fuzzy logic systems // 2015 IEEE Symposium Series on Computational Intelligence IEEE, 2015. P. 1561-1568.

201. Mohammed, M.F., A.H. Ahmad, and A.T. Humod. Design of isolated IGBT driving and control circuits for an interleaved boost converter // Engineering and Applied Science Research, 2021. Vol. № 1. P. 48-55.

202. Jaber, S.F. and A.M. Shakir. Design and simulation of a boost-microinverter for optimized photovoltaic system performance // Int. J. SMART GRID (ijSmartGrid), 2021. Vol. № 2. P. 94-102.

203. I. Breesam, W., et al. Speed Control of a Multi-Motor System Based on Fuzzy Neural Model Reference Method // Actuators. 11 MDPI, 2022. P. 123.

204. Qasim, M., et al. DESIGN AND SIMULATION OF A SOLAR-WIND STAND-ALONE SYSTEM WITH A SEVEN-LEVEL INVERTER // Вестник Южно-Уральского государственного университета. Серия: Энергетика, 2022. Vol. № 3. P. 5-17.

205. Mohammed, M.F. and M.A. Qasim. Single Phase T-Type Multilevel Inverters for Renewable Energy Systems, Topology, Modulation, and Control Techniques: A Review // Energies, 2022. Vol. № 22. P. 8720.

206. Abbas, F.A., et al. An efficient energy-management strategy for a DC microgrid powered by a photovoltaic/fuel cell/battery/supercapacitor // Clean Energy, 2022. Vol. № 6. P. 827-839.

207. Ecodirect, “Ameresco 30J > Ameresco Solar 30 Watt Solar Panel - Class 1 Div 2”,. URL: https://www.ecodirect.com/Ameresco-30J-Ameresco-Solar-30-Watt-Solar-Panel-p/ameresco-30j.htm.

208. Mohammed, M.F., M.A. Qasim, and V.I. Velkin. Stand-alone transformer-less multilevel inverter fed by solar energy for irrigation purposes // materials today: proceedings, 2022.